Coupled Electron and Nuclear Dynamics in Model Systems

Dissertation

zur Erlangung des
naturwissenschaftlichen Doktorgrades
der Bayerischen Julius-Maximilians-Universität Würzburg

vorgelegt von

Marco Erdmann

aus

Würzburg

Würzburg 2004

Eingereicht am: ....

bei der Fakultät für Chemie und Pharmazie

1. Gutachter: ....

2. Gutachter: ....

der Dissertation

1. Prüfer: ....

2. Prüfer: ....

3. Prüfer: ....

des Öffentlichen Promotionskolloquiums

Tag des Öffentlichen Promotionskolloquiums: ....

Doktorurkunde ausgehändigt am: ....

Contents

Introduction **6**

1 Theoretical background **11**

1.1 The Born-Oppenheimer approximation and its limitations 11

1.2 Accuracy of the Born-Oppenheimer approximation 16

1.3 Matter-field interaction 18

1.4 Time-dependent perturbation theory 21

1.5 Strong-field Hamiltonian 23

1.6 Electron localization function 24

2 Numerical methods **28**

2.1 Solving the time-dependent Schrödinger equation 28

2.1.1 Improving accuracy 29

2.1.2 Obtaining eigenstates 30

2.2 Calculation of absorption spectra 32

3 Combined electron and nuclear dynamics: A simple model system **35**

3.1 Introduction 35

3.2 The model Hamiltonian 36

3.3 Adiabatic approximation 39

3.3.1 Adiabatic potential curves 40

3.3.2 Electronic eigenfunctions 42

3.3.3 Kinetic coupling elements 44
3.3.4 Transition dipole moments 46
3.4 Quantum dynamics 47
3.4.1 Time-dependent electron and nuclear densities 47
3.4.2 Time-dependent Laplacians 54
3.5 Inverse Born-Oppenheimer approximation 56
3.6 Summary 58

4 Electronic predissociation 61
4.1 Introduction 61
4.2 Modifications to the model 62
4.3 Electronic structure 64
4.4 Predissociation dynamics 66
4.5 Summary 70

5 Spectroscopic transitions 71
5.1 Introduction 71
5.2 One-photon transitions 72
5.2.1 Absorption spectra 72
5.2.2 Electron and nuclear dynamics during spectroscopic transitions 81
5.3 Strong-field dynamics 84
5.4 Summary 88

6 Localization in a two-electron system 91
6.1 Introduction 91
6.2 Definition of ELF for exact wave functions 92
6.3 The extendend model Hamiltonian 94
6.4 Adiabatic potentials and eigenfunctions 96
6.5 Quantum dynamics 100
6.6 Summary 103

7 Outlook: Electron localization in the anti-parallel spin case **104**

Summary **111**

Zusammenfassung **116**

A Diabatization of two coupled adiabatic potentials **122**

B Thomas-Fermi kinetic energy density in one dimension **125**

Bibliography **129**

Dank **134**

Lebenslauf **135**

Introduction

The dynamical features of atomic and molecular systems have been of interest in quantum mechanics since its very beginnings [1]. The equation of motion in (non-relativistic) quantum mechanics is the *time-dependent Schrödinger equation*

$$i\hbar \frac{\partial}{\partial t}\Psi = H\Psi, \tag{1}$$

where H denotes the system's Hamiltonian. The wide search for methods to solve the time-dependent Schrödinger equation started only in the late 1970's, although some fundamental principles were already formulated in the 1930's [1]. The theoretical description of time-dependent molecular phenomena gained additional momentum with the foundation of femtochemistry by A. Zewail in the late 1980's [2].

Chemistry focuses its interest on molecules and the exact theoretical description of time-dependent processes makes it necessary to solve the Schrödinger equation for the coupled electronic and nuclear motion. As the computational effort to find a solution scales exponentially with the degrees of freedom in a system, this is only possible for very small molecules.

The traditional approach to address this problem is a separation of nuclear and electronic variables. Within the *Born-Oppenheimer adiabatic approximation* (see chapter 1.1) the electronic problem is solved first for fixed nuclear geometry. This is the concern of quantum chemistry. The solution yields electronic eigenfunctions and eigenenergies which depend parametrically on the nuclear geometry. The calculated eigenenergies for different nuclear geometries build potential energy surfaces belonging to one electronic state. These potential energy curves are used in quantum dynamics to solve the time-dependent Schrödinger equation for the nuclei and several integration schemes have been developed [3–6].

Within the Born-Oppenheimer approximation the dynamics of the nuclei is limited to a single electronic state. The adiabatic approximation also generally fails in describing the dynamics in excited states. Prominent examples for this breakdown are the Jahn-Teller effect [7], electronic predissociation [8] or internal conversions [9]. Furthermore, conical intersections, originating from the coupling of electronic and vibrational motion, are of central significance in many photochemical processes [10].

These nonadiabatically coupled cases can still be treated — in principle exactly — by propagating nuclear wave functions in coupled electronic states. This is usually done in a *diabatic* representation, where the Hamiltonian contains diagonal and off-diagonal potential matrix elements, see reference [11] and references therein. Coupling between electronic states can also be induced by external perturbations, e.g. electric fields, and can be described by explicit time-dependent coupling elements in the Hamiltonian.

The exact propagation of the nuclear wave function gets very cumbersome, if more than a few degrees of freedom have to be computed. A promising attempt to reduce the many-body Schrödinger equation for the nuclei to a set of coupled equations for each nuclear coordinate is the *time-dependent self-consistent field* [12] or time-dependent Hartree approximation. It was extended to a multiconfigurational approach [13] and also to treat nonadiabatically coupled cases [14].

Over the last 20 years many methods have been devised to investigate electronic and nuclear motion simultaneously. All of them truncate the full quantum mechanical description to some extent in order to keep the numerical effort controllable. Among those are the *Car-Parinello* method [15,16] or *electron-nuclear dynamics* (END) which was developed by Öhrn and co-workers [17,18]. Another large group of mixed classical/quantum mechanical methods employs a *time-dependent Hartree-Fock* description of the electrons and a classic description for the nuclei [19–26]. This list is of course by no means complete.

Only recently, several attempts have been made to address the full coupled problem: Bandrauk and co-workers performed calculations on the H_2^+ molecule in strong laser fields for fixed molecular orientation [27,28]. The Bandrauk group also introduced linear models for the combined electronic and nuclear motion [29–31]. This model of reduced dimensionality, which becomes very useful in ultraintense laser fields [32–35], was recently applied to the H_2 molecule [36].

Within the framework of the *Graduiertenkolleg 690 "Electron density"* this work investigates the full quantum mechanical description of a coupled electronic and nuclear motion. The focus of our interest lies in the temporal changes of electron and nuclear density during a coupled electron and nuclear dynamics. For that it is necessary to solve the time-dependent Schrödinger equation exactly for all nuclear and electronic degrees of freedom. We already mentioned that this is very demanding for real molecules. However, it is possible to find a model system that is small enough to be tractable computationally and, on the other hand, contains all physics of a coupled electronic and nuclear dynamics. Therefore, we employ a simple model which was introduced by Shin and Metiu [37,38] for the description of charge-transfer processes. It involves only a single nuclear and a single electronic degree of freedom and the particle interactions are parameterized in such a way as to allow for a facile transition from a Born-Oppenheimer behaviour to a situation where the adiabatic approximation breaks down. Within this model we can easily explore features beyond a limiting Born-Oppenheimer description. By adding another electron the physics of a many-electron system is also available.

This work is organized as follows: The first two chapters give an overview of the employed theoretical (chapter 1) and numerical (chapter 2) methods. We discuss the Born-Oppenheimer approximation, the theoretical description of matter-field interaction and give the original definition of the *electron localization function* (ELF). Furthermore, we describe how the time-dependent Schrödinger equation can be solved by the *split-operator algorithm* and how to obtain eigenstates and absorption spectra.

Chapter 3 investigates the changes in the eigenstates and potential energy surfaces, obtained from an adiabatic approximation, when switching from a typcial Born-Oppenheimer situation to a strongly coupled one. The changes in the dynamical behaviour of electron and nucleus due to nonadiabatic coupling are discussed by means of wave packet calculations employing the full Hamiltonian. Furthermore, we discuss how usually not easily available quantities like the kinetic coupling elements and the transition dipole moments between adiabatic states change under the influence of vibronic coupling. Finally, we shortly discuss why reversing the Born-Oppenheimer approximation leads to an unphysical description.

In chapter 4 the model Hamiltonian is modified for the purpose to describe an *electronic predissociation* process. Wave packet calculations demonstrate the change of electron and nuclear densities during the fragmentation.

Chapter 5 regards perturbations imposed by external electric fields and investigates how absorption spectra change in the presence of strong nonadiabatic coupling. In this way a clear illustration of the commonly employed *Franck-Condon principle* for spectroscopic transitions can be found in terms of time-dependent electron and nuclear densities. The interaction with strong laser pulses leads to the formation of nuclear and electronic wave packets.

An extension of the simple model (chapter 6) illustrates the concept of electron localization in a many-electron system and how localization changes as a function of time during a vibrational motion in an electronically excited state. Therefore, it was necessary to extend the definition of the widely used *electron localization function* using an exact, time-dependent wave function.

Finally, we give a short outlook (chapter 7) on how to define electron localization in the case of anti-parallel electron spins. We derive a similar function as the ELF and demonstrate its usefulness in a numerical example.

The aim of this work is to provide a deeper insight and a more fundamental understanding of how nonadiabatic coupling changes nuclear and electron densities as a function of time, not restricted to the electronic ground state. Therefore, it is not sufficient to rely on common concepts of the electron density alone. One rather has to simultaneously regard the time-dependent perturbation of the density by the nuclear motion which is crucial to concepts of, e.g. charge transfer or localization.

Chapter 1

Theoretical background

1.1 The Born-Oppenheimer approximation and its limitations

Solving the many-particle Schrödinger equation is a tedious task. Without any approximations an analytical solution can only be obtained for systems of no more than two interacting particles. The Born-Oppenheimer approximation [39] is a special case of an adiabatic approximation and it serves as a starting point for many methods of modern quantum chemistry. While this work tries to avoid this approximation, it is nevertheless necessary to obtain a basic understanding of its features.

The total Hamiltonian of a given molecular system — neglecting spin-orbit interactions — is of the form [9]:

$$H_{\text{tot}} = T_{\text{el}}(x) + T_{\text{nucl}}(R) + V(x, R) \tag{1.1}$$

Here, x and R denote the sets of electronic and nuclear coordinates. $T_{\text{el}}(x)$ and $T_{\text{nucl}}(R)$ are the operators of the kinetic energy of electrons and nuclei, respectively, while $V(x, R)$ is the Coulomb interaction of all particles (using atomic units, $\hbar = m_e = e = 1$):

$$\begin{aligned} T_{\mathrm{el}}(x) &= -\frac{1}{2}\sum_i \nabla_i^2 \\ T_{\mathrm{nucl}}(R) &= -\sum_\alpha \frac{1}{2M_\alpha}\nabla_\alpha^2 \\ V(x,R) &= \sum_i\sum_{j>i}\frac{1}{|\vec{x}_i-\vec{x}_j|}+\sum_\alpha\sum_{\beta>\alpha}\frac{Z_\alpha Z_\beta}{\left|\vec{R}_\alpha-\vec{R}_\beta\right|}-\sum_i\sum_\alpha\frac{Z_\alpha}{\left|\vec{x}_i-\vec{R}_\alpha\right|} \end{aligned} \tag{1.2}$$

Here, i and j count the electrons, while α and β count the nuclei. M_α are the masses of the nuclei. In the following we will omit the vector signs of the coordinates in order to simplify the notation, i.e. $\vec{x}_i = x_i$ and $\vec{R}_\alpha = R_\alpha$.

The adiabatic approximation has its foundation in the large difference between the electronic and nuclear masses, which means that in the time average the electrons are expected to move much faster than the nuclei. This allows for a partitioning into the “slow” (nuclear) and “fast” (electronic) subsystems [9]. Thus, assuming that the electron density only depends on the position, but not on the momenta (i.e. masses) of the nuclei, the mean electron density can be described by a set of electronic wave functions $\varphi(x, R)$ evaluated at fixed values of the nuclear coordinates R:

$$\rho(x) = \int |\varphi(x,R)|^2 \; |\chi(R)|^2 \; dR \tag{1.3}$$

The second term describes the density of the probability distribution of the nuclear coordinates. It has the meaning of a *nuclear wave function* which will soon become clearer.

Evaluating equation (1.3) makes it necessary to determine the wave function of the “fast” subsystem for fixed values of R. We apply above partitioning to the molecular Hamiltonian (1.1) and rewrite it in terms of centre-of-mass coordinates [40]:

$$\begin{aligned} H_{\mathrm{tot}} &= T_{\mathrm{nucl}} + H_{\mathrm{el}} \\ H_{\mathrm{el}} &= T_{\mathrm{el}} + V(x, R) \end{aligned} \tag{1.4}$$

Here, H_{el} denotes the *electronic Hamiltonian.* The *adiabatic electronic wave functions* $\varphi_n(x, R)$ are determined by the *electronic Schrödinger equation*:

$$H_{\mathrm{el}}(R)\varphi_n(x, R) = \epsilon_n(R)\varphi_n(x, R) \tag{1.5}$$

Here, n counts the adiabatic electronic states and $\epsilon_n(R)$ are the eigenenergies that depend *parametrically* on the nuclear coordinates. The set of electronic functions $\{\varphi_n(x, R)\}$ are eigenfunctions of a Hermitian operator and form a complete basis set. They may be chosen *orthogonal* and *orthonormal*:

$$\langle \varphi_n(x, R) \mid \varphi_{n'}(x, R) \rangle = \delta_{nn'} \tag{1.6}$$

We may now expand the complete wave function $\Psi_{\mathrm{tot}}(x, R)$ into the basis of electronic eigenfunctions:

$$\Psi_{\mathrm{tot}}(x, R) = \sum_n \varphi_n(x, R)\chi_n(R) \tag{1.7}$$

As already mentioned above, the expansion coefficients $\chi_n(R)$ are functions of the nuclear coordinate. The index n counts the different electronic states. Inserting this expansion into the *Schrödinger equation* yields the following set of coupled equations:

$$\sum_n \left(T_{\text{nucl}} + H_{\text{el}}\right) \varphi_n(x,R)\chi_n(R) = E_{tot} \sum_n \varphi_n(x,R)\chi_n(R) \tag{1.8}$$

No approximations were introduced so far. Equation (1.8) is just a re-writing of the *Schrödinger equation* in terms of a basis set expansion. The nuclear kinetic energy operator T_{nucl} is a differential operator and absorbing mass dependence, sign and summation into the Nabla operator allows for an easier notation:

$$T_{\text{nucl}} = \sum_\alpha -\frac{1}{2M_\alpha} \nabla_\alpha^2 \overset{!}{=} \nabla_{\text{nucl}}^2 \tag{1.9}$$

Expanding the single terms of equation (1.8) leads to the following expression:

$$\begin{aligned}
\sum_n \left(\nabla_{\text{nucl}}^2 + H_{\text{el}}\right) \varphi_n\chi_n &= E_{\text{tot}} \sum_n \varphi_n\chi_n \\
\sum_n \left\{\nabla_{\text{nucl}}^2 \left(\varphi_n\chi_n\right) + H_{\text{el}}\, \varphi_n\chi_n\right\} &= E_{\text{tot}} \sum_n \varphi_n\chi_n \\
\sum_n \{\nabla_{\text{nucl}} \left[(\varphi_n \nabla_{\text{nucl}}\chi_n) + (\chi_n \nabla_{\text{nucl}}\varphi_n)\right] & \\
+ \chi_n H_{\text{el}}\varphi_n\} & \\
&= E_{\text{tot}} \sum_n \varphi_n\chi_n \qquad (1.10)\\
\sum_n \left\{\varphi_n \left(\nabla_{\text{nucl}}^2\chi_n\right) + 2\left(\nabla_{\text{nucl}}\varphi_n\right)\left(\nabla_{\text{nucl}}\chi_n\right)\right. & \\
\left. + \chi_n \left(\nabla_{\text{nucl}}^2\varphi_n\right) + \chi_n\epsilon_n\varphi_n\right\} &= E_{\text{tot}} \sum_n \varphi_n\chi_n
\end{aligned}$$

Projection onto *one* electronic state $\langle\varphi_m|$ and integration over the electronic coordinates, transforms equation (1.10) into:

$$\begin{aligned}
\nabla_{\text{nucl}}^2\, \chi_n + \epsilon_m\, \chi_n + \sum_n \{2\langle\varphi_m \left|\nabla_{\text{nucl}}\right| \varphi_n\rangle \left(\nabla_{\text{nucl}}\chi_n\right) & \\
+ \langle\varphi_m \left|\nabla_{\text{nucl}}^2\right| \varphi_n\rangle\, \chi_n\} &= E_{\text{tot}}\chi_m \qquad (1.11)
\end{aligned}$$

Here we used the *orthonormality* (1.6) of the electronic basis set. The first two terms now contain no longer electronic functions, while the terms in the curly bracket couple different electronic states via derivatives with respect to nuclear coordinates. The terms of the form $T_{mn}^{(k)} = \langle\, \varphi_m \left|\nabla_{\text{nucl}}^k\right| \varphi_n\rangle$ (with $k = 1, 2$) are called kth-order *non-adiabatic coupling elements*, respectively, while the last term of the bracket is the mass polarization.

The *adiabatic approximation* restricts the total wave function to one electronic state, i.e. all coupling elements in equation (1.11) are neglected. Thus only the terms with $m = n$ survive. Also, the diagonal first-order non-adiabatic coupling elements are zero if we take equation (1.6) into account:

$$
\begin{aligned}
\langle\varphi_n \,|\varphi_n\rangle &= 1 \\
\Rightarrow \nabla_{\text{nucl}}\langle\varphi_n \,|\varphi_n\rangle &= 0 \\
\nabla_{\text{nucl}}\langle\varphi_n \,|\varphi_n\rangle &= \underbrace{\langle\varphi_n \,|\nabla_{\text{nucl}}|\, \varphi_n\rangle}_{\text{diagonal coupling 1st order}} + \langle\nabla_{\text{nucl}}\,\varphi_n \,|\, \varphi_n\rangle = 0 \qquad (1.12) \\
\overset{\varphi_n\in\mathbb{R}}{\Longrightarrow} \langle\varphi_n \,|\nabla_{\text{nucl}}|\, \varphi_n\rangle &= -\langle\nabla_{\text{nucl}}\,\varphi_n \,|\, \varphi_n\rangle \\
\Leftrightarrow \langle\varphi_n \,|\nabla_{\text{nucl}}|\, \varphi_n\rangle &= \langle\nabla_{\text{nucl}}\,\varphi_n \,|\, \varphi_n\rangle = 0
\end{aligned}
$$

We may now rewrite equation (1.11) with the surviving terms:

$$
\left(\nabla_{\text{nucl}}^2 + \epsilon_m + \langle\varphi_m \left|\nabla_{\text{nucl}}^2\right| \varphi_m\rangle\right) \chi_m = E_{\text{tot}}\chi_m \qquad (1.13)
$$

Re-introduction of the kinetic energy operator (eqn. (1.9)) yields:

$$
\left(T_{\text{nucl}} + \epsilon_m + \langle\varphi_m \left|\nabla_{\text{nucl}}^2\right| \varphi_m\rangle\right) \chi_m = E_{\text{tot}}\chi_m \qquad (1.14)
$$

The term $\langle\varphi_m \,|\nabla_{\text{nucl}}^2|\, \varphi_m\rangle$ is the so-called *diagonal correction* and is much smaller than ϵ_m, as the mass of the nuclei enters into the denominator. The shape of the field, acting on the nuclei, is therefore determined almost entirely by ϵ_m [41].

In the *Born-Oppenheimer approximation* the diagonal correction is also neglected and equation (1.11) takes now again the form of the Schrödinger equation:

$$[T_{\mathrm{nucl}} + \epsilon_m(R)]\,\chi_m(R) = E_{\mathrm{tot}}\chi_m(R) \tag{1.15}$$

We have now arrived at the point of the *Born-Oppenheimer picture*, where the motion of the nuclei is restricted to a single electronic state *potential energy surface* $|m\rangle$. The corresponding eigenenergies $epsilon_m(R)$, which are obtained from the *electronic Schrödinger equation* (1.5), serve as the potenial term for the nuclear motion.

1.2 Accuracy of the Born-Oppenheimer approximation

In order to get an estimate of the accuracy of the Born-Oppenheimer approximation one has to find an estimate for the off-diagonal kinetic coupling elements $T^{(k)}_{mn}$, where m, n are quantum numbers and $k = 1, 2$. A central quantity of the approximation is the mass ratio between electrons and nuclei that may be expressed as *Born-Oppenheimer parameter* $\kappa = (1/M)^{1/4}$ (in a.u., $m_e = 1$). We will only present the results here, for a detailed discussion the reader should refer to reference [9].

It is possible to calculate the first-order correction to the Born-Oppenheimer wave function $\Psi_n(R, x) = \psi(R)\varphi_n(x, R)$ from perturbation theory [42]. It takes the form:

$$\delta\Psi_{mn} = \sum_{m'\neq m}\sum_{n'} \frac{L_{m'n'mn} + K_{m'n'mn}}{E_{mn} - E_{m'n'}}\,\Psi_{m'n'} \tag{1.16}$$

The perturbation term contains matrix elements of the operators L and K which are defined as (in atomic units):

$$\begin{aligned} L_{mn}(R) &= -\sum_{\alpha}\frac{1}{M_\alpha}\langle\varphi_m(x,R)|\frac{\partial}{\partial R_\alpha}|\varphi_n(x,R)\rangle\frac{\partial}{\partial R_\alpha} \\ K_{mn}(R) &= -\sum_{\alpha}\frac{1}{M_\alpha}\langle\varphi_m(x,R)|\frac{\partial^2}{\partial R_\alpha^2}|\varphi_n(x,R)\rangle \end{aligned} \tag{1.17}$$

The first-order correction term to the energy is the diagonal electronic matrix element $K_{nn}(R)$ which generates no coupling and thus does not violate the adiabatic approximation. It is just a coordinate dependent correction to the adiabatic potential. The second-order correction to the energy is:

$$\delta E_{mn} = \sum_{m'\neq m}\sum_{n'} \frac{|L_{m'n'mn} + K_{m'n'mn}|^2}{E_{mn} - E_{m'n'}} \tag{1.18}$$

One can show that the matrix elements of K can be neglected if the electronic energy seperation is not too small. The non-adiabaticity stems mostly from the $L_{m'n'mn}$ matrix elements. For small quantum numbers n and only electronic state contributing to the sum over m' one obtains the following non-adiabatic corrections:

$$\begin{aligned} \delta\Psi_{mn} &\approx \kappa^3(\mathcal{E}/\Delta\mathcal{E})^2\Psi_{m'n'} \\ \delta E_{mn} &\approx \kappa^6\mathcal{E}(\mathcal{E}/\Delta\mathcal{E})^3 \end{aligned} \tag{1.19}$$

Here $\mathcal{E}$ denotes the electronic energy and $\Delta\mathcal{E}$ the energy seperation between electronic states. Thus, if $\Delta\mathcal{E} \approx \mathcal{E}$ (as is usually true for the first excited state), the corrections to the wave function, the adiabatic potential[1] and the energy are on the order of κ^3, κ^4 and κ^6.

From equation (1.19) follows that the accuracy of the adiabatic approximation is the higher, the larger the gap between the electronic states is. For excited electronic states the level spacing gets increasingly smaller and it is evident that the non-adiabaticity effects for the ground state are much smaller then for highly excited states, that always show effects of degeneration and quasi-degeneration.

If for a certain nuclear configuration R the gap between two electronic states $\mathcal{E}_m(R)$ and $\mathcal{E}_{m'}(R)$ gets negligibly small, the nuclear motion in the vicinity of such a configuration is no longer adiabatic. The motion of the electronic subsystem has the period $2\pi/\Delta\mathcal{E}$ and the condition for adiabaticity takes the form (ω is the frequency of the nuclear motion):

$$\omega/\Delta\mathcal{E} \ll 1 \tag{1.20}$$

If this condition is not fulfilled, the states m and m' get strongly mixed by nuclear motion. An exception is the case where the crossing electronic states belong to different symmetries. Then the integrals over the electronic states in equation (1.17) vanish and $K_{mn}(R) = L_{mn}(R) = 0$.

1.3 Matter-field interaction

The exact description of the interaction of a molecule with an intense laser pulse involves the coupling of all degrees of freedom of the molecule to the quantum states of the external field. This is very cumbersome and so throughout this work we will treat the laser field as purely classical. The interaction term $W(t)$ in the

---

[1] The correction to the adiabatic potential can be written as $\delta\mathcal{E}_m \approx \frac{1}{2}\kappa^4\mathcal{E}(\mathcal{E}/\Delta\mathcal{E})^2$.

Hamiltonian describes the interaction of a particle with the electric field. In the following we will shortly derive its mathematical form.

The electric field $\vec{E}$ with wave vector $\vec{k}$ and frequency ω may be written as:

$$\vec{E}(\vec{R},t) = \vec{\epsilon}\, f(t)\, E_0 \left(e^{i\left(\vec{k}\vec{R}-\omega t\right)} + e^{-i\left(\vec{k}\vec{R}-\omega t\right)}\right) \tag{1.21}$$

Here, $\vec{\epsilon}$ is the polarization vector, $f(t)$ is the envelope function of the laser pulse and E_0 half of the maximal field strength. Under the assumption that the wave length of the fields is much larger than the range of a given molecule [43], we can safely neglect the position dependency (*dipole approximation*):

$$\vec{E}(t) = \vec{\epsilon}\, f(t)\, E_0 \left(e^{-i\omega t} + e^{i\omega t}\right) \tag{1.22}$$

The interaction term $W(t)$ takes now the form [44]

$$W(t) = -\vec{\mu}\vec{E}(t). \tag{1.23}$$

where $\vec{\mu}$ is the dipole moment of the molecule. Inserting equation (1.23) into the time-dependent Schrödinger equation (2.1) yields (in a.u.):

$$i\frac{\partial}{\partial t}\Psi(t) = \left[H - \vec{\mu}\vec{E}(t)\right]\Psi(t) \tag{1.24}$$

Expanding the wave function into the basis of electronic and vibrational eigenstates of the Hamiltonian yields *time-dependent* expansion coefficients $a_{n,v}(t)$ (thus defining a wave packet):

$$|\Psi(t)\rangle = \sum_n \sum_v a_{n,v}(t)\, e^{-iE_{n,v}t}\, |\Psi_{n,v}\, \varphi_n\rangle \tag{1.25}$$

Here, n counts the electronic and v the vibrational states of the molecule. $|\Psi_{n,v}\rangle$ denotes an vibrational eigenstate in electronic state n and $E_{n,v}$ is its eigenenergy. Projection onto an eigenstate $\langle\Psi_{m,v'}\,\varphi_m|$ yields a set of coupled equations for the coefficients:

$$i\frac{\partial}{\partial t}a_{m,v'}(t) = E_{m,v'}\,a_{m,v'}(t) + \sum_n\sum_v \mu_{m,v',n,v}(t)\,a_{n,v}(t)\,e^{i\omega_{m,v',n,v}t} \tag{1.26}$$

In above equation $\mu_{m,v',n,v}(t)$ are the *transition dipole moments* which result from the projection of the electric field vector $\vec{E}(t)$ onto the dipole moment $\vec{\mu}$ and are of the form:

$$\mu_{m,v',n,v}(t) = \langle\Psi_{m,v'}\varphi_m| - \vec{\mu}\cdot\vec{E}(t)|\Psi_{n,v}\varphi_n\rangle = -E(t)\,\mu_{m,v',n,v} \tag{1.27}$$

The *transition frequencies* $\omega_{m,v',n,v}$ are given by (in a.u.):

$$\omega_{m,v',n,v} = E_{m,v'} - E_{n,v} \tag{1.28}$$

In equation (1.26) all electronic and vibrational states are coupled by the external field and finally takes the form:

$$\begin{aligned} i\hbar\frac{\partial}{\partial t}a_{m,v'}(t) &= E_{m,v'}\,a_{m,v'}(t) \\ &- f(t)\,E_0\left\{e^{-i\omega t} + e^{i\omega t}\right\}\sum_v\sum_n \mu_{m,v',n,v}\;a_{n,v}(t)\;e^{i\omega_{m,v',n,v}t} \\ &= E_{m,v'}\,a_{m,v'}(t) \\ &- f(t)\,E_0\sum_v\sum_n \mu_{m,v',n,v}\;\left\{e^{i\omega_{m,v',n,v}+\omega t} + e^{i\omega_{m,v',n,v}-\omega t}\right\}\;a_{n,v}(t) \end{aligned} \tag{1.29}$$

For an absorption process the first exponential varies very fast as a function of time. This means that all observables averaged over time-intervals larger than several optical cycles of the external field (several femtoseconds in the case of an UV excitation) have no contributions from terms containing the sum of the laser frequency and the transition frequency and are neglected (*rotating wave approximation*). The reverse holds true for a stimulated emission process (*counter-rotating wave approximation*) [45].

The complicated equations that arise from matter-field interaction may be solved approximately in terms of *time-dependent perturbation theory* as we will see in the next section.

1.4 Time-dependent perturbation theory

A simplified description of the interaction of matter with a weak electromagnetic field may be obtained in terms of the *time-dependent perturbation theory* [46,47]. In this approach the field is treated classically whereas the interaction with the quantum system is a time-dependent perturbation. Let us regard a quantum system whose time evolution for times $t < 0$ is given by equation (2.1) (in a.u.):

$$i\frac{\partial}{\partial t}\Psi_0(t) = H_0\Psi_0(t) \tag{1.30}$$

Here H_0 is the Hamiltonian of the unperturbed system. At $t = 0$ a small, time-dependent perturbation $W(t)$ acts on the system, thus equation (1.30) has to be modified:

$$i\frac{\partial}{\partial t}\Psi(t) = \left[H_0 + W(t)\right]\Psi(t) = H\Psi(t) \tag{1.31}$$

We are looking for solutions of this equation under the condition that $\Psi(t) = \Psi_0(t)$ for times $t \leq 0$. The wave function can formally be written as:

$$\Psi(t) = e^{-iHt}\,\varphi(t) \tag{1.32}$$

Inserting equation (1.32) into (1.31) yields:

$$i\frac{\partial}{\partial t}\phi(t) = W_t\phi(t) \tag{1.33}$$

$\phi(t)$ is the wave function in the *interaction picture*, while the pertubation takes the form:

$$W_t = e^{iHt}\,W(t)\,e^{-iHt} \tag{1.34}$$

Integration of the partial differential equation (1.33) gives the following expression:

$$\phi(t) = \phi(0) + \frac{1}{i}\int\limits_0^t W_{t'}\phi(t')\,dt' \tag{1.35}$$

Solving this equation is quite difficult, as the wave function $\phi(t)$ also appears in the time integral. It is, however, possible to obtain an approximate solution via an iterative procedure. For that we replace the exact function in the integral by $\phi(0)$ and get the *first-order correction*:

$$\phi^{(1)}(t) = \phi(0) + \frac{1}{i}\int\limits_0^t W_{t'}\phi(0)\,dt' \tag{1.36}$$

Replacing $\phi(t)$ in equation (1.35) by the first order function (1.36) yields the *second-order correction*:

$$\phi^{(2)}(t) = \phi(0) + \frac{1}{i}\int\limits_0^t W_{t'}\phi(t')\,dt' + \frac{1}{i^2}\int\limits_0^t\int\limits_0^{t'} W_{t'}W_{t''}\phi(0)\,dt''dt' \tag{1.37}$$

This iteration may be continued to higher orders.

While this formalism gives corrections to the wave function in the *interaction picture*, our interest lies in the *Schrödinger picture*. Using equation (1.32) one finds for the first-order wave function:

$$\Psi^{(1)}(t) = e^{-iHt}\Psi(0) + \frac{1}{i}\int_0^t e^{-iH(t-t')}W_{t'}e^{-iHt'}\Psi(0)\,dt' \tag{1.38}$$

Here $\phi(0) = \Psi(0)$. The second-order wave function may be obtained similarly.

1.5 Strong-field Hamiltonian

The interaction of molecules with intense laser fields shows interesting phenomena like bond-softening or above-threshold ionization (ATI) [48]. A theoretical description is no longer possible in terms of time-dependent perturbation theory (see section 1.4) as considerable amounts of population are transferred between electronic states. In the following we shortly describe how to incorporate the matter-field interaction into the usual Born-Oppenheimer picture of non-coupled electronic states.

Consider a system that consists only of two electronic states $|1\rangle$ and $|2\rangle$. The system is initially in its electronic ground state $|1\rangle$. Population may be transferred by an intense laser pulse to the excited state $|2\rangle$. The Hamiltonian now transforms into a matrix $\mathbf{H}$ with coupling off-diagonal elements:

$$\mathbf{H} = \begin{pmatrix} H_1 & W_{12} \\ W_{21} & H_2 \end{pmatrix} \tag{1.39}$$

H_n $(n = 1, 2)$ are the Hamiltonians of the electronic states $|1\rangle$ and $|2\rangle$. The coupling by the field W_{nm} is of the form:

$$W_{nm} = -E_0\, \mu_{nm}\, f(t)\, cos(\omega t) \tag{1.40}$$

Here μ_{nm} is the *transition dipole moment* ($\mu_{nm} = \langle n\, |\hat{\mu}|\, m\rangle$), E_0 is the field strength and $f(t)$ is the envelope function of the pulse. The nuclear wave function has two components ψ_n ($n = 1, 2$) that describe the nuclear motion in the electronic states. The equation of motion now turns into a matrix equation (in a.u.):

$$\begin{pmatrix} H_1 & W_{12} \\ W_{21} & H_2 \end{pmatrix} \begin{pmatrix} \psi_1 \\ \psi_2 \end{pmatrix} = i\frac{\partial}{\partial t} \begin{pmatrix} \psi_1 \\ \psi_2 \end{pmatrix} \tag{1.41}$$

The interaction with a strong laser pulse transfers considerable amounts of population from the ground state to higher states and often strong oscillations in the populations are seen during the interaction time. They are known as *Rabi oscillations* [46, 49]. The solution of equation (1.41) can be found in terms of *diabatic states* or by solving the full, coupled problem of electronic and nuclear motion.

1.6 Electron localization function

According to Thomas A. McCormick the *electron localization function* (*ELF*) is:

> “Qualitatively ELF assigns high values to a point in space where there is significant electron density, but few or no nodes pass through the point. It assigns lower values to points that either have little electron density or through which enough nodes from one or more occupied orbitals pass that these nodes can overcome the contribution of the density to ELF at that point.” [50]

In the following we provide the basic definition as developed by Becke and Edgecombe [51]. However, their definition is not applicable straighforward to an exact wave function and we have to re-define the ELF later on (chapter 6.2).

The basic definition of ELF starts from the Hartree-Fock probability of finding two particles of the same spin σ at positions r_1 and r_2 in a multielectron system:

$$P_2^{\sigma\sigma}(r_1, r_2) = \rho_\sigma(r_1)\rho_\sigma(r_2) - \left|\rho_1^\sigma(r_1, r_2)\right|^2, \tag{1.42}$$

where $P_2^{\sigma\sigma}(r_1, r_2)$ is the same-spin *pair probability* and $\rho_1^\sigma(r_1, r_2)$ is the σ-spin *one-body density matrix* of the Hartree-Fock determinant:

$$\rho_1^\sigma(r_1, r_2) = \sum_i^\sigma \psi_i^*(r_1)\psi_i(r_2) \tag{1.43}$$

Summation is restricted to orbitals of σ spin only. If an electron of spin σ is located at r_1 *with certainty* (r_1 is called the *reference point*), then we can define a *conditional probability* of finding a second σ-spin electron at position r_2 by dividing equation (1.42) by the total σ-spin density at r_1:

$$\begin{aligned} P_{\text{cond}}^{\sigma\sigma}(r_1, r_2) &= \frac{P_2^{\sigma\sigma}(r_1, r_2)}{\rho_\sigma(r_1)} \\ &= \rho_\sigma(r_2) - \frac{\left|\rho_1^\sigma(r_1, r_2)\right|^2}{\rho_\sigma(r_1)} \end{aligned} \tag{1.44}$$

It is necessary to mention here, that the HF density and density matrix are invariant with respect to unitary transformations and thus the pair probabilities are as well. If $r_1 = r_2$ the density matrix shows the following features:

$$\rho_1^\sigma(r_1, r_1) = \rho_\sigma(r_1) \tag{1.45}$$

and

$$\int \left|\rho_1^\sigma(r_1, r_2)\right|^2 dr_2 = \rho_\sigma(r_1) \tag{1.46}$$

From that, it is easy to verify that the conditional probability of finding a second electron at the reference point vanishes:

$$P^{\sigma\sigma}_{\text{cond}}(r_1, r_1) = 0 \tag{1.47}$$

The total conditional probability is then given by:

$$\int P^{\sigma\sigma}_{\text{cond}}(r_1, r_2)\, dr_2 = N_\sigma - 1, \tag{1.48}$$

where N_σ is the total number of electrons with σ-spin in the given system. Equation (1.47) is of course a consequence of the *Pauli principle*.

Becke and co-workers emphasized that very useful information is contained in the *short-range* behaviour of the HF exchange correlation when r_2 approaches the reference point r_1 [52,53]. Because of the Pauli principle one cannot examine $P^{\sigma\sigma}_{\text{cond}}$ directly, but Becke showed that the leading term of the Taylor expansion of the *spherically averaged* conditional pair probability is given by [54]

$$P^{\sigma\sigma}_{\text{cond}}(r, s) = \frac{1}{3}\left[\tau_\sigma - \frac{1}{4}\frac{(\nabla\rho_\sigma)^2}{\rho_\sigma}\right] s^2 + \ldots \tag{1.49}$$

Here, the arguments (r, s) denote the spherical average on a shell of radius s about the reference point r. τ_σ is the positive-definite *kinetic energy density* which is defined by (further details are found in [55])

$$\tau_\sigma = \sum_i^\sigma |\nabla\psi_i|^2 . \tag{1.50}$$

Here again the sum runs over all electrons with the same spin. The smaller the probability of finding a second electron of the same spin near the reference point gets, the more localized is the reference electron. That means, electron localization is measured by the following expression:

$$D_\sigma = \tau_\sigma - \frac{1}{4}\frac{\left(\nabla\rho_\sigma\right)^2}{\rho_\sigma} \tag{1.51}$$

It can be shown that D_σ is nonnegative [56]. D_σ vanishes in the special case of one-electron systems and therefore also vanishes in multi-electron systems where regions are dominated by a single, localized σ-spin orbital. Equation (1.51) takes *small* values when the reference electron is highly localized. Thus Becke and Edgecombe defined the *electron localization function* (ELF) as:

$$\mathrm{ELF} = \left(1 + \chi_\sigma^2\right)^{-1} \tag{1.52}$$

In above equation $\chi_\sigma = D_\sigma / D_\sigma^0$ and is normalized to the *uniform electron gas* with a spin density equal to the local value of $\rho_\sigma(r)$. Thus D_σ^0 takes the form:

$$D_\sigma^0 = \frac{3}{5}\left(6\pi^2\right)^{\frac{2}{3}} \rho_\sigma^{\frac{5}{3}} \tag{1.53}$$

By its definition the ELF can only take values of $0 \leq \mathrm{ELF} \leq 1$. In chapter 6.2 we will redefine the ELF for exact wave functions and also introduce a similar quantity for electrons with differents spins.

Chapter 2

Numerical methods

2.1 Solving the time-dependent Schrödinger equation

In order to describe the dynamical changes in the probability density of a quantum system, one has to find solutions to the *time-dependent Schrödinger equation* (in atomic units):

$$i\frac{\partial}{\partial t}\Psi(t) = H\,\Psi(t) = (V + T)\,\Psi(t) \tag{2.1}$$

Here, H denotes the Hamiltonian which — if we neglect spin-orbit interactions — has only contributions by the kinetic (T) and potential energy (V). $\Psi(t)$ is the time-dependent wave function. If we choose an infinitesimal time step dt, a formal solution to above equation is [57]:

$$\Psi(t + dt) = e^{-i(V+T)dt}\,\Psi(t) \tag{2.2}$$

The exponential is called the propagator of the system. As the kinetic energy operator contains derivatives with respect to the particle coordinates, one cannot apply the propagator directly to the wave function. Usually one chooses a symmetric splitting of the evolution operator $exp(-iHdt)$ that gives rise to a third-order error in dt because of the non-zero commutator between T and V [58]:

$$e^{-iHdt} = e^{-i\frac{V}{2}dt}\, e^{-iTdt}\, e^{-i\frac{V}{2}dt} + \mathcal{O}(dt^3) \tag{2.3}$$

In configuration space the wave function can be multiplied directly with the terms only containing the potential energy, while the same holds true for the kinetic energy term in momentum space. The two respresentations are connected by a Fourier transformation:

$$\tilde{\Psi}(p) = \frac{1}{\sqrt{2\pi}} \int e^{-ipx}\Psi(x)\, dx \tag{2.4}$$

The *split-operator method* can easily be implemented if the wave function is represented on a spatial grid of a finite number of points. In that case very efficient Fast Fourier Transform (FFT) algorithms can be applied that scale with $N \log N$, where N is the number of grid points.

Throughout this work we employed the FFTW package by Matteo Frigo and Steven G. Johnson [59], which adopts itself to the underlying hardware and is one of the fastest FFT routines available nowadays.

2.1.1 Improving accuracy

Under certain conditions the second order accuracy of the split-operator (SPO) algorithm is not sufficient anymore. Several attempts have been made to improve its accuracy and we present two of them here. The advantage of a higher order SPO scheme is the possibility to increase the time step without losing accuracy in the propagation.

Bandrauk and Shen proposed a splitting of the time evolution operator $exp(-iHdt)$ into seven exponentials to achieve an *SPO* scheme that is accurate to third order [60] . The propagator takes the form:

$$\begin{aligned} e^{-iHdt} &= e^{-i\gamma\frac{T}{2}dt}\, e^{-i\gamma V dt} \\ &\cdot e^{-i(1-\gamma)\frac{T}{2}dt}\, e^{-i(1-2\gamma)V dt} \\ &\cdot e^{-i(1-\gamma)\frac{T}{2}dt}\, e^{-i\gamma V dt}\, e^{-i\gamma\frac{T}{2}dt}, \\ &\text{with } \; \gamma = 1/\left(2-2^{1/3}\right) \end{aligned} \tag{2.5}$$

Bandrauk and Shen were able to show that this propagator yields better accuracy for time-dependent problems than the standard split-operator (equation (2.3)) and produces better phases for time-independent problems.

A year earlier already Yoshida proposed a general scheme to construct higher order propagators [61]. While one cannot find a closed, analytical form for the higher order propagators, Yoshida found a fourth-order accurate splitting that also contains seven exponentials:

$$\begin{aligned} e^{-iHdt} &= e^{-ix_1\frac{V}{2}dt}\, e^{-ix_1 T dt} \\ &\cdot e^{-i(x_1+x_0)\frac{V}{2}dt}\, e^{-ix_0 T dt} \\ &\cdot e^{-i(x_1+x_0)\frac{V}{2}dt}\, e^{-ix_1 T dt}\, e^{-ix_1\frac{V}{2}dt} \end{aligned} \tag{2.6}$$

Here, $x_0 = 2^{\frac{1}{3}}/(2-2^{\frac{1}{3}})$ and $x_1 = 1/(2-2^{\frac{1}{3}})$.

2.1.2 Obtaining eigenstates

One of the most useful features of the *SPO* algorithm is the possibility to calculate highly precise eigenstates of a given potential. As we will see later on, it is inevitable for our discussion to know the electronic eigenstates of our system. Kosloff introduced the so-called *relaxation method* [62] for that, which is based on the split-operator algorithm. One starts from an nearly arbitrary[1] function $\Psi(t = 0)$ and replaces the time in the propagator by $t = -i\tau$ (*imaginary time propagation*). The time evolution over an infinitesimal time step $d\tau$ can be written in terms of the eigenstates φ_n with eigenenergies E_n:

$$\Psi(\tau + d\tau) = \sum_n \langle \varphi_n | \Psi(\tau) \rangle e^{-E_n d\tau} \varphi_n \tag{2.7}$$

Applying the split-operator algorithm, as described in section 2.1, it follows immediately from equation (2.7), that the state with the lowest eigenenergy suffers least damping. This, of course, works only for a completely positive spectrum. In order to converge the propagation, the wave function must be renormalized in each time step. Using a sensible convergence criterion one obtains the normalized ground state wave function. A "good" convergence criterion is the eigenenergy which can be calculated from the wave function and the wave function of a time step earlier:

$$E_0 = \lim_{\tau \to \infty} -\frac{1}{2d\tau} \ln \left\{ \frac{\langle \Psi(\tau + d\tau) | \Psi(\tau + d\tau) \rangle}{\langle \Psi(\tau) | \Psi(\tau) \rangle} \right\} \tag{2.8}$$

The relaxation method can be used to obtain higher states as well. However, due to small numerical instablilities, it is necessary to project out the already found lower states in each time step.

---

[1] The initial state must not be orthogonal to the ground state. Small numerical errors always yield *non*-orthogonal contributions, though.

2.2 Calculation of absorption spectra

By calculating the *absorption spectrum* of a molecule, we get information about its eigenstates that may be populated via a spectroscopic transition. Let us first regard a general wave packet $\Psi_f(q,t)$ in an excited electronic state. As a wave packet is a *coherent superposition of eigenstates* of the molecule, it may be written in terms of eigenfunctions of the molecular Hamiltonian (in atomic units):

$$\Psi_f(q,t) = \sum_{v=0}^{v_{\max}} c_v \, \varphi_v(q) \, e^{-iE_v t} \tag{2.9}$$

Here q are the molecular degrees of freedom, v counts the eigenstates $\varphi_v(q)$ with energy E_v, and c_v are the expansion coefficients. Now we fix the coefficients c_v by imposing as initial condition:

$$\Psi_f(q,t=0) = \Psi_f(0) = \mu_{fi}\Psi_i(q) \tag{2.10}$$

Thus the excited state wave packet resembles the initial state wave function multiplied by the *transition dipole function* μ_{fi}. Using the orthonormality of the basis set and the initial condition, the expansion coefficients can be expressed in terms of the basis set functions:

$$c_v = \langle \varphi_v(q) | \mu_{vi} | \Psi_i(q) \rangle \tag{2.11}$$

Multiplying equation (2.9) with $\Psi_f(0)$ from the left and integrating over all coordinates, yields:

$$\begin{aligned} S(t) &= \langle \Psi_f(0) | \Psi_f(t) \rangle \\ &= \sum_{v=0}^{v_{\max}} c_v \langle \Psi_f(0) | \varphi_v(q) \rangle \, e^{-iE_v t} \\ &= \sum_{v=0}^{v_{\max}} |c_v|^2 \, e^{-iE_v t} \end{aligned} \tag{2.12}$$

Here we used $\langle \Psi_f(0) | \varphi_v(q) \rangle = c_v^*$. $S(t)$ is called *autocorrelation function.*

According to *Fermi's golden rule* the *absorption spectrum* may be written as [45]:

$$\sigma(\omega) \propto \sum_f |\langle \Psi_i | \mu_{fi} | \Psi_f \rangle|^2 \, \delta(E_i + \omega - E_f) \tag{2.13}$$

The sum runs over all final states Ψ_f that are selected by the argument of the delta function which ensures that only resonant transitions can occur. Replacing the Dirac delta function by [63]

$$\delta(E_i + \omega - E_f) = \frac{1}{2\pi} \int e^{i(E_i + \omega - E_f)t} \, dt, \tag{2.14}$$

we can rewrite $\sigma(\omega)$ as:

$$\begin{aligned} \sigma(\omega) &\propto \frac{1}{2\pi} \sum_f \langle \Psi_i | \mu_{fi} | \Psi_f \rangle \langle \Psi_f | \mu_{fi} | \Psi_i \rangle \int e^{i(E_i+\omega)t} \, dt \\ &= \frac{1}{2\pi} \int e^{i(E_i+\omega)t} \sum_f \langle \Psi_i | \mu_{fi} | \underbrace{e^{-iE_f t} \Psi_f}_{= e^{-iHt} \Psi_f} \rangle \langle \Psi_f | \mu_{fi} | \Psi_i \rangle \, dt \\ &= \frac{1}{2\pi} \int e^{i(E_i+\omega)t} \langle \Psi_i | \mu_{fi} e^{-iHt} \underbrace{\sum_f |\Psi_f\rangle \langle \Psi_f|}_{= \mathbb{1}} \mu_{fi} | \Psi_i \rangle \, dt \\ &= \frac{1}{2\pi} \int e^{i(E_i+\omega)t} \langle \Psi_i | \mu_{fi} e^{-iHt} | \mu_{fi} \Psi_i \rangle \, dt \\ &= \frac{1}{2\pi} \int e^{i(E_i+\omega)t} \langle \mu_{fi} \Psi_i | e^{-iHt} | \mu_{fi} \Psi_i \rangle \, dt \end{aligned} \tag{2.15}$$

In the last step of above derivation we replaced μ_{fi} by its complex conjugate, which is possible because the dipole operator is *self-adjoint*. Taking a closer look, one finds that the term in the bracket is nothing else than the above defined autocorrelation function $S(t)$. Thus, the absorption spectrum is directly proportional to the Fourier transform of $S(t)$:

$$\sigma(\omega) \propto \frac{1}{2\pi} \int S(t)\, e^{i(E_i+\omega)t}\, dt \tag{2.16}$$

We have found now a unique relation between the time-resolved molecular motion in an excited state and the frequency-resolved absorption spectrum. $S(t)$ can easily be calculated in terms of the split-operator algorithm (see section 2.1) by solving the time-dependent Schrödinger equation with $\mu_{fi}\Psi_i(q)$ as initial function and propagating in the excited state potential. As $\Psi_f(0) = \mu_{fi}\Psi_i(q)$ is a real function, $S(t)$ fulfills the symmetry relation:

$$S(-t) = S^*(t) \tag{2.17}$$

This guarantees that $\sigma(\omega)$ is real as well. In practice one propagates the wave packet starting from $t = 0$ up to a given time and then adds the negative branch by copying the complex conjugate of the positive branch of the function.

Chapter 3

Combined electron and nuclear dynamics: A simple model system

3.1 Introduction

In this chapter we introduce the simple model system that was developed by Metiu and co-workers to describe charge-transfer processes [37, 38]. Within this model system it is possible to characterize the coupled motion of a nucleus and an electron simultaneously. The electron-nucleus interaction is parameterized in such a way as to allow for an easy transition from an adiabatic (Born-Oppenheimer type) behaviour to a situation where the motion of the particles is strongly coupled. In this chapter our main interest focusses on the dynamical changes of electron and nuclear probability densities that are introduced by a nonadiabatic coupling.

As a first step we apply the Born-Oppenheimer approximation to our model and solve the electronic Schrödinger equation for fixed nuclear geometry (chapter

3.3). The resulting adiabatic potential curves and electronic eigenfunctions are then used to calculate other quantities that are usually not easily available, e.g. the diagonal and off-diagonal kinetic coupling elements and the transition dipole moments. From the gathered data a prediction is made of what is to be expected for the nuclear dynamics.

After that we illustrate by means of wave packet calculations the dynamical changes of nuclear and electron density for the case of an adiabatic motion and during a nonadiabatic transition (chapter 3.4). Furthermore, the influence of coupling on the transport of electron density between different nuclei is characterized with the help of time-dependent Laplacians.

The chapter closes with a short passage about reversing the Born-Oppenheimer approximation and the resulting picture of electrons moving on potential energy surfaces that are obtained from solving the Schrödinger equation for fixed electron geometry (chapter 3.5). We close this chapter with a short summary.

3.2 The model Hamiltonian

We describe the coupled electronic-nuclear motion in a simple model system that consists of three ions and one electron arranged in a line. Figure 3.1 illustrates the situation: two ions are fixed at a distance of 10 Å, the third ion and the electron are allowed to move on the internuclear axis. The masses of the ions are chosen to be that of a proton, while all charges are $Z = +1$, respectively. The system has two degrees of freedom: the position of the nucleus R and the position of the electron x. The interaction of the electron with the nuclei is parameterized in the form of screened Coulomb interactions. The Hamiltonian of the full system then takes the form (in a.u.):

$$H = -\frac{1}{2}\frac{\partial^2}{\partial x^2} - \frac{1}{2M}\frac{\partial^2}{\partial R^2} + V(x,R) \tag{3.1}$$

Here M denotes the ion mass and $V(x,R)$ are the particle interactions which are of the form:

$$\begin{aligned} V(x,R) = {} & \frac{1}{|R_L - R|} + \frac{1}{|R_R - R|} - \frac{\operatorname{erf}(|R_L - x|/R_f)}{|R_L - x|} \\ & - \frac{\operatorname{erf}(|R_R - x|/R_f)}{|R_R - x|} - \frac{\operatorname{erf}(|R - x|/R_c)}{|R - x|} + E_0 \end{aligned} \tag{3.2}$$

In the expression for the potential energy all electron-nuclei interactions are cut off with *error functions* (erf). The value of E_0 was chosen such that the global minimum of the full potential was zero in all regarded cases. R_L and R_R denote the positions of the fixed ions and were chosen to be -5 Å and +5

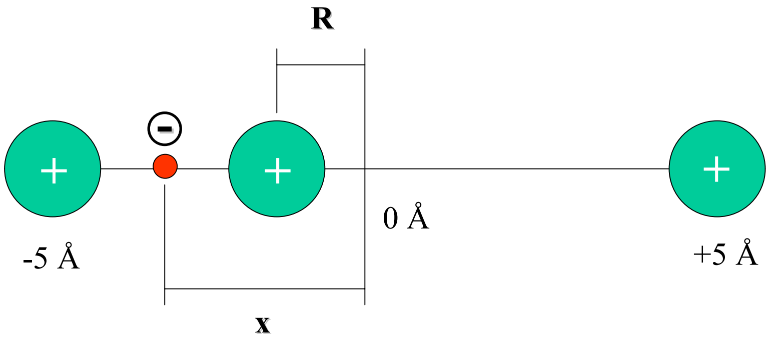

Figure 3.1: Illustration of the geometry of the model system consisting of a central ion and an electron which move between two fixed ions.

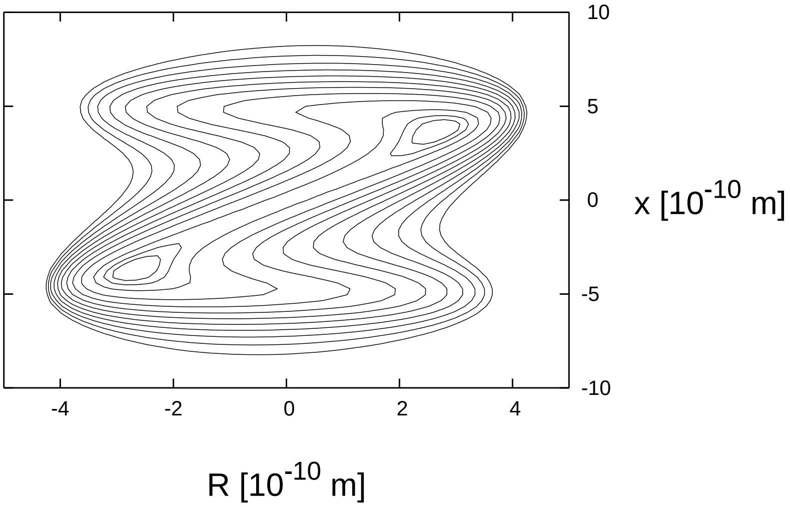

Figure 3.2: Contour plot of the potential energy surface $V(x,R)$ *(*$R_c = 1.5$ *Å). The contour lines have values of 0.25 eV, 0.5 eV and then rise between 1 to 10 eV in increments of 0.1 eV.*

Å, respectively. The parameter R_f which appears in the interaction between electron and stationary ions was taken to be 1.5 Å. The interaction with the mobile ion was determined by different values of the parameter R_c. Its influence on the system will be discussed in detail in the next section.

A contour plot of the full potential is shown in figure 3.2. The symmetry of the system allows for two stable ground state configurations: either the electron is located between the left fixed and the moving ion with the moving ion shifted closer to the left or the electron is right of the central nucleus which then is shifted more to the right hand side. The first situation is illustrated in figure 3.1.

3.3 Adiabatic approximation

In order to gain insight into the electronic structure of the model system, we apply the Born-Oppenheimer approximation to the full Hamiltonian (eqn. (3.1)). Within this approach one first solves the electronic Schrödinger equation (1.5) for a fixed nuclear coordinate R. This leads to the following equation:

$$\left\{-\frac{1}{2}\frac{\partial^2}{\partial x^2} + V(x,R)\right\}\varphi_n(x,R) = V_n(R)\varphi_n(x,R) \tag{3.3}$$

Here $V_n(R)$ are the adiabatic potential curves corresponding to electronic state n and the electronic eigenfunctions $\{\varphi_n(x,R)\}$ define a complete orthonormal basis set for all values of R. This basis set may be used to expand the total wave function $\Psi(x,R)$ as:

$$\Psi(x,R) = \sum_n \psi_n(R)\varphi_n(x,R) \tag{3.4}$$

As mentioned earlier, projection onto one electronic function $\varphi_m(x,R)$ transforms the Schrödinger equation into a set of coupled differential equations:

$$\begin{aligned}\left\{-\frac{1}{2M}\frac{\partial^2}{\partial R^2} + V_m(R) - E\right\}\psi_m(R)& \\ = \sum_n \left\{T^{(1)}_{mn}(R)\frac{\partial}{\partial R} + T^{(2)}_{mn}(R)\right\}\psi_n(R)&\end{aligned} \tag{3.5}$$

Applying the Born-Oppenheimer equation means that the right hand side of equation (3.5) becomes zero, as the nuclear motion solely takes place in a fixed electronic state (m). $V_m(R)$ then acts as the potential energy operator for the nuclear motion. Within this approximation diagonal correction terms $T^{(j)}_{mm}(R)$ as well as couplings to other electronic states $T^{(j)}_{mn}(R)$ are neglected. These kinetic coupling elements are usually quite small, but play an important role when the adiabatic curves get close to each other, as will be discussed in the next sections. The explicit mathematical form of the coupling elements is

$$T_{mn}^{(j)}(R) = \frac{1}{2M} \int \varphi_m(x,R) \frac{\partial^{(j)}}{\partial R^{(j)}} \varphi_n(x,R)\, dx \tag{3.6}$$

with $j = 1, 2$.

3.3.1 Adiabatic potential curves

Figures 3.3 and 3.4 contain the adiabatic potential curves, calculated for two different values of R_c. The values of R_c were chosen in accordance to references [37, 38]. In the first case [$R_c = 1.5$ Å, in the following referred to as Born-Oppenheimer case] ground and first excited electronic state are clearly separated by a large energy gap of $\Delta = 1.28$ eV. Intuitively, it is expected that the Born-Oppenheimer approximation is valid in that case. However, taking a closer look at figure 3.3 also shows that the $n = 2$ and $n = 3$ electronic states approach each other closely at $R = 0$. This already questions the validity of the BO approximation for higher electronic states. In the case of $R_c = 2.5$ Å ground and first excited state are only separated by a gap of $\Delta = 0.05$ eV at the nuclear position $R = 0$. The energy spacing corresponds to a period of magnitude $\tau_{\mathrm{el}} = 2\pi/\Delta = 82$ fs for the electronic motion which is of the same order as a typical vibrational motion. This situation should lead to a strong coupling between electronic and nuclear motion (see section 1.2).

It should be noted here, that the model Hamiltonian allows for a facile transition between the two regarded cases by varying the parameter R_c. Mathematically, the parameter changes the electron-moving ion attraction from strong ($R_c = 1.5$ Å) to weak ($R_c = 2.5$ Å).

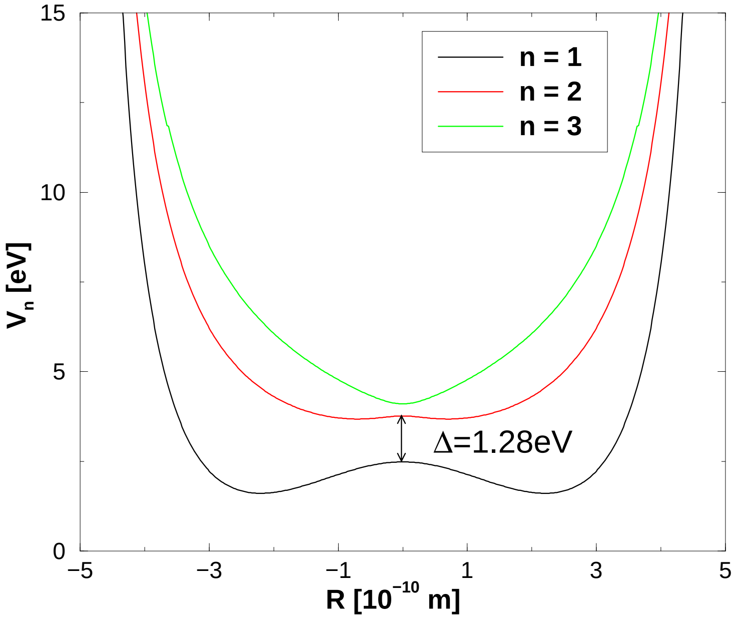

Figure 3.3: Adiabatic potentials for the electronic quantum numbers $n = 1 - 3$ *for* $R_c = 1.5$ Å.

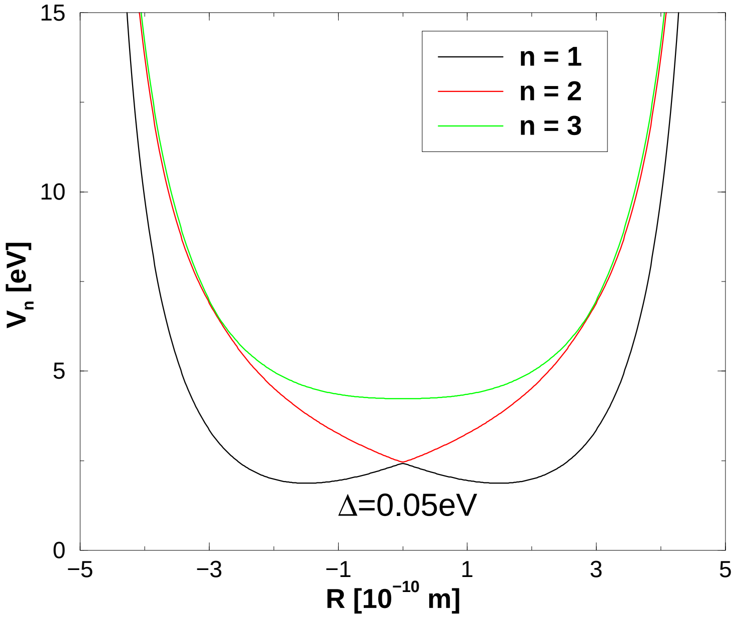

Figure 3.4: The same adiabatic potentials as above, but for $R_c = 2.5$ Å.

3.3.2 Electronic eigenfunctions

In the last section we presented the adiabatic potential curves generated from the model Hamiltonian. These eigenvalues and the corresponding eigenfunctions were obtained by solving the electronic Schrödinger equation with the method described in chapter 2.1.2. For a visualization it is easiest to consider the electronic basis functions $\varphi_n(x,R)$ as functions of both, the electronic coordinate x and the nuclear position R which serves as a parameter. The modulus squared of the electronic ground state functions in the weak and strong coupling case are displayed in figure 3.5. In the Born-Oppenheimer (BO) case (left part) the shape of the wave function does not change much with varying nuclear position R, while the center of the distribution shifts smoothly on the x-axis.

For $R_c = 2.5$ Å the strong nonadiabatic coupling between the ground and first excited state leads to a rapid change of the electronic wave function in the coupling region around $R = 0$ (figure 3.5, right part). This is the expected behaviour: the electronic function changes considerably as a function of the nuclear coordinate in a region where the coupling cannot be neglected. Figure 3.6 shows

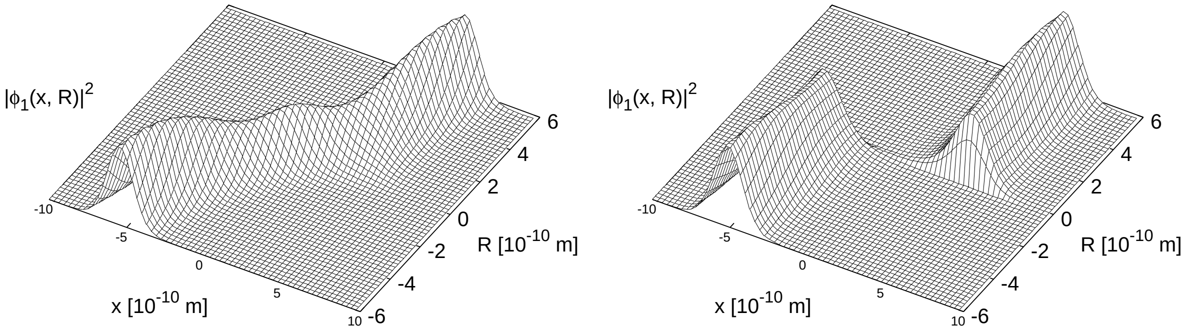

Figure 3.5: Variation of the modulus squared of the electronic ground state eigenfunctions $|\varphi_1(x,R)|^2$ with the nuclear coordinate R. The weak (left part) and the strong (right part) coupling case are displayed.

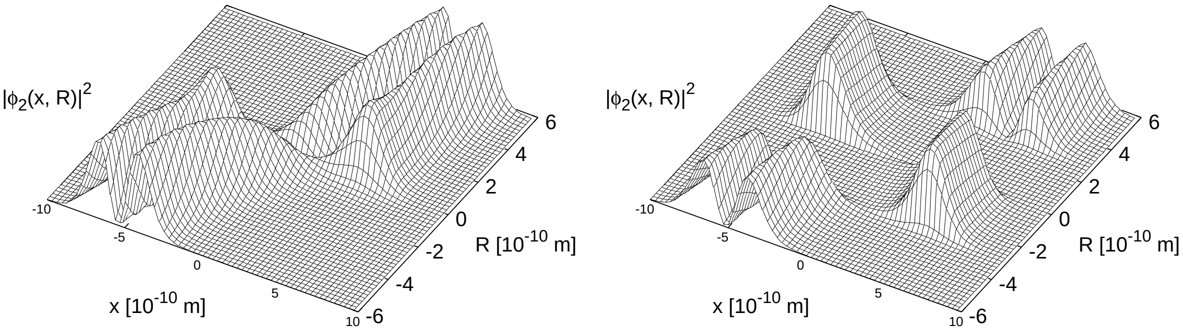

Figure 3.6: First ($n = 2$) excited state electronic wavefunctions for $R_c = 1.5$ Å (left part) and $R_c = 2.5$ Å (right part).

the eigenfunctions for the first electronically excited state. Even for the BO case (left part) the coupling to the $n = 2$ state leads to tremendous changes of the electronic wave function around $R = 0$. The strong coupling case (figure 3.6) exhibits a very complex coupling pattern.

In order to illustrate this situation even better, figure 3.7 shows cuts through the ground and first excited state wave functions for several values of R in the vicinity of $R = 0$. Panels (a) – (c) correspond to values of $R = 0.05$ Å, $R = 0$ Å and $R = -0.05$ Å. In passing the barrier, the main maximum of $\varphi_1(x, R)$ shifts from positive to negative x values. Simultaneously the minimum of $\varphi_2(x, R)$ shifts from a negative to positive x coordinate. At the barrier $R = 0$, where the adiabatic curves $V_1(R)$ and $V_2(R)$ are almost degenerate, the two wave functions are symmetric and antisymmetric with respect to $x = 0$.

In conclusion, we have seen that the electronic eigenfunctions exhibit considerable changes as a function of the nuclear coordinate in the presence of nonadiabatic coupling. It is to be exptected that this behaviour is also reflected in the time-dependent changes of the electron density if the system gets perturbed by the motion of the nucleus or by an external electric field.

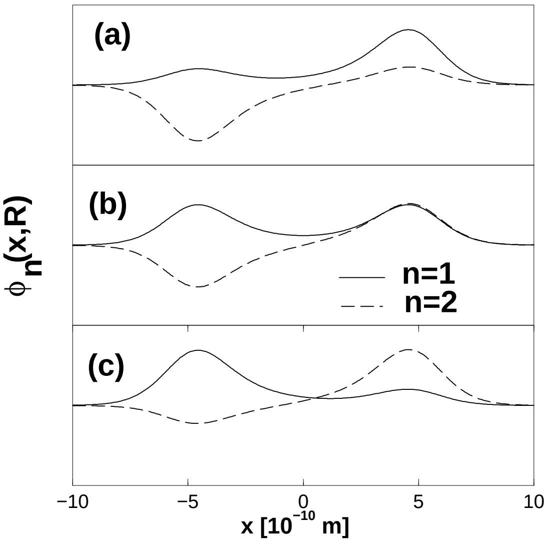

Figure 3.7: Variation of the electronic eigenfunctions $\varphi_n(x,R)$ in the vicinity of the symmetric ion configuration $R=0$. The ground and excited state wave functions are shown for values of (a) $R=0.05$ Å, (b) $R=0$ Å and (c) $R=-0.05$ Å.

3.3.3 Kinetic coupling elements

As mentioned before, the kinetic coupling elements $T_{nm}^{(j)}$ play a crucial role when the BO approximation breaks down, as they couple nuclear and electronic motion. They are usually difficult to obtain, but can be calculated exactly for our model system. First, the diagonal elements $T_{nn}^{(1)}$ are zero due to the normalization of the adiabatic electronic basis functions. The other elements of first and second order are displayed in figure 3.8 for the strong coupling case ($R_c = 2.5$ Å). Regarding the off-diagonal couplings one finds that the first-order function ($j=1$) is symmetric, whereas for $j=2$ it is antisymmetric with respect to $R=0$. The symmetry of the coupling elements stems from the inversion symmetry of the Hamiltonian itself which is transferred to the electronic basis functions, i.e.:

$$\varphi_n(x,R) = (-1)^{(n+1)}\varphi_n(-x,-R) \tag{3.7}$$

This is illustrated in figures 3.5 and 3.6. One finds the following relations:

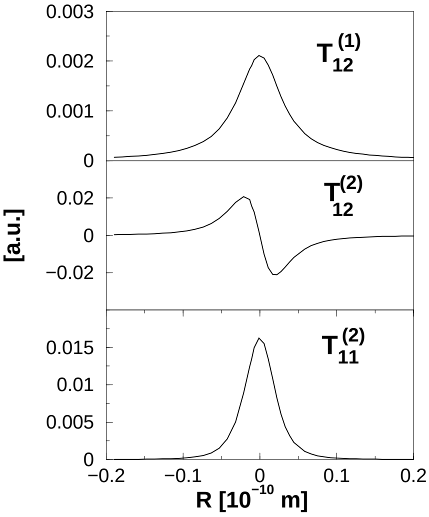

Figure 3.8: Kinetic coupling elements obtained in the strong coupling case $R_c = 2.5$ Å.

$$\begin{aligned} T_{nm}^{(j)}(-R) &\sim (-1)^j \, \langle \varphi_n(x,-R)| \frac{\partial^j}{\partial R^j} |\varphi_m(x,-R)\rangle_x \\ &= (-1)^j \, \langle \varphi_n(-x,-R)| \frac{\partial^j}{\partial R^j} |\varphi_m(-x,-R)\rangle_x \\ &= (-1)^{n+m+j} \, T_{nm}^{(j)}(R) \end{aligned} \tag{3.8}$$

The off-diagonal kinetic coupling elements show a strong variation as a function of the nuclear distance. We find that the function containing the second derivative is of an overall much larger magnitude than the element $T_{12}^{(1)}$. This is — however — not true at the symmetric configuration $R = 0$, where $T_{12}^{(2)}$ vanishes identically, see equation (3.8). The diagonal element $T_{11}^{(2)}$ is contained in the lower panel of figure 3.8. We note, that the element $T_{22}^{(2)}$ in the region, as shown in the figure, is equal to $T_{11}^{(2)}$. This is due to the high barrier between the two wells of the potential $V(x,R)$ which are obtained for fixed R in the vicinity of $R = 0$. As a consequence one finds approximately (see figure 3.7) $\varphi_2(x,R) = -\varphi_1(-x,R)$ which, in turn, produces equal matrix elements.

3.3.4 Transition dipole moments

Figure 3.9 shows the transition dipole moments for a transition from the electronic ground state to the first excited state for the $R_c = 1.5$ Å and $R_c = 2.5$ Å case. They can be calculated from the electronic basis functions and are defined as follows:

$$\mu_{2\leftarrow 1}(R) = \langle \varphi_1(x,R)|\mu|\varphi_2(x,R)\rangle_x \tag{3.9}$$

Here, μ is the dipole moment operator and corresponds to $\mu = R - x$ (in a.u.) within our model system. In this context, it is noteworthy that these quantities are usually not easily accessible and are set constant in most numerical applications (*Condon approximation*). For the weak coupling case (figure 3.9, left panel) the transition dipole moment shows a modest variation with respect to the nuclear position R. Remarkably is the rapid change in curvature around $R = \pm 1.25$ Å. This can be understood from the fact that the electronic functions $\varphi_2(x,R)$ change muchfaster as a function of R than the functions of the electronic ground state (see figures 3.5, left panel and 3.6, left panel). This is a consequence

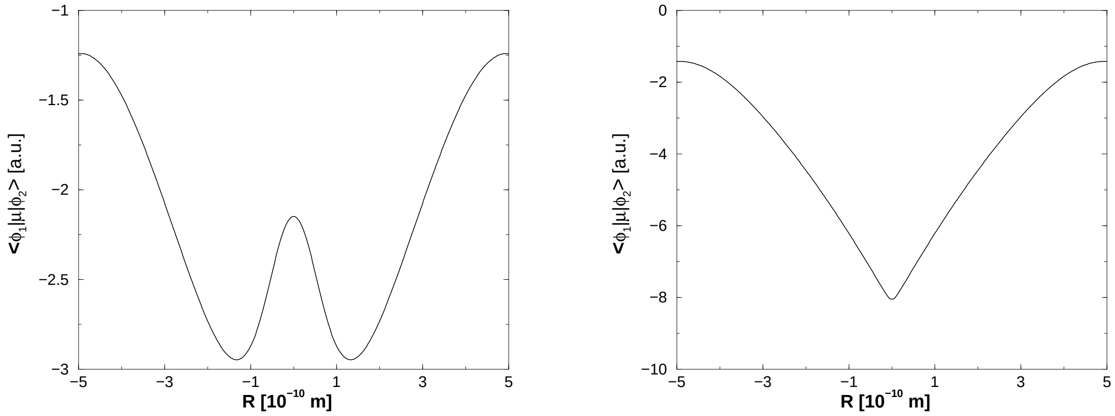

Figure 3.9: The transition dipole moments for a $2 \leftarrow 1$ transition $\mu_{2\leftarrow 1}(R) = \langle \varphi_1(x,R)|\mu|\varphi_2(x,R)\rangle$. The weak (left panel) and the strong coupling case (right panel) are displayed.

of a coupling between states $n = 2$ and $n = 3$. In the case of strong nonadiabatic coupling (figure 3.9, right panel) the variation with respect to R is nearly twice as large as in the latter case and the transition dipole moment exhibits a minimum at the coupling site around $R = 0$ Å.

Finally, we can conclude that the transition dipole moments reflect the behaviour of the corresponding electronic eigenfunctions: In presence of a strong nonadiabatic coupling the transition dipole moment exhibits large variations with respect to the nuclear coordinate (figure 3.9, right panel), whereas in the Born-Oppenheimer case the changes are less pronounced. Still, due to a coupling of states $n = 2, 3$ in that case, the transition dipole moment shows a double minimum structure. Furthermore, the often used *Condon approximation* which neglects the dependency of the transition dipole moments on the nuclear geometry does not apply in the presence of strong nonadiabatic coupling.

The data we have collected up to now allow us to predict some features of the nuclear dynamics in the model system. First, in the Born-Oppenheimer case the preparation of a localized wave packet in the electronic ground state will result in a nuclear dynamics taking place exclusively in that electronic state. On the other hand, if a strong coupling is present, the vibrational motion cannot be restricted to a single electronic state. This implies that the BO approximation is not a good description of the $R_c = 2.5$ Å case. In the following we will turn to the quantum dynamics in our system, where we have to prove above predictions.

3.4 Quantum dynamics

3.4.1 Time-dependent electron and nuclear densities

We now turn to the quantum dynamics in our model system. In order to get insight into the coupled electronic and nuclear dynamics, we solve the time-dependent Schrödinger equation using the Hamiltonian of equation 3.1 employing first a cut-off parameter of $R_c = 1.5$ Å. The initial wave packet was restricted to a certain electronic state and was of the form

$$\Psi(x, R, t = 0) \;=\; \varphi_1(x, R)e^{-\beta(R-R_0)^2}, \tag{3.10}$$

with the parameters $\beta = 7.14$ Å^{-2} and $R_0 = -0.9$ Å. Thus, we start in the electronic ground state ($n = 1$) with a Gaussian wave packet for the nuclear degree of freedom. In the general case there exists a multiple component wave function with the nuclear wave packet in state (n) as

$$\psi_n(R, t) = \langle\varphi_n(x, R)|\Psi(x, R, t)\rangle_x \tag{3.11}$$

These components can be used to calculate the populations in different states:

$$P_n(t) = \int |\psi_n(R, t)|^2 \, dR \tag{3.12}$$

In order to follow the motion of the nucleus and the electron we also calculate the time-dependent electron and nuclear densities. They are defined as follows:

$$\rho(R, t) = \int |\Psi(x, R, t)|^2 \, dx \tag{3.13}$$

$$\rho(x, t) = \int |\Psi(x, R, t)|^2 \, dR \tag{3.14}$$

Figure 3.10 displays the dynamics of the nuclear and electron density. Due to the special choice of the initial wave function the nuclear wave packet shows a vibrational motion which is restricted to positions of R smaller than zero, i.e., it moves in a single potential well and tunneling is negligible within the displayed

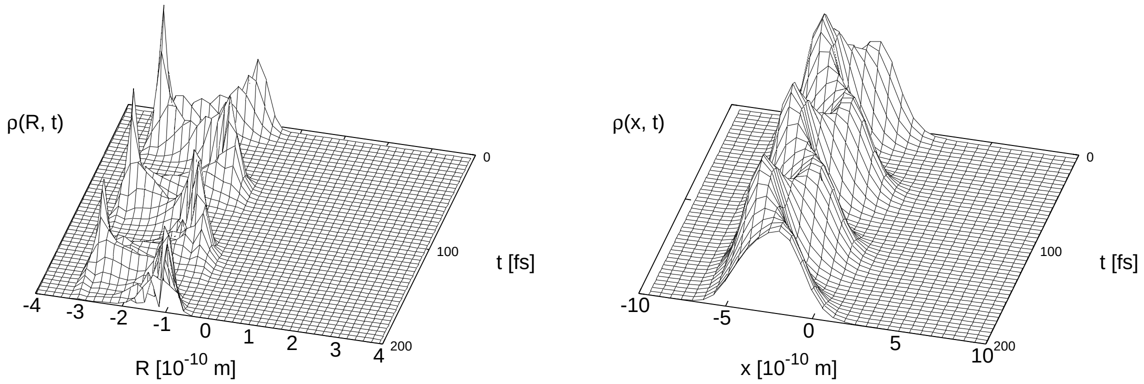

Figure 3.10: Time-dependence of the nuclear and electronic density in the Born-Oppenheimer case ($R_c = 1.5$ Å). The initial state is chosen such that the wave packet dynamics is restricted to a single potential well.

time interval. The periodic changes of the nuclear density induce a temporal variation of the electron density which takes place with the same period. In other words, the electron density follows the displacement of the moving ion. In the present case, the population $P_1(t)$ in the electronic ground state is equal to one, so that the component $|\psi_1(R,t)|^2$ equals the nuclear density $\rho(R,t)$. The same applies if the initial conditions are modified such that the wave packet has enough average energy to move over the symmetry point $R = 0$. This case, where we used $R_0 = -4$ Å as parameter in the representation of the initial wave packet, is illustrated in figure 3.11. Initially, the nuclear density splits into a smaller part which remains at negative values of R and a larger fraction moving over the barrier. Already after about 100 fs, the density is completely delocalized and no clear periodic motion can be distinguished at later times. On the other hand, the electron density shows much clearer features. It follows the motion of the nucleus changing its position from negative to positive x values. However, after some time the electron density shows a bimodal distribution with maxima around $x = \pm 5.0$ Å. Thus the nuclear motion induces an electron transfer between the two potential wells. It is noteworthy that in the cases as discussed until now, higher electronic states are not populated, i.e., we have a Born-Oppenheimer dynamics in the electronic ground state.

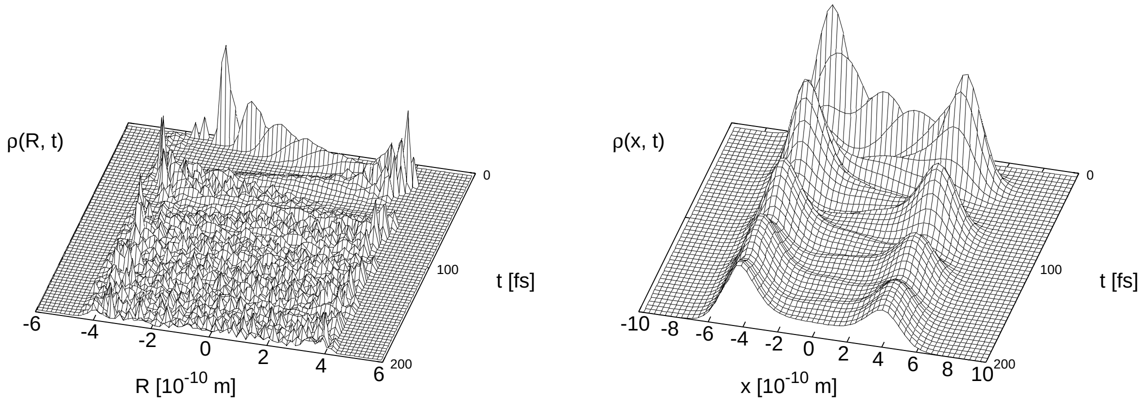

Figure 3.11: Time-dependence of the nuclear and electronic density in the Born-Oppenheimer case ($R_c = 1.5$ Å). The initial state is chosen such that the wave packet is able to move between the two potential wells.

Now, let us turn to the strong coupling case ($R_c = 2.5$ Å). Here, the initial state was again of the form given by equation (3.10) with the parameters $\beta = 7.14$ Å^{-2} and $R_0 = -3.0$ Å. The nuclear density dynamics is displayed in the left part of figure 3.12. A localized vibrational wave packet motion can be observed which extends over the central potential barrier at $R = 0$. In comparison to the Born-Oppenheimer dynamics shown in figure 3.11, the amplitude of the vibration is much smaller. Also, the accumulation of electron density at positive values of the coordinate x takes somewhat longer and no density is found around $x = 0$. This stems from the fact that both, the $n = 1$ and $n = 2$ electronic basis functions have a very small amplitude in this region (see figure 3.7).

The motion of the total nuclear density does not exhibit features of a nonadiabatic transition. Therefore, we calculate the projections $|\psi_n(R,t)|^2$, i.e., the components of the nuclear wave function in the ground ($n = 1$) and first excited ($n = 2$) electronic state. This is not necessary in the Born-Oppenheimer situa-

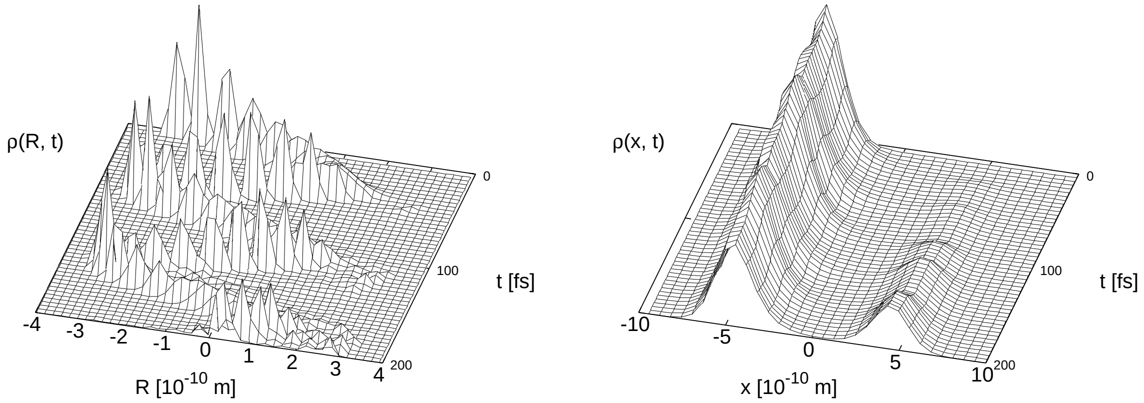

Figure 3.12: Time-dependence of the nuclear and electronic density in the strong coupling case ($R_c = 2.5$ Å).

tion since there, as was stated above, the nuclear component in the ground state is identical to the total nuclear density $\rho(R, t)$. The time-evolution of the two projections is displayed in figure 3.13. Starting in the electronic ground state (left panel), the nuclear wave packet moves towards positive R values. After about 25 fs, the probability density vanishes almost completely. Simultaneously, density appears in the excited electronic state. The latter wave packet moves outward reaching a turning point at $R = 2$ Å and returns until its magnitude decreases to zero. Naturally, due to norm conservation, the ground electronic state is populated again. This finding is consistent with an interpretation based on the adiabatic potential curves as displayed in figure 3.4: a wave packet, starting in the $n = 1$ state moves towards the coupling region and a change of the electronic state takes place. This process repeats itself as time goes on.

The obtained results can also be understood in terms of an electron transfer process. In the Born-Oppenheimer case (figure 3.11), the vibrational motion transfers electron density from negative to positive values of the electronic coordinate. This transfer proceeds stepwise and without involving a change of the electronic quantum number. At early times both, the nuclear and electron densi-

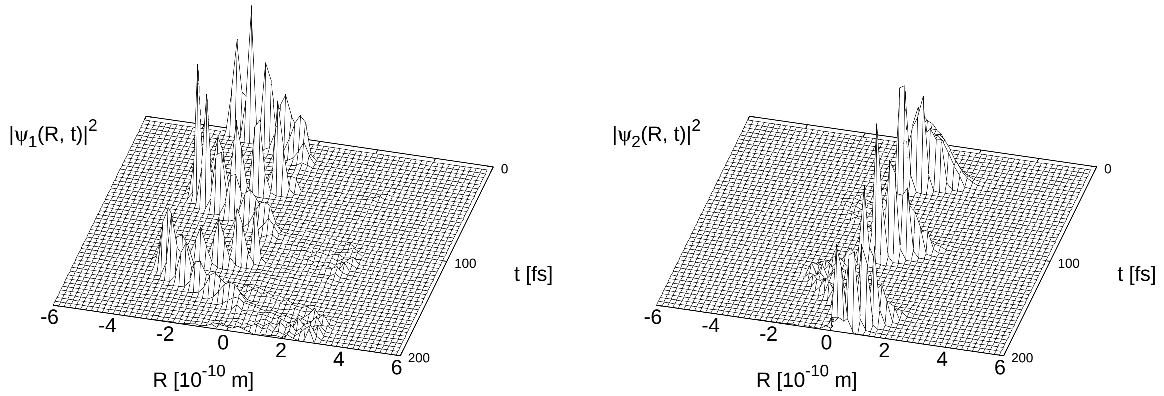

Figure 3.13: Nuclear components $|\psi_n(R,t)|^2$ *in the electronic states* $n = 1$ *and* $n = 2$*, as indicated (*$R_c = 2.5$ *Å).*

ties, i.e., the entire wave packet $\Psi(x, R, t)$, moves from one potential well to the other. An alternative interpretation is in terms of an isomerization process: the geometry of the ion chain changes since the middle ion oscillates between the two stable ground state configurations. This, of course, goes along with an alternating bonding situation: the electron density binds the movable ion temporarily to the left and then to the right ion which illustrates nicely that during an isomerization process electron density is transferred. At some point both stable configurations are assumed with equal probability. However, this configuration is not equilibrated; in contrary, as time proceeds, the initial wave packet is restored, a phenomenon known as wave packet revival [64–68].

The situation is different in the case of strong coupling. Here the transfer of density being located left of the middle ion to the region right of it goes in hand with a nonadiabatic transition. This is documented in figure 3.14 which shows various time-dependent functions. The upper panel contains the population $P_1(t)$ in the lowest electronic state whereas the expectation value of the nuclear coordinate is displayed in the lower panel of the figure. Additionally, the middle curve shows the population

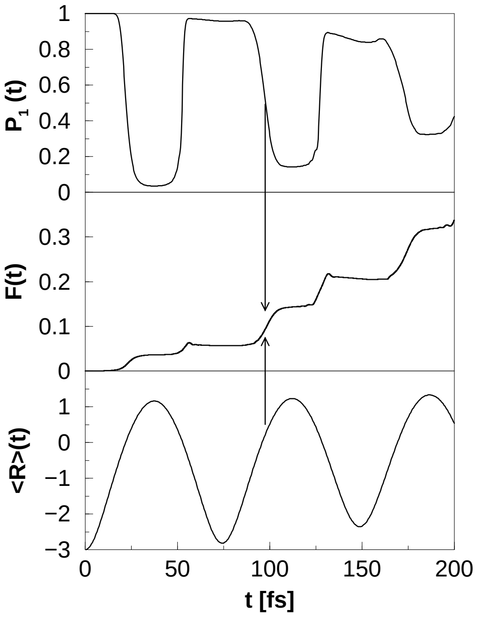

Figure 3.14: Electron transfer dynamics in the strong coupling case: the upper panel shows the population in the electronic ground state $P_1(t)$. In the middle panel the population corresponding to positive values of the electronic coordinate x is shown [see equation (3.15)]. The lower panel contains the expectation value of the nuclear coordinate.

$$F(t) = \int_0^{R_R} \rho(x,t)\, dx \tag{3.15}$$

which measures how much of the electron density is located at positive values of the electron coordinate, i.e, has been transferred into the region of the second potential minimum. As it is suggested by the arrows in figure 3.14, the population increases, when the lower electronic state is depopulated at the times the nonadiabatic transition takes place. Likewise, if the back transition occurs, another increase of $F(t)$ can be observed. This stepwise electron transfer process is efficient when the nuclear density is located in the vicinity of $R = 0$. As can be taken from the temporal variation of the R expectation value, the transfer occurs on the outward and inward motion of the nuclear density. Note that it takes several vibrational periods until a substantial amount of electron density is accumulated in the right potential well.

The interpretation of the nuclear dynamics as an isomerization also differs from what has been said above: for not too long time, the ion oscillates but the electron remains, with a high probability, between the left and center nucleus. This means that this, in fact, is not an isomerization process as might be inferred from the nuclear density dynamics (figure 3.12) but is a simple vibrational motion where the electron density does not follow the vibration and remains almost stationary. This is in contrast to the BO dynamics taking place in a single potential well (figure 3.10), where the density follows the vibrational motion.

3.4.2 Time-dependent Laplacians

Electron density is a rather insensitive quantity. Usually even low levels of theory produce the same density as higher levels. Therefore, chemical bonding has been investigated using various tools as applied to the electron density [51, 69]. One quantity, as is often discussed, is the Laplacian of the density, which in our case of a single electronic degree of freedom is

$$L(x,t) = \Delta\rho(x,t) = \frac{d^2}{dx^2}\rho(x,t). \tag{3.16}$$

Note that, whereas the conventional analysis does not include time, we here deal with a time-dependent electron density. The negative time-dependent Laplacian of the electron density is depicted in figure 3.15 for selected times during the first vibrational period of the ionic motion. The over-the-barrier Born-Oppenheimer casse [panels (a)] is compared to the strong coupling case [panels (b)]. The usual interpretation is that regions, where $-L(x)$ is positive, indicate a concentration of electron density, whereas regions with a negative $-L(x)$ characterize areas with a depletion of electron density [69]. In the BO situation, the

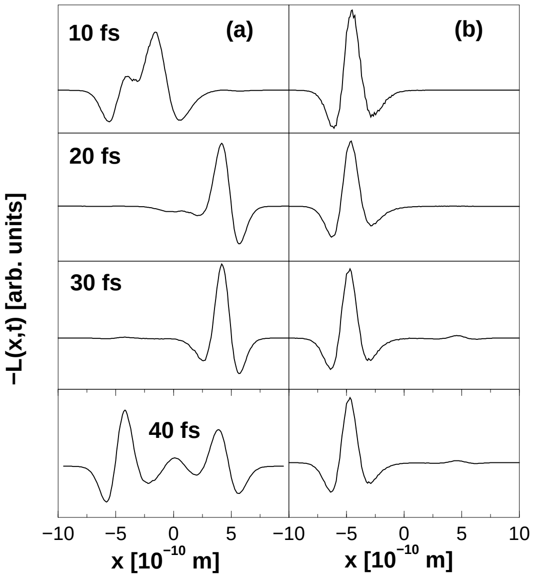

Figure 3.15: The time-dependent negative Laplacians of the electron density are displayed for selected times, as indicated. The Born-Oppenheimer case [panels (a)] is compared to the strong coupling case [panels (b)].

concentration of the electron density is first limited to a small region of space and exhibits a dynamics following the ionic motion (10, 20 and 30 fs). At a time of 40 fs, where the nuclear density is very delocalized, one observes three regions with enhanced electron concentration. These regions correspond to a sharing of the electron density between the three ions with a separation by areas with substantial depletion. The strong coupling case, as depicted in panels (b) of figure 3.15, is characterized by an almost time-independent electron concentration at negative values of the electron coordinate. The build-up of density at positive values for times of 30 fs and 40 fs can hardly be seen.

Altogether, the time-dependent Laplacians illustrate the density dynamics in a clearer way as the density itself, which is to be expected because of the sensitivity of higher order derivatives to functional changes.

3.5 Inverse Born-Oppenheimer approximation

When performing the Born-Oppenheimer approximation one usually takes it for granted that the electrons move much faster than the nuclei. This leads to the picture of nuclei moving on potential surfaces that are determined by the electronic structure of the molecule (see chapter 1.1). While this picture is reasonable and has proven to be useful over the years, nothing prevents one to reverse the procedure in a gedankenexperiment: Let us regard a total wavefunction $\Psi(x, R)$ that can be expanded into a basis of nuclear wave functions $\psi_v(R, x)$, obtained by fixing the electronic coordinate x.

$$\Psi(x, R) = \sum_v \psi_v(R, x)\varphi_v(x) \tag{3.17}$$

Here, x and R again denote the electronic and nuclear degrees of freedom, $\varphi_v(x)$ is an electronic wave function in a fixed vibrational state $|v\rangle$ and the nuclear wave function $\psi_v(R, x)$ depends parameterically on the electronic coordinate. The meaning of this expansion is not immediately clear, but the resulting picture is about the following: Electrons move now on adiabatic surfaces for the different vibrational states, obtained by solving the Schrödinger equation for fixed electronic geometry. We will not go through all the mathematics here, as the theoretical description is analogous to the Born-Oppenheimer approximation, where R and x have been exchanged.

From what has been said so far, the critic would naturally conclude that such a kind of treatment is not physical. However, we can calculate the adiabatic states that would result, if one solves the Schrödinger equation for fixed electronic coordinate. The resulting curves for the already regarded cases (see section 3.3) $R_c = 1.5$ Å (left panel) and $R_c = 2.5$ Å case (right panel) are shown in figure 3.16.

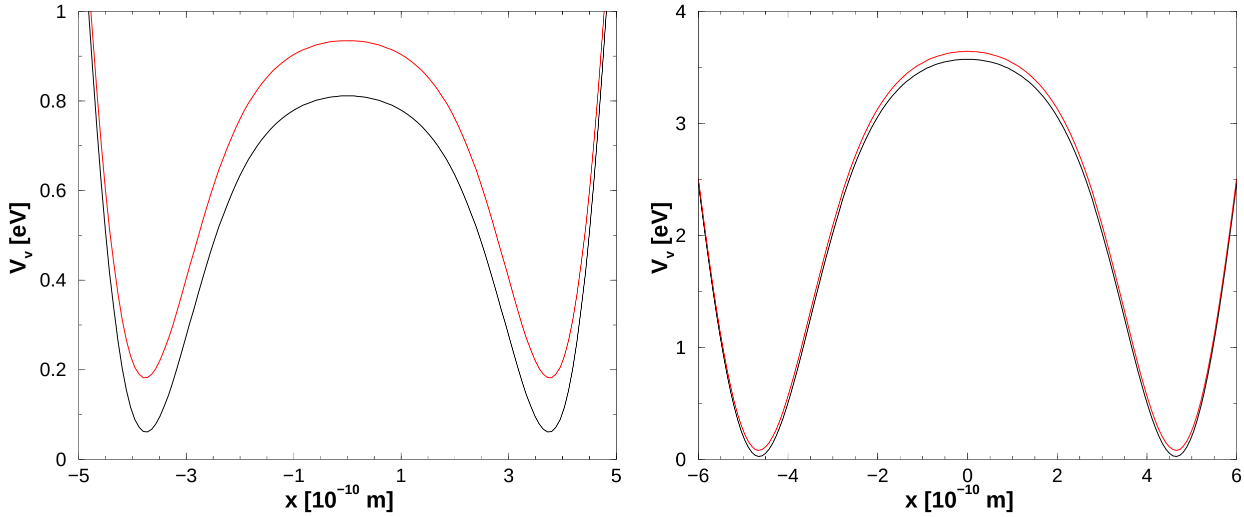

Figure 3.16: Calculated adiabatic curves for fixed electronic coordinate x. The weak (left panel) and the strong coupling case (right panel) are displayed.

The calculated potential curves exhibit two clear minima, one at positive, the other at negative values of x. Looking at the $R_c = 2.5$ Å curves (left panel, figure 3.16) the barrier between left and right potential well is approximately four times as high as in the weak coupling case (right panel). This is in accordance with the dynamical behaviour regarded in section 3.4, where the time-dependent electron density remains nearly stationary during the vibrational motion of the nucleus and only small amounts of density get transferred from the left to the right fixd ion when the nucleus passes the coupling region around $R = 0$ Å. The ground state energies are predicted as 0.81 eV ($R_c = 1.5$ Å) and 1.85 eV ($R_c = 2.5$ Å), respectively, where the correct ground state energies are 1.64 and 1.90 eV. This discrepancy can easily be understood, if one concludes what kind of interactions are neglected in this kind of treatment. As was mentioned earlier, the BO approximation neglects coupling elements of the form (see equation (3.6)):

$$T_{mn}^{(j)}(R) = \frac{1}{2M} \int \varphi_m(x,R) \frac{\partial^{(j)}}{\partial R^{(j)}} \varphi_n(x,R)\, dx \tag{3.18}$$

In our reversed Born-Oppenheimer picture these coupling elements then transform into:

$$T^{(j)}_{vv'}(x) = \frac{1}{2m_e} \int \psi_v(R,x) \frac{\partial^{(j)}}{\partial x^{(j)}} \psi_{v'}(R,x)\, dR \tag{3.19}$$

Now the fundamental difference is immediately clear: Whereas in the usual Born-Oppenheimer treatment the mass of the nuclei enters into the denominator of the coupling elements which results in usually small numbers, the “reverse” coupling elements are devided by the electron mass m_e. Thus the $T^{(j)}_{vv'}$ are at least three orders of magnitude larger than the coupling elements in the Born-Oppenheimer treatment. In other words one could say that the $T^{(j)}_{mn}$ are negligibly small within the BO picture, but that in the reversed treatment the neglect of the coupling elements $T^{(j)}_{vv'}$ results in an unphysical description.

3.6 Summary

The purpose of this chapter was to characterize a combined electronic and nuclear quantum dynamics. Therefore we performed calculations on a model system incorporating a single electronic and nuclear degree of freedom. In order to obtain as much information about the static properties of the system as possible, we determined the electronic eigenfunctions, the adiabatic potential curves, the kinetic coupling elements and the transition dipole moments between the ground and first excited state. The potentials obtained for different parameterizations of the particle interaction show, a larger gap or a close-lying avoided crossing. In the latter case, this is accompanied by nonvanishing coupling elements.

The two cases, which are typical for a situation where the Born-Oppenheimer approximation is valid and for the case of a strong nonadiabatic coupling which results in the breakdown of adiabatic approximations, give rise to a different quantum mechanical motion. The differences were illustrated employing solutions of the time-dependent Schrödinger equation which allow for the calculation of electronic and nuclear densities as a function of time. In the Born-Oppenheimer case, the electron density follows the vibrational motion of the nucleus. Choosing the initial condition for the two-dimensional wave packet such that an isomerization process occuring between two potential minima takes place, the binding situation first changes periodically. However, the transfer of electron density during the motion of the nucleus results in an accumulation of density in different regions of configuration space.

In the strong coupling case, neither the nuclear density nor the electron density (and thus the entire two-dimensional probability density) reflects directly the influence of the nonadiabatic coupling. In calculating the nuclear components in the ground and excited electronic state, the usual picture as it is obtained from solutions of the nuclear Schrödinger equation involving coupled electronic states, appears: during the transition, one component of the nuclear wave function vanishes whereas the other component simultaneously appears. In the particular example we chose, the electron density initially remains stationary, although the nuclear motion extends over a large interval of the nuclear coordinate. This is remarkable, because the existence of a strong coupling suggests dramatic density changes taking place at times when the electronic transition occurs. At the latter times, a small fraction of electron density is transferred between the ions which then, at later times, leads as well to an accumulation of electron density at positive and negative values of the electronic coordinate.

The concentration and depletion of electron density during the wave packet motion can effectively be illustrated using time-dependent Laplacians. These functions, which are often used to reveal properties of the electron density in static problems, prove to be useful also in the analysis of dynamical processes.

The attempt to reverse the Born-Oppenheimer approximation by freezing the electron coordinate and solving the nuclear Schrödinger equation leads to the unphysical picture of electrons that move on “nuclear” potential surfaces belonging to different vibrational levels. From the energetics alone it is clear that this results in a bad description as, e.g., an electronic excitation would take place on a single potential energy surface and the vibrational motion of the nuclei would not change. This is also clear if one considers the neglected coupling elements which turn out to be rather large.

Chapter 4

Electronic predissociation

4.1 Introduction

In this chapter we regard some distinct bonding situations that are often encountered in real molecules. A famous example for the breakdown of the Born-Oppenheimer adiabatic approximation (see chapter 1.1) is the electronic predissociation of molecules [8]. Two theoretical frameworks to describe such a decay mechanism are commonly employed: Within the so-called diabatic picture [70] this process takes place, when a bound (diabatic) potential energy curve V_n^d is intersected by another repulsive potential V_m^d. Including an off-diagonal potential element leads to a coupling of the bound states to the continuum, so that the molecule dissociates. This effect is visible in the energy dependence of observables such as absorption spectra [45] or scattering cross sections [71, 72] in the form of resonances. In the case of a small diabatic coupling (the "diabatic limit"), the decay is associated with a long lifetime of the quasi-bound complex which, in turn, means that the resonances have a small spectral width.

In the adiabatic picture one chooses a different physical description of a predissociation. The adiabatic potential curves $V_n^a(R)$ are uniquely obtained from the solution of the electronic Schrödinger equation (equation (1.5)) for fixed nuclear geometry R. In the case where nonadiabatic effects are large, an adiabatic curve exhibits an avoided crossing (diatomic molecule) [73] or a conical intersection (polyatomic molecule) [10] with the potential surface of another electronic state. The interaction is provided by kinetic coupling elements containing derivatives of the electronic wave function with respect to the nuclear coordinate. The case of a strong coupling, corresponding to a large probability to change the adiabatic electronic state, is identical to the case of a weak diabatic coupling which often leads to confusion if the couplings and the zeroth-order picture of the description are not accurately defined.

The above mentioned predissociation process can easily by studied within the earlier introduced model system (chapter 3) and only minor modifications to the Hamiltonian are necessary to generate the corresponding binding situation. We focus our interest again on the quantum dynamics and we mainly illustrate the nucleus mediated transient electronic structure during the molecular fragmentation. The next section describes the modifications to the model Hamiltonian of chapter 3.2. The following section then deals with the resulting changes to the dynamic behaviour.

4.2 Modifications to the model

We use the same model system already introduced in chapter 3.2 consisting of three ions aligned in a row and a single electron. The Hamiltonian of the model system (equation (3.1)) is modified as follows (in a.u.):

$$H = -\frac{1}{2}\frac{\partial^2}{\partial x^2} - \frac{1}{2M}\frac{\partial^2}{\partial R^2} + V^{\mathrm{mod}}(x, R), \tag{4.1}$$

where

$$\begin{aligned} V^{\mathrm{mod}}(x,R) = \frac{Z_1 Z_3}{|R_L - R|} + Z_2 Z_3 \frac{\mathrm{erf}(|R_R - R|/R_{23})}{|R_R - R|} - Z_1 \frac{\mathrm{erf}(|R_L - x|/R_{1e})}{|R_L - x|} \\ - Z_2 \frac{\mathrm{erf}(|R_R - x|/R_{2e})}{|R_R - x|} - Z_3 \frac{\mathrm{erf}(|R - x|/R_{3e})}{|R - x|} + E_0. \end{aligned} \tag{4.2}$$

In above equation Z_n ($n = 1-3$) are the charges of the nuclei which follow the numbering left ion (1), right ion (2) and moving ion (3). Contrarily to our former model, we employ a screened Coulomb interaction between ions (2) and (3) which is parameterized by an error function (erf). The same kind of functional form is used to describe the ion-electron attraction. The repulsion between ions (1) and (2) is omitted, as it just adds a constant energy shift to the Hamiltonian. The positions of the fixed ions are chosen as $R_L = -5$ Å and $R_R = +5$ Å. Various parameters allow for a manipulation of the interaction: The mass of the moving ion M, the charges of the ions Z_n ($n = 1-3$) and the screening radii R_{ne} ($n = 1-3$). The constant E_0 shifts the global minimum of the full potential to 0 eV.

Again, we solve for fixed nuclear geometry R the electronic Schrödinger equation to obtain the adiabatic potential curves and the corresponding electronic eigenfunctions $\varphi_n(x,R)$ in electronic state $|n\rangle$ (in a.u.):

$$\left\{ -\frac{1}{2}\frac{\partial^2}{\partial x^2} + V(x,R) \right\} \varphi_n(x,R) = V_n^a(R)\varphi_n(x,R) \tag{4.3}$$

Also, to characterize the dynamics in the system, we solve the time-dependent Schrödinger equation for the full Hamiltonian (4.1), applying the split-operator formalism (see chapter 2.1). Furthermore, the time-dependent motion is analyzed by calculating the integrated nuclear and electron densities from the time-dependent wave function (eqns. (3.13) and (3.14)). The nuclear densities in a particular electronic state $|n\rangle$ (see eqn. (3.11)) are obtained by projecting the full wave function $\Psi(x, R, t)$ onto the electronic basis functions defined in equation (4.3).

4.3 Electronic structure

The functional form of the potential energy (equation (4.2)) allows us to modify the particle interaction in a convenient way. In the following we show, that, using this parameterization, it is possible to generate adiabatic potential energy curves $V_n^a(R)$ for the nuclear motion describing various generic electronic structures which also occur in diatomic molecules. In order to restrict the parameter space the mass of the moving ion is fixed to the hydrogen mass and the stationary ions (1) and (2) are kept at a distance of 10 Å ($R_L = -5$ Å and $R_R = +5$ Å). The screening radii corresponding to the electron's interaction with the fixed ions were set to $R_{1e} = R_{2e} = 1.5$ Å. The charges are allowed to be non-integer values, thus having the interpretation of effective charges.

Figure 4.1 displays the potential curves for the electronic ground ($|1\rangle$) and first excited state ($|2\rangle$), calculated for different parameters. The upper panel a) contains the case where the ground state potential exhibits a double-minimum structure and the first excited state is separated by a larger gap of about 0.5 eV. In calculating the curves, all charges were set to $Z_n = 1$, the electron-nuclear interaction was determined with $R_{3e} = 1.5$ Å and the nuclear interaction of ions (2) and (3) contained the parameter $R_{23} = 1$ Å. The plot illustrates the situation where the adiabatic approximation between the nuclear and electronic degree of freedom applies. This case was already investigated in detail in chapter 3.

A situation where the ground state is bound and the first excited state is dissociative can be constructed by decreasing the repulsion between ions (2) and (3). Therefore we set $Z_1 = Z_3 = 1$ and $Z_2 = 0.001$. The resulting curves are

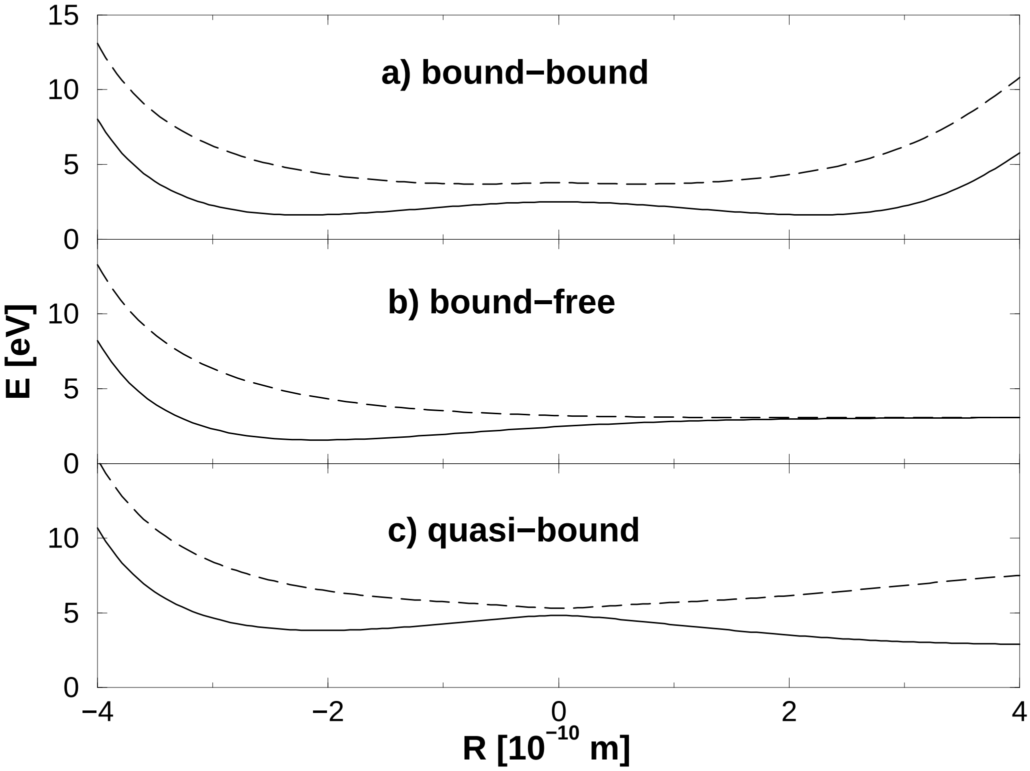

Figure 4.1: Adiabatic potential energy curves for the electronic ground (solid line) and first excited state (dashed line), calculated using different parameters entering into the interaction potential of the model system. Panel a) shows the case of an electronic ground state having a double minimum potential and an energetically seperated excited state ($Z_n = 1$, $R_{3e} = 1.5$ Å, $R_{23} = 1.0$ Å). The case of a bound ground state and dissociative first excited state is illustrated in panel b) ($Z_1 = Z_3 = 1$, $Z_2 = 0.001$, $R_{3e} = R_{23} = 1.5$ Å). Panel c) contains curves where ground and excited state potentials exhibit an avoided crossing which is typical for a predissociation process ($Z_n = 1$, $R_{3e} = 1.75$ Å, $R_{23} = 2.3$ Å).

displayed in panel b) of figure 4.1. This is the typical situation of a bound-to-free transition upon electronic excitation, as is already obtained in a simple LCAO-approach to e.g. the H_2^+ molecule using two basis functions.

Regarding panel c) of figure 4.1 the model interaction was modified such that the lower and the upper adiabatic potential curves exhibit an avoided crossing around $R = 0$. Here the lower curve decreases in energy for distances of R larger than $R = 0$, i.e. the system is not stable. This is the characteristic situation of an electronic predissociation where a diabatic 'quasi-bound' initial state decays via a coupling to a continuum. The construction of such a situation is possible by setting all charges $Z_n = 1$ and choosing $R_{3e} = 1.75$ Å and $R_{23} = 2.3$ Å.

Altogether, we find from figure 4.1 that, within the parameterization of the potential energy (equation (4.2)), it is possible to generate adiabatic potential curves which are generic for ground and excited state configurations belonging to a bound-bound, bound-free and quasi-bound nuclear dynamics.

4.4 Predissociation dynamics

In this section we take a look at the changes in the dynamical behaviour that are caused by the modification of the model Hamiltonian. Our discussion focusses on the system that exhibits predissociation (figure 4.1, panel c)). Usually nuclear dynamics is treated by propagating wave packets on diabatic potentials, including a potential coupling between the different states. Within our model system we can abstain from that and regard the coupled electron-nuclear motion directly. The initial wave packet was of the form

$$\Psi(x, R, t = 0) = e^{-\beta(R-R_0)^2}\, \varphi_1(x, R), \tag{4.4}$$

where $\beta = 2.12\,\text{Å}^{-1}$ and $R_0 = -3.4$ Å. The wave packet was initially located in the electronic ground state. The time evolution of the nuclear density is displayed in figure 4.2 (left panel). The initially localized Gaussian function moves towards larger distances and spreads considerably during the first few fs. The spreading proceeds and at 40 fs the density is almost totally localized at positive values of R. At later times, probability density moves inward again, after it has been reflected on the right end of the grid. As the electronic ground state is dissociative and the wave function is absorbed at the right grid boundary, this must be due to nonadiabatic processes taking place. At about 80 fs the nuclear density shows a larger maximum around $R = 0$.

Regarding the total nuclear density it is not possible to decide which electronic states participate in the predissociation process. Therefore, we regard the

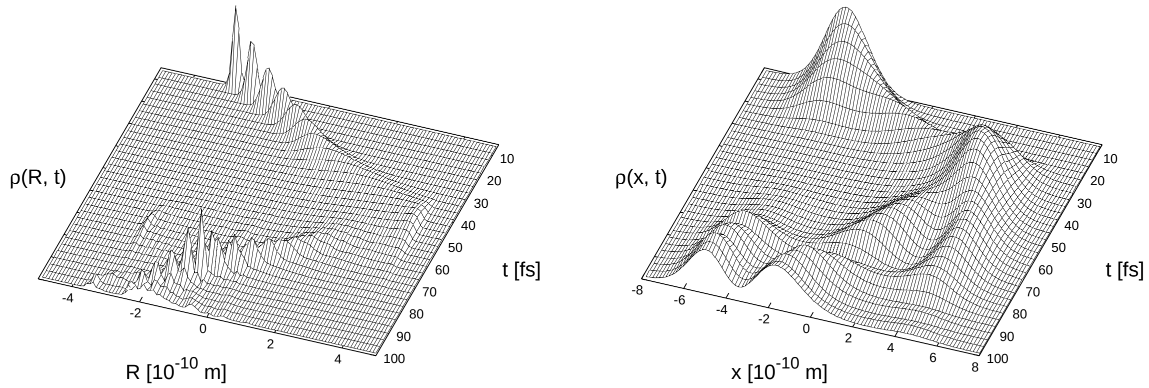

Figure 4.2: Time-dependent nuclear and electron densities during a predissociation process. The original wave packet was located in the electronic ground state centered left from the avoided crossing at $R = 0$. The detailed parameters are given in the text.

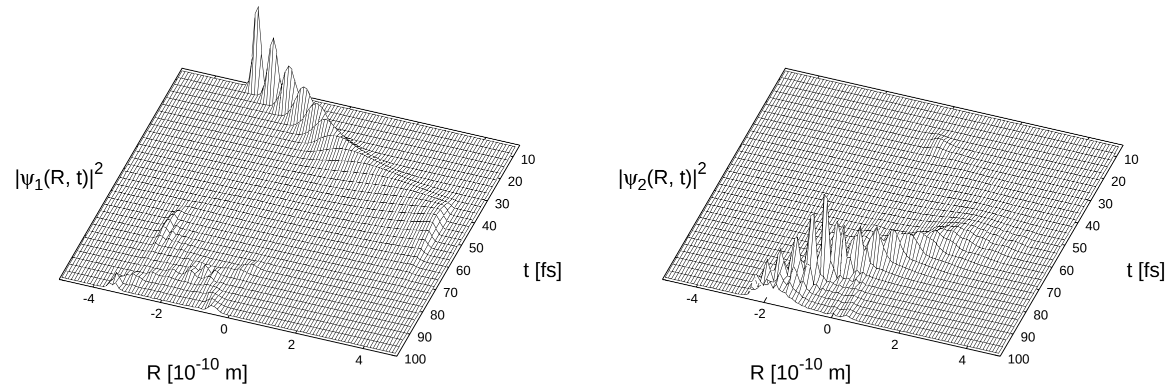

Figure 4.3: Modulus squared of the projections of the total wave function $\Psi(R, x, t)$ onto the electronic ground (left panel) and first excited state (right panel).

modulus squared of the projections $\psi_n(R,t)$ (eqn. (3.11)), which are shown in figure 4.3. Since the wave packet of equation (4.4) is, by definition, a ground state function, the projection $\psi_1(R,t=0)$ is identical to the total nuclear density $\rho(R,t=0)$, see figure 4.2. As is seen in the total density, the function moves outward until it reaches the crossing region where the nonadiabatic coupling is effective ($\sim$ 20 fs). Then, part of the total density is transferred to the first electronically excited state (around 40 fs), the rest remains in the electronic ground state. At a time of about 60 fs, the excited state density is reflected at the outer potential wall, thus exhibiting an oscillatory structure which is caused by the superposition of inward and outward moving components. There is, besides the dissociative part, another ground state component seen at negative distances which corresponds to a flux reflected at the potential barrier. Finally, at a time of about 80 fs, a re-population of the electronic ground state occurs, but most of the density remains in the excited state. The dynamics taking place at longer times proceeds accordingly and is not shown here.

The nuclear wave packet dynamics for our model system is in accordance with the general quantum mechanical description of a motion taking place on coupled potential energy surfaces (see also references [74, 75]). The advantage here is that we are in the position to simultaneously monitor changes of the electron density, i.e. we might answer our initial question for the changes in the electronic structure during a predissociation process. Figure 4.2 (right panel) displays the electron density $\rho(x,t)$. In order to analyze the electron density, it is necessary to compare the density to the electronic eigenfunctions $\varphi_n(x,R)$. The modulus squared of the electronic ground and first excited state functions are plotted in figure 4.4.

Now, in the beginning the nucleus is located around $R=-3$ Å and electron density resembles that of the electronic ground state ($\varphi_1(x,R)$). A little later (around 20 fs), the mobile ion has reached the coupling region around $R=0$,

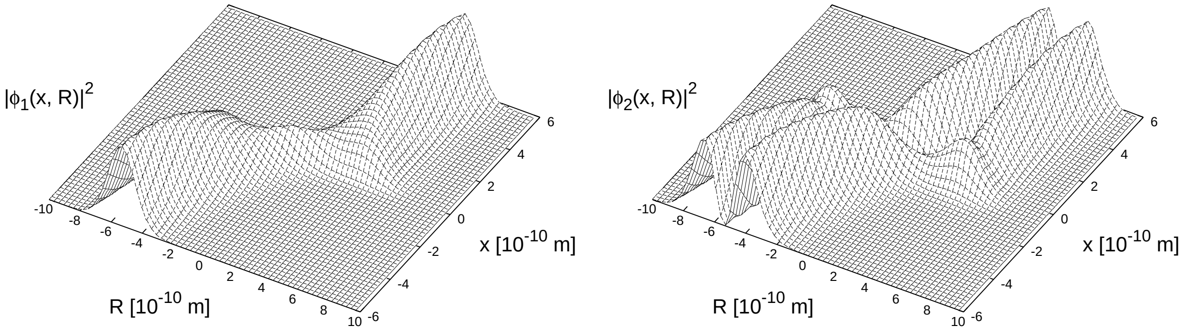

Figure 4.4: Electronic eigenfunctions for the predissociation case. The electronic ground (left panel) and first excited (right panel) state are shown. The corresponding adiabatic potential curves can be found in figure 4.1, panel c).

but still most of the population is in the $n = 1$ state. Accordingly, the electron density is dominated by the features of the respective electronic wave function. Even some time later (40 fs), where fragmentation has occured with a relatively high probability the electron density does not exhibit any nodes from the excited state electronic function. At 60 fs, however, the nodal structure of the excited state function becomes visible in the electron density for positive values of x. As most of the population stays in the excited electronic state, the electron density at about 100 fs still shows the nodal structure of the excited state wave function. Again, it follows from this analysis that the dynamics in the system is dominated by a strong nonadiabatic coupling. We find the typical nuclear dynamics of coupled electronic states, whereas the electron density exhibits a complicated structure due to the mixing of ground and excited state properties due to the coupled motion.

4.5 Summary

In this chapter we showed that it is possible to modify our model system to mimic distinct bonding situations that are often encountered in real diatomic molecules. These situations can be characterized in terms of adiabatic potential curves with bound and dissociative character. In the case of electronic predissociation, where the electronic ground state is dissociative in the asymptotic limit, the adiabatic curves also exhibit an avoided crossing. Our model system has the huge advantage that we are not restricted to a Born-Oppenheimer description and thus, we need not apply a diabatic description for the nuclear dynamics. In contrary, we could demonstrate how the character of the electron density changes during the fragmentation. The nonadiabatic coupling mixes properties of ground and excited state electronic wave functions, giving rise to a complicated transient electronic structure of the system.

Chapter 5

Spectroscopic transitions

5.1 Introduction

In chapter 3 we investigated the quantum dynamics in a simple model system in the cases of weak and strong coupling. There, our interest was focussed on the properties of time-dependent nuclear and electron densities. Chapter 4 then attended the possibility to modify the original Hamiltonian (equation (3.1)) to model various generic electronic structures. In particular we studied a predissociation case. In this chapter we turn to spectroscopic transitions, employing again the model of chapter 3.2 to characterize the quantum dynamics in the case of the interaction with weak and strong electric fields. The motivation for this study is to investigate the influence of nonadiabatic coupling on spectral properties of a system and to follow *simultaneously* electronic and nuclear motion in laser fields without adopting approximations.

The interaction of an atom or molecule with a weak electric field is usually described within first-order perturbation theory, as outlined in chapter 1.4. Essentially, the interaction term is introduced (into the Hamiltonian) as a small time-dependent perturbation. In the case of strong fields a perturbative treatment is no longer valid. The interaction with the electromagnetic field has to be considered explicitly. This means, even within the Born-Oppenheimer picture the adiabatic states are no longer decoupled and population transfer can occur. The explicit coupling between the adiabatic states can be implemented in a similar way as in the diabatic description of nonadiabatic coupling. In the latter case the states are coupled by off-diagonal potential coupling terms, in the former the field couples different states (see chapter 1.5). Fortunately, we are in the position to omit the Born-Oppenheimer approximation in our model system, so that the interaction term with the field can be included into the full model Hamiltonian. Section 5.2 treats one-photon transitions in the weak field regime. The case of strong fields and multiphoton processes is described in section 5.3.

5.2 One-photon transitions

5.2.1 Absorption spectra

In this section we treat one-photon electric dipole transitions within the framework of first-order perturbation theory. Starting from the initial state ψ_i with energy E_i, the absorption spectrum can be written according to *Fermi's golden rule* expression (see chapter 2.2):

$$\sigma_i(E) \sim \sum_f |\langle\psi_f|\mu|\psi_i\rangle|^2\, \delta(E_f - E), \tag{5.1}$$

where $|\psi_f\rangle$ is a final state of energy E_f. The energy $E = E_i + \omega$ is the sum of the inital state energy E_i and the photon energy ω and μ denotes the projection of the dipole operator onto the polarization vector of the electric field. The expression for the absorption spectrum can be recasted in a time-dependent form as [76]:

$$\sigma_i(E) \sim \int e^{iEt} c_i(t)\, dt, \tag{5.2}$$

where the time-dependent correlation function $c_i(t)$ is defined as

$$c_i(t) = \langle \mu\psi_i | e^{-iHt} \mu\psi_i \rangle, \tag{5.3}$$

and H denotes the Hamiltonian of the system.

In our model, the dipole operator is of the simple form (in a.u.)

$$\mu = -x + R \tag{5.4}$$

and thus is of odd parity.

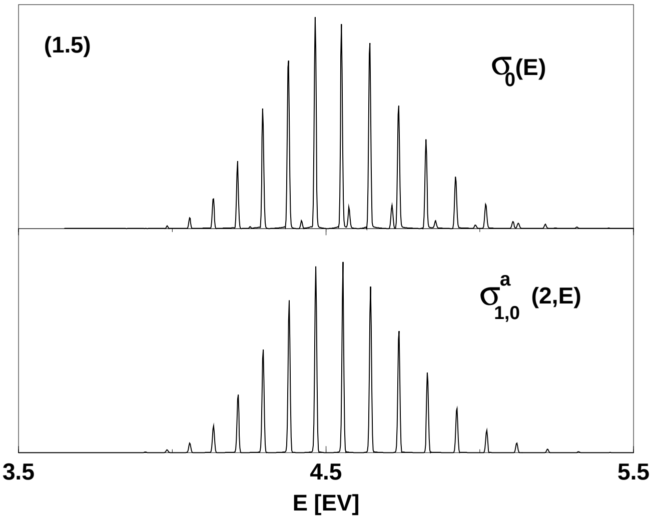

Figure 5.1: Upper panel: absorption spectrum for a cut-off parameter of $R_c = 1.5$ Å. *Only a restricted energy range between 3.5 and 5.5 eV is displayed. The lower panel displays the spectrum as calculated within the adiabatic approximation.*

We first treat the case where the parameter appearing in the electron-nuclear interaction (equation (3.2)) has a value of $R_c = 1.5$ Å. Here, we find a ground state energy of $E_0 = 1.6488$ eV. The absorption spectrum is plotted in figure 5.1, upper panel, in an energy range around $E = 4.5$ eV. Many low intensity peaks are seen for higher energies outside the displayed energy range. Additionally, there is a single large peak at an energy close to E_0 corresponding to a transition to the first vibrationally excited state which is energetically almost degenerate with the ground state. The absorption spectrum exhibits a clear vibrational progression. However, there is a set of peaks with much smaller intensity.

In order to understand the structure of the spectrum, the latter was calculated using the adiabatic approximation. Therefore the nuclear Schrödinger equation (1.15) was solved employing the adiabatic potential curves $V_n(R)$. The spectrum takes the form

$$\sigma^a_{n,v}(m, E) \sim \int e^{iEt} c^a_{n,v}(m, t)\, dt, \tag{5.5}$$

where $E = E_{n,v} + \omega$ contains the vibrational energy $E_{n,v}$ in the electronic state $|n\rangle$ and the autocorrelation function is

$$c^a_{n,v}(m, t) = \langle \mu^a_{mn} \psi_{n,v} | e^{-iH_m t} \mu^a_{mn} \psi_{n,v} \rangle. \tag{5.6}$$

Here enters the initial vibrational wave function $\psi_{n,v}(R)$, the nuclear Hamiltonian H_m of the final electronic state $|m\rangle$ and the transition dipole moment

$$\mu^a_{mn}(R) = \langle \varphi_m(x, R) | - x + R | \varphi_n(x, R) \rangle. \tag{5.7}$$

We calculated the initial wave function $\psi_{1,0}(R)$ in the electronic ground state $|1\rangle$ with the eigenenergy of $E_{1,0} = 1.6490$ eV which is in very good agreement with the numerically exact value. Using the electronic wave functions for the ground and first excited electronic state, the transition dipole moment was determined and found to be only weakly R-dependent in the region where $\psi_{1,0}(R)$

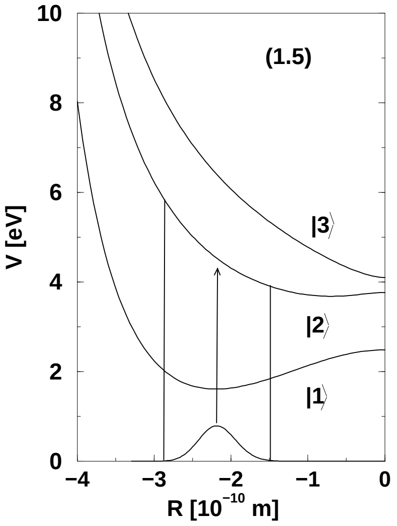

Figure 5.2: Adiabatic potential energy curves for the case $R_c = 1.5$ Å. Also shown is the vibrational ground state in $|1\rangle$. The lines indicate the borders of the Franck-Condon window for the electronic transition and the arrow marks the energetic position for a vertical transition.

is localized. This means that the commonly employed Condon approximation, which neglects the dependence of μ_{mn} on the nuclear coordinates, is valid in the present case. The spectrum, as calculated within the adiabatic approximation, is shown in figure 5.1, lower panel. The intensity distribution and the locations of the peaks coincide with those of the high intensity lines in the numerically exact spectrum $\sigma_0(E)$. However, the progression of smaller peaks is not found within the adiabatic approximation. In order to understand the features of the spectra we may regard the adiabatic potential curves $V_n(R)$ $(n = 1, 2)$ which are displayed in figure 5.2 for negative values of R. Note that the potentials are symmetric with respect to $R = 0$.

The vibrational ground state wave function $\psi_{1,0}(R)$ is also shown. The vertical lines indicate the Franck-Condon window, i.e., the region where transitions from the initial state are most likely to occur. The arrow starting at the maximum of the vibrational function marks a vertical transition, in accordance with the

Franck-Condon principle (see also section 5.2.2).

Regarding the absorption spectrum $\sigma_0(E)$ in figure 5.1, it is obvious that the larger set of peaks correlate with an excitation into the second electronic state $|2\rangle$. Within the adiabatic approximation, a transition to vibrational states in state $|3\rangle$ having energies in the displayed energy range, are not to be expected since the vibrational wave functions have no overlap with the initial state. Thus, the small set of peaks missing in the spectrum $\sigma^a_{1,0}(2, E)$ are due to nonadiabatic effects. Although the coupling between the excited electronic states $|2\rangle$ and $|3\rangle$ is weak (see chapter 3), it induces a mixture of vibrational components corresponding to different electronic states. It is this mixing which then results in the additional peaks.

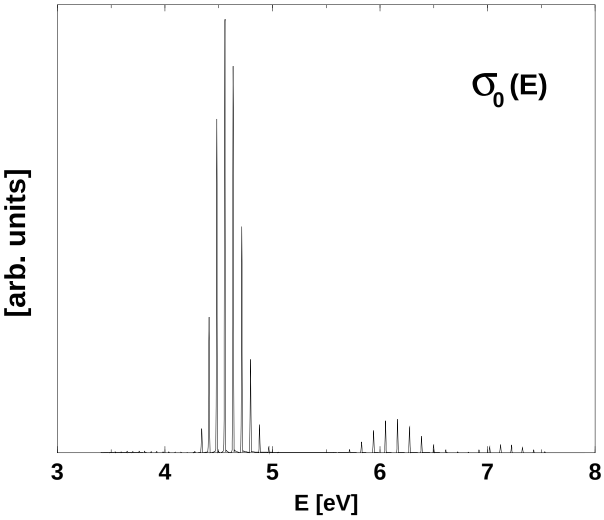

Figure 5.3: Absorption spectrum for the case $R_c = 2.5$ Å.

Next, we regard the case $R_c = 2.5$ Å which induces a strong nonadiabatic coupling between the two lowest electronic states (see chapter 3). The absorption spectrum obtained from a two-dimensional time propagation is contained in figure 5.3. Several electronic bands with a vibrational progression can be identified, the largest being centered around an energy of 4.8 eV. As for the case treated above,

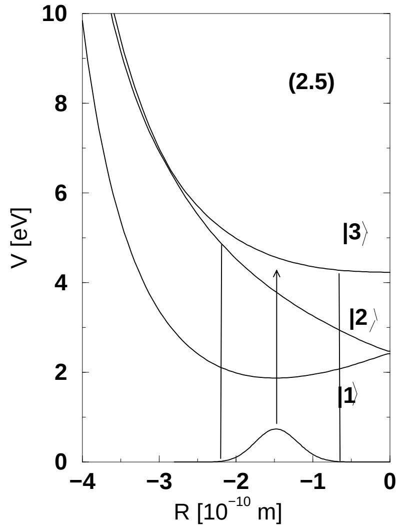

Figure 5.4: Adiabatic potential curves for the case $R_c = 2.5$ Å. The Franck-Condon window defined by the location of the inital wave function and the region for a vertical transition are marked.

we calculated adiabatic potentials $V_n(R)$ which, for quantum numbers $n = 1 - 3$, are displayed in figure 5.4. As was indicated earlier (chapter 3), a substantial electron-nucleus coupling occurs in the region around $R = 0$ where the potential curves for the two lowest states exhibit only a small energy gap of 0.05 eV. The displayed Gaussian indicates the vibrational ground state wave function. The lines mark the Franck-Condon window for transitions to excited electronic states. From the figure one would expect a first absorption band centered around an energy of $\sim$ 3.7 eV ($|2\rangle \leftarrow |1\rangle$). This band indeed can be seen in the complete absorption spectrum $\sigma_0(E)$ (figure 5.3), however, it appears with a very low intensity compared to other bands, in particular to the next one corresponding to a $|3\rangle \leftarrow |1\rangle$ transition. Let us concentrate on the first absorption band which may be determined using various levels of approximation. Within the adiabatic approximation, we can calculate the spectrum for the $|2\rangle \leftarrow |1\rangle$ transition using equations (5.5) - (5.7). The result is diplayed in figure 5.5, lower panel. Neither the line positions nor the vibrational spacing is comparable to the exact spectrum which is shown on an enlarged scale in the upper panel of the same figure. As a conclusion, the strong nonadiabatic coupling of the two electronic states with quantum numbers $n = 1, 2$ leads to a complicated spectrum and the adiabatic approximation breaks down completely.

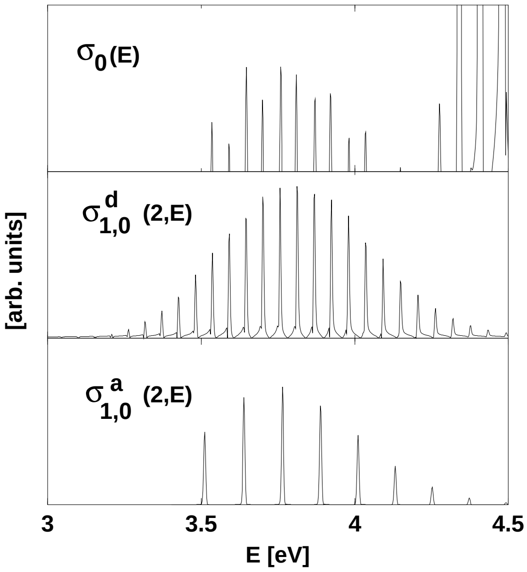

Figure 5.5: Comparison of adiabatic (lower panel), diabatic (middle panel) and complete absorption spectrum (lower panel) for the case $R_c = 2.5$ *Å.*

The electron-nuclei coupling can be introduced using a potential coupling between the electronic states. The concept behind this approach is that of "diabatization" of electronic states, which, by definition, minimizes the kinetic coupling elements appearing in the coupled Schrödinger equation for the nuclear wave functions in different electronic states (equation (1.11)) [11]. The problem to construct diabatic potential curves has been discussed extensively; see e.g. the reviews [77, 78]. Here we take a simple approach: the intersecting (diabatic) potentials are constructed starting with the adiabatic potentials V_1 and V_2. In the coupling region around $R = 0$ we introduce a linear fit which connects the upper potential for positive values of R continuously with the branch of the lower potential for negative values of R. Likewise the two other branches are connected.

This yields intersecting potentials $V_1^d(R)$ and $V_2^d(R)$. Using the diabatic and adiabatic potentials we may determine potential coupling matrix elements V_{12}^d so that the diagonalization of the diabatic potential matrix yields the adiabatic potentials. Further details on the diabatization is given in appendix A. In order to calculate the spectrum, an initial nuclear wave function has to be propagated with the Hamiltonian involving two coupled electronic states. In more detail, the spectrum takes the form

$$\sigma_{n,v}^d(m,E) \sim \int e^{iEt} c_{n,v}^d(m,t)\,dt, \tag{5.8}$$

where $E = \omega + E_{n,v}$ and the autocorrelation function is

$$c_{n,v}^d(m,t) = \langle \mu_{mn}^d \psi_{m,v} | e^{-iH_{mn}t} \mu_{mn}^d \psi_{n,v} \rangle. \tag{5.9}$$

Here enters the vibrational Hamiltonian (for $n = 1$ and $m = 2$):

$$H_{21} = \begin{pmatrix} T(R) + V_1^d(R) & V_{12}^d(R) \\ V_{21}^d(R) & T(R) + V_2^d(R) \end{pmatrix}, \tag{5.10}$$

where $T(R)$ is the operator of the kinetic energy. Note that the nuclear wave function consists of two components, i.e., $\psi_{nm}(R,t) = (\psi_n(R,t), \psi_m(R,t))$, where the initial condition is $\psi_{nm}(R,0) = (0, \mu_{mn}^d \psi_{n,v})$. Within the ideal diabatic representation, the transition dipole moment μ_{mn}^d is a constant and we set it to unity in what follows. The time propagation is performed as is described in reference [79]. The diabatic spectrum is shown in figure 5.5, middle panel. Here we find a vibrational progression where the single lines coincide with those in the complete spectrum σ_0 (upper panel). This confirms that one indeed has to consider the nonadiabatically coupled ground and first excited state in order to find a reliable spectrum. Of course, since the diabatic transition dipole moment was set to unity, the intensity of the spectrum cannot be compared to σ_0. As for the intensity of the $|2\rangle \leftarrow |1\rangle$ relative to the $|3\rangle \leftarrow |1\rangle$ transition, we calculated the transition dipole moments around distances of $R = 1.5$ Å, i.e., within the Franck-Condon window for the electronic transitions. These moments vary only weakly with the nuclear coordinate R. For the ratio of the square of the dipole moments $|\mu_{31}/\mu_{21}|^2$ we found a value of about 1600 which explains the intensity variations in the spectral lines for the two transitions. The reason for the different magnitude of the moments lies in the electronic wave functions which enter into the calculation: whereas the function for $n = 3$ is located in the same region as the ground state electronic function at negative values of x, the $n = 2$ function is located almost exclusively at positive values of x and thus has small overlap with the ground state (see also chapters 3.3.2 and 3.3.4).

It should be noted that the choice of diabatic states "is not unique and it is up to each investigator to find the one that is most convenient for the problem at hand" [37]. This can be illustrated by regarding the absorption spectrum in the $R_c = 2.5$ Å case. Above we showed that the interpretation of the spectrum at lower energies is possible within our choice of diabatic states. This, as well, applies to the next intense absorption band appearing around 4.5 eV (see figure 5.3) which, by inspection of figure 5.4, can be identified as belonging to the $|3\rangle \leftarrow |1\rangle$ transition. Here the third diabatic curve, if constructed as described above, will be the one intersecting the potential curve $V_2^d(R)$ around $R = -2.9$ Å. Shin and Metiu constructed another set of three diabatic states. Whereas the diabatic potentials for the two lowest states are identical to ours, the curve of the third state (describing an "atomic" situation, where the electron interacts only with the movable ion) differs substantially from the one of our third state. The potential of the atomic like diabatic state crosses our curve $V_2^d(R)$ at a distance of $R = -1.5$ Å, i.e., in the Franck-Condon region for the $|2\rangle \leftarrow |1\rangle$ transition (see figure 5.4). This means that the $|3\rangle \leftarrow |1\rangle$ absorption band cannot be described within the choice of the three diabatic states used in reference [37]. However, as is discussed in detail by Shin and Metiu, valuable physical insight into the nature of charge-transfer processed can be gained employing their set of electronic basis states.

5.2.2 Electron and nuclear dynamics during spectroscopic transitions

We turn now to the transient features of our system occuring during the interaction of the particles with an external electric field. In particular, we are interested in temporal changes of the vibrational and electronic parts of the wave function. Equations (5.1) and (5.2) are based on first-order time-dependent perturbation theory. The first-order correction to the total wave function, created by a perturbation $W(t)$ is of the form (see chapter 1.4)

$$|\psi^{(1)}(t)\rangle = \frac{1}{i} \int\limits_{-\infty}^{t} e^{-iH(t-t')}\, W(t')\, e^{-iHt'}\, |\psi_i\rangle\, dt'. \tag{5.11}$$

For dipole transitions induced by a field with carrier frequency ω, the interaction energy $W(t)$ is

$$W(t) = -\frac{1}{2}\, \mu\, g(t)\, e^{-i\omega t}, \tag{5.12}$$

where we are interested in absorption processes. In the numerical example, the pulse envelope $g(t)$ is chosen as

$$g(t) = \begin{cases} e^{-\beta(t-t_0)^2} & (t < t_0), \\ 1.0 & (t \geq t_0). \end{cases} \tag{5.13}$$

This is a Gaussian pulse which rises to its maximum at $t = t_0$ and then remains constant. The Gaussian was chosen to have a full-width-at-half-maximum (FWHM) of 50 fs and a center at $t_0 = 50$ fs.

Instead of following the time dependence of the wave function $\Psi^{(1)}(x, R, t)$, we regard again the electron and nuclear densities defined as

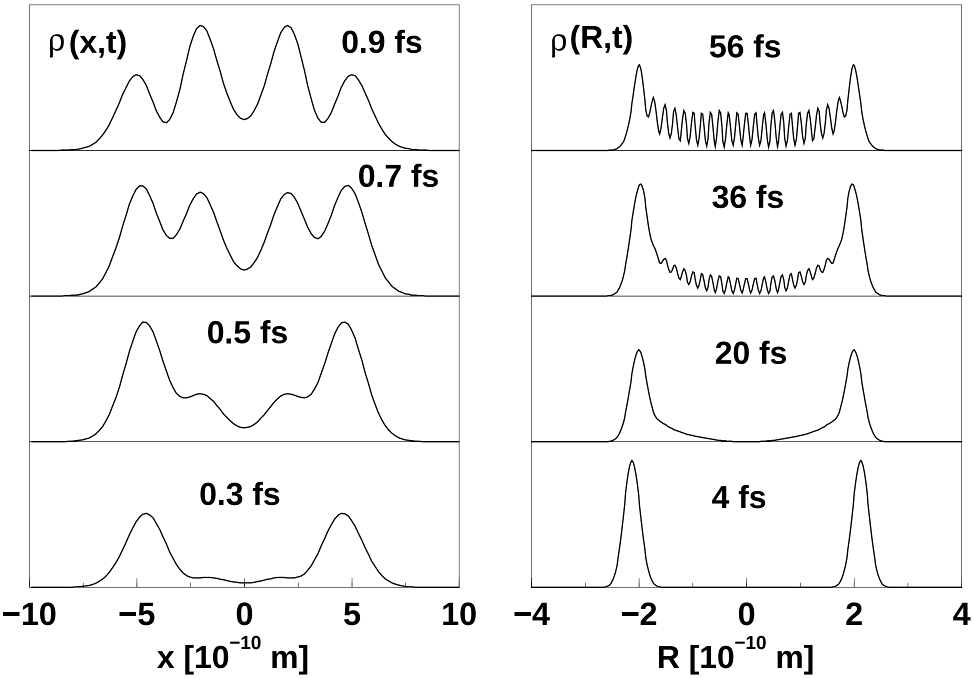

Figure 5.6: Dynamics of the excited state electronic density (left panels) and the nuclear density (right panels), during a weak field excitation for the case of $R_c = 1.5$ Å. The electron density becomes stationary within the first femtosecond of the excitation, whereas it takes about 60 fs for the vibrational state to settle into a stationary state.

$$\rho(x,t) = \int |\Psi^{(1)}(x,R,t)|^2 \, dR, \tag{5.14}$$

$$\rho(R,t) = \int |\Psi^{(1)}(x,R,t)|^2 \, dx. \tag{5.15}$$

Figure 5.6 (left panels) displays the time-dependent electron density within the first femtosecond of the field-system interaction ($R_c = 1.5$ Å). A photon energy of $E = E_i + \omega = 2.815$ eV was chosen which corresponds to the largest peak in the first absorption band occuring at a total energy of 4.464 eV (see figure 5.1. At a time of 0.3 fs, the density resembles the density of the initial state which is symmetric with respect to x and is approximately zero around $x = 0$. With increasing time, a nodal structure builds up between the two maxima (0.5 and 0.7 fs). Finally, at 0.9 fs, the outer maxima have reached values which are smaller than the new maxima appearing in the intermediate region. For longer times, the electron density does not change its form anymore, only the norm increases. Thus, with respect to the electronic degree of freedom a stationary state is obtained. The corresponding electronic eigenstate has to be antisymmetric, thus, by inspection of figure 5.6, it has a single node, i.e., the electronic quantum number is $n = 2$ (in our notation where the symmetric electronic ground state has the label $n = 1$). This, of course can directly be seen in the complete wave function $\Psi(x, R, t)$.

Next, we regard the nuclear densities which are displayed in figure 5.6, right panels. The density at 4 fs has the structure of the initial vibrational state. With increasing time, probability density builds up around the symmetry point $R = 0$. At about 36 fs, a nodal structure appears which becomes more pronounced as time elapses. Only minor changes are seen after 56 fs (not shown), so that the stationary structure of the vibrational wave function is prepared within a time scale of 60 fs.

A comparison of the electronic and nuclear densities in figure 5.6 documents that the electronic motion proceeds on a much faster time scale than the nuclear motion. Here we see the *Franck-Condon principle* at work, stating that, during an electronic excitation process, the nuclei do not move [80]. Regarding the electronic and nuclear wave functions (or densities) this, more precisely, means that during a field-induced transition, the electronic wave function becomes stationary (in the sense that its structure remains the same and only its norm increases with time) on a very short time scale, whereas it takes much longer for the nuclei to settle into a stationary state.

5.3 Strong-field dynamics

In what follows, we investigate the interaction of the electron/nuclei system with a strong electric field. As already mentioned above, perturbation theory has to be abandoned and the propagator now contains the Hamiltonian of the unperturbed system and an additional interaction term as

$$W(x, R, t) = -\mu(x, R)g(t)cos(\omega t). \tag{5.16}$$

In propagating the wave function with the time-dependent Hamiltonian, we use small time steps $\Delta t = 0.01$ fs so that, during a propagation step, the interaction term can be approximated as being constant [81]. The numerical calculation used a Gaussian pulse envelope with a FWHM of 50 fs, a frequency of $\omega = 2.65$ eV and an intensity of 5×10^{12} W/cm^2. Thus the field is in resonance with the electronic transition $|3\rangle \leftarrow |1\rangle$ in the case of $R_c = 2.5$ Å which is treated here. In order to evaluate the efficiency of multiphoton transitions, we have used the time-dependent wave function after the excitation pulse stopped at a time of $t_0 = 150$ fs to calculate a spectrum as

$$\sigma(E) = \int e^{iEt} \langle \psi(t_0) | \psi(t_0 + t) \rangle \, dt. \tag{5.17}$$

The first four high intensity bands of the spectrum are displayed in figure 5.7. Additionally, the absorption band around 4.5 eV is included in an extra panel on an enlarged scale. Many more peaks of lower intensity appear outside the displayed energy range. The spectrum documents that the interaction with the

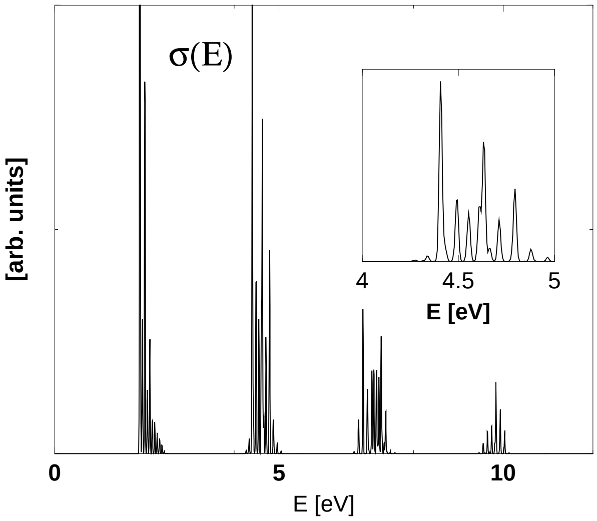

Figure 5.7: Spectrum after strong-field excitation of the model system ($R_c = 2.5$ Å). The band around 4.5 eV is depicted on an enlarged scale in the extra panel.

intense field leads to multiphoton transitions of high order so that many electronic states are excited. Within each electronic state several vibrational states are populated as is revealed by the vibrational fine structure of the spectrum (see, e.g., the extra panel in figure 5.7).

The dynamics of the driven system is illustrated in figure 5.8. For the employed frequency, the optical cycle of the pulse is about 1.5 fs. Figure 5.8 (left panels) shows that the electron density follows the periodic variation of the field. Thus the *quiver* motion as is found for a free electron in an oscillating field is seen here as well, but is modified by the presence of the field of the nuclei. On the other hand, the much heavier nucleus cannot follow the fast field oscillations. The time-evolution of the nuclear density is diplayed in figure 5.8 (right panels) for various times during the external perturbation. From the irregular features of the density it is to be expected (which is also evident from the spectrum in figure 5.7) that many vibrational states participate in the nuclear dynamics. This can be further analyzed by regarding times, for which the interaction has stopped so that an unperturbed time evolution takes place. Figure 5.9 documents that

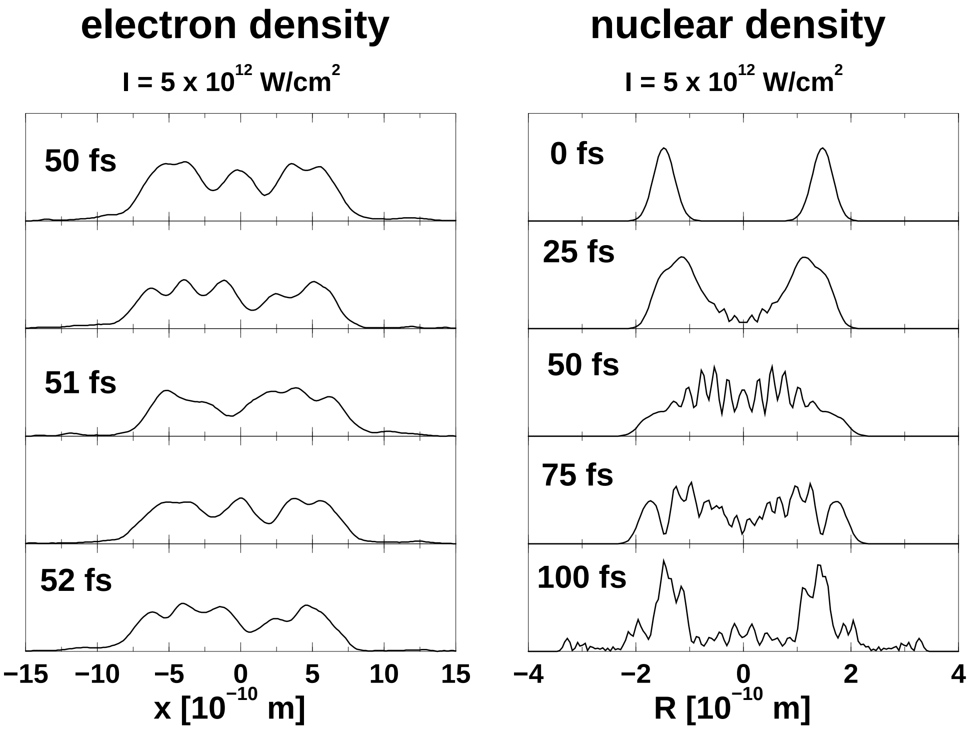

Figure 5.8: Electron and nuclear dynamics during the interaction with an intense laser pulse. Whereas the electron density follows the optical period of the applied field, the nuclear density exhibits a dynamics only after about 50 fs.

the field has prepared an electronic and vibrational wave packet: the electron, as well as the vibrational density exhibit temporal changes. Here the time scale for the electronic motion can be estimated by the energetic separation $\Delta E_{\rm el}$ of the absorption bands in figure 5.7. This yields a time scale of $T_{\rm el} = 2\pi/\Delta E_{\rm el} \approx 1.6$ fs and indeed the variation of the electron density takes place on this time scale. On the other hand, many vibrations with different level spacings $\Delta E_{\rm vib}$ are excited yielding times $T_{\rm vib} = 2\pi/\Delta E_{\rm vib}$ ranging from 30 to 100 fs. This leads to the complicated vibrational dynamics as is documented in the nuclear densities displayed in figure 5.9.

In atoms, electronic wave packets can be prepared by an external field and their dynamics may be tracked in real time [82]. On the other hand, the discussion of strong field interactions with molecular systems is centered around the

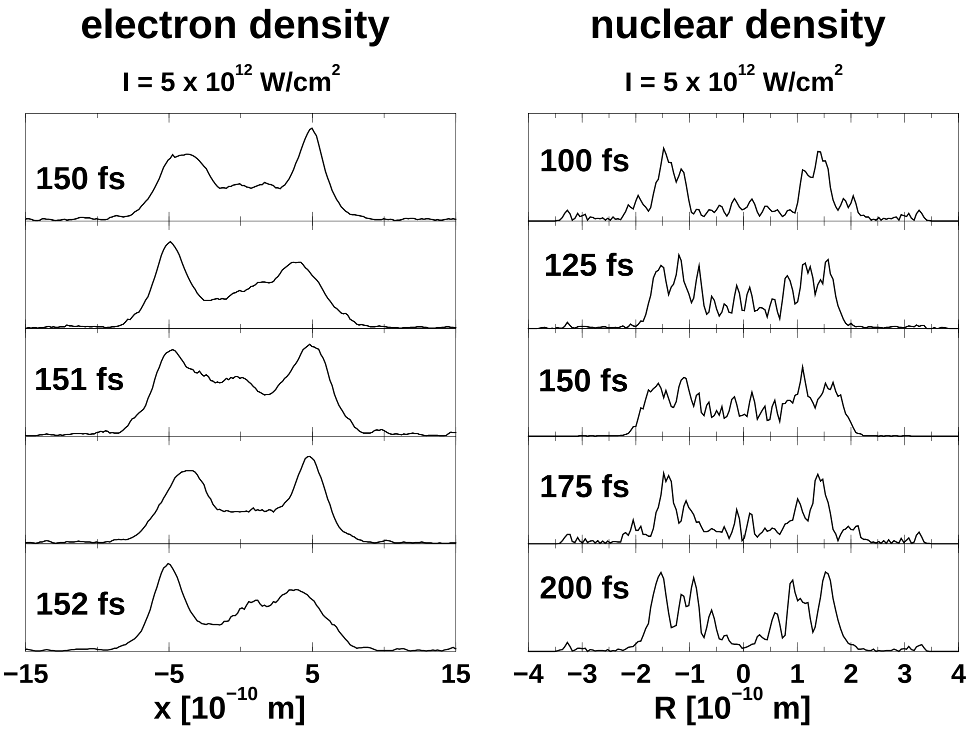

Figure 5.9: Electron and nuclear dynamics after the interaction with an intense laser pulse. The interaction has prepared a coherent superposition of electronic and vibrational states. The fast motion of the electronic wave packet (left panels) and the slower vibrational wave packet (right panels) can be distinguished.

production of nuclear (rotational-vibrational) wave packets; see, e.g. the review by Giusti-Suzor *et al.* [83]. Here, we are able to follow the electronic and nuclear wave packets simultaneously. This stresses the power of the employed model, with respect to an analysis of quantum dynamics beyond adiabatic approximations.

It is clear that the quantum dynamics will be reflected in any kind of time-dependent observable. As an example, we regard the expectation value of the dipole moment defined as

$$\mu(t) = \langle \psi(t) | \mu | \psi(t) \rangle. \tag{5.18}$$

Figure 5.10, lower panel, contains this quantity which exhibits very fast oscillations and a more slowly varying amplitude. The period of the faster time variation is about 1.5 fs., i.e., is equal to the time scale for the electronic motion T_{el} as estimated above. Then, the longer periods which are reflected in the beating structure of the overall amplitude are due to the vibrational motion. One has to keep in mind that the electronic motion here is much too fast to be directly observed in an experiment owing to the limited time resolution. To illustrate this point we regard the absolute square of the dipole moment which is proportional, under certain conditions, to the intensity of the emitted radiation, see reference [84]. Performing an average using a square window function of 10 fs yields the curve as displayed in the upper panel of figure 5.10. Now the fast oscillations (for electronic coherences) are washed out and the remaining time dependence can be assigned to the vibrational quantum dynamics.

5.4 Summary

The simplified description of the dynamics of an electron and a nucleus within our model system allows for the characterization of the correlated dynamics during and after the interaction with an external electric field. Employing adiabatic potential energy curves it is possible to understand the structure of absorption spectra as obtained in the limiting case of weak fields. For a small nonadiabatic coupling, the adiabatically calculated spectrum is in excellent agreement with the exact one. Still, the existence of even a weak coupling produces extra peaks which cannot be explained within the adiabatic approximation. For a strong coupling, the adiabatic approximation yields a spectrum which does not agree with the exact spectrum. The introduction of a potential coupling and the thus induced diabatic two-component wave packet motion can be used to calculate an absorption spectrum in much better agreement.

The well-known Franck-Condon principle states that during an electronic

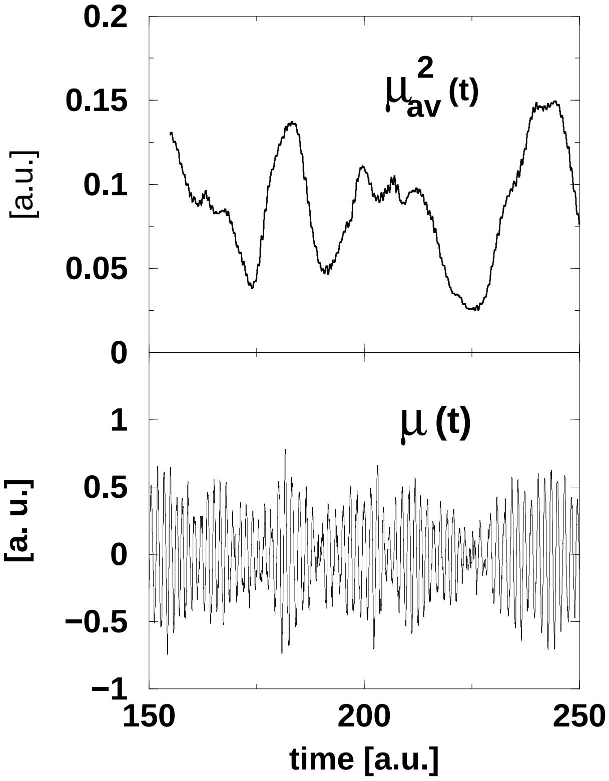

Figure 5.10: Lower panel: expectation value of the dipole moment. The oscillations reflect the combined vibrational and electronic dynamics. By using a time average of the absolute square of the dipole moment, the electronic motion is averaged out and the signal reflects exclusively the vibrational motion (upper panel).

transition the nuclei do not move. In terms of time-dependent electron and nuclear densities, we have illustrated this principle. Regarding the dynamics during a laser excitation process we may state that within a very short time scale the electronic part of the wave function reaches a stationary state in the sense that its structure remains unchanged. During this short time interval, the nuclear wave function indeed does not exhibit structural changes. Only at longer times the nuclear wave function becomes stationary.

The interaction of the constraint particles with a strong laser pulse leads to the excitation of many bound electronic and vibrational states. The electronic density shows that during the excitation process, the electron performs the classical-like quiver motion induced by the fast variations of the field. The much larger mass of the nucleus prevents that it follows the oscillations of the electric field. In general, the interaction prepares an electronic and vibrational wave packet motion which will — if properly detected — be seen in any observable depending on both the electronic and nuclear coordinates or momenta.

Chapter 6

Localization in a two-electron system

6.1 Introduction

In the last chapters we used a simple model of a moving ion and an electron to determine the influence of nonadiabatic coupling on the electron density; we investigated spectroscopic transitions in weak and strong electric fields and also treated a predissociation case by slightly modifying the original model. In those examples only one electron was involved and we did not need to pay attention to the symmetry of the electronic wave function.

In this chapter we present an extension to the one-electron model. By adding a second electron, complications arise, as the electronic wave functions must be anti-symmetric with respect to exchange of the two electrons (*Pauli principle*). Within the calculation, the total symmetry of the wave function is determined by either choosing a symmetric or anti-symmetric coordinate-space wave function, corresponding to the cases of anti-parallel and parallel spins, respectively.

While the structure of the electron density gets more complex in a multi-electron system, one also loses the ability to identify regions of localization of single electrons. However, the concept of the *electron localization function* (ELF) as introduced by Becke and Edgecombe [51] to "measure" localization of electrons with identical spin has turned out to be extremely beneficial in chemistry. The ELF was used to investigate the shell-structure of atoms and the bonding situation in a variety of molecules an crystals. For a review see reference [85].

In order to deploy ELF to our system, one has to re-define it for an exact wave function. This will be done in the next section. After that we introduce the extended model Hamiltonian and finally provide an example of how the ELF can be employed to investigate a time-dependent wave packet motion.

6.2 Definition of ELF for exact wave functions

In chapter 1.6 we defined the electron localization function in terms of a Hartree-Fock wave function. This original definition by Becke and Edgecombe [51] is not applicable to an exact wave function, but we follow the same strategy to adopt the ELF to our needs. The probability density to find the two electrons with spin σ and τ at positions x and y and the nucleus at position R is given by the diagonal of the three-particle density matrix:

$$D_{\sigma\tau}(x, y, R) = |\Psi(x\sigma, y\tau, R)|^2 \tag{6.1}$$

In principle, one might investigate the correlation of all three particles, but we focus our interest on the electrons here. An averaging over the nuclear degree of freedom yields:

$$D_{\sigma\tau}(x, y) = \int |\Psi(x\sigma, y\tau, R)|^2 \, dR \tag{6.2}$$

The *conditional probability* to find one electron with spin σ at x, if we know with certainty that the other electron with spin τ is located at position y, is given by

$$P_{\sigma\tau}(x,y) = \frac{D_{\sigma\tau}(x,y)}{\rho_\tau(y)}, \tag{6.3}$$

where $\rho_\tau(y)$ is the spin density which can be calculated from the full wave function via integration:

$$\rho_\tau(y) = \int |\Psi(x\sigma, y\tau, R)|^2 \; dR \, dx \, d\sigma \tag{6.4}$$

At this point one has to distinguish between the cases of parallel (denoted $\alpha\alpha$) and anti-parallel spin ($\alpha\beta$). It should be noted that we exclude cases where *spin polarization* occurs, i.e. cases where the spatial wave functions of electrons with different spin are not identical. This means $\rho_\sigma(x) = \rho_\tau(y)$ in all regarded cases.

In the case of anti-parallel spins the coordinate-space wave function is symmetric with respect to an exchange of the electrons and the function

$$P_{\alpha\beta}(x) = P_{\alpha\beta}(x,x) \tag{6.5}$$

is a direct measure for the localization of one electron. The interpretation is as follows: $P_{\alpha\beta}(x)$ is the conditional probability to find one electron at position x, if we know with certainty that the other electron with opposite spin is at the same place. If $P_{\alpha\beta}(x)$ is small, the first electron is strongly localized, whereas for large $P_{\alpha\beta}(x)$ the probability density of the first electron is diffuse.

In the case of parallel spins $P_{\alpha\alpha}(x,y)$ vanishes identically for $x = y$ as a consequence of the Pauli principle. Following the treatment of Becke and Edgecombe one transforms equation (6.3) to the relative coordinate $s = x - y$. For our linear model a spherical averaging around $s = 0$ is not necessary and $P_{\alpha\alpha}(x, s)$ is directly expanded into a Taylor-series around $s = 0$:

$$P_{\alpha\alpha}(x, s)|_{s=0} = P(x, 0) + \frac{\partial P_{\alpha\alpha}(x, 0)}{\partial s} s + \frac{1}{2} \frac{\partial^2 P_{\alpha\alpha}(x, 0)}{\partial s^2} s^2 \tag{6.6}$$

The first term is zero because of the Pauli principle. The linear term must also vanish, as, according to Kato's theorem [86,87], the many-body wave function Ψ is proportional to s for small s, which means $|\Psi|^2$, D and P are proportional to s^2 in this limit. Thus, the first non-zero term of the expansion (6.6) is of quadratic order and may be written as:

$$P_{\alpha\alpha}(x, s) = \frac{1}{2} \frac{\partial^2 P_{\alpha\alpha}(x, 0)}{\partial s^2} s^2 = C_{\alpha\alpha}(x) s^2 \tag{6.7}$$

The quantity $C_{\alpha\alpha}(x)$ enters directly into the definition of the electron localization function (ELF) and one finds:

$$\mathrm{ELF}(x) = \left[1 + \left(C_{\alpha\alpha}(x)/C^0_{\alpha\alpha}(x)\right)^2\right]^{-1} \tag{6.8}$$

Here, $C^0_{\alpha\alpha}(x)$ is the *Thomas-Fermi (TF) kinetic energy density* with the same local spin density $\rho_\alpha(x)$. The TF kinetic energy density of our system is given by

$$C^0_{\alpha\alpha}(x) = \frac{16}{3} \pi^2 \rho^3_\alpha(x) \tag{6.9}$$

and will be derived in appendix B.

6.3 The extendend model Hamiltonian

In this section we describe how an additional electron can be included into the previously investigated model (chapters 3 – 5). Again three ions are aligned in a row, where the two outer nuclei are fixed at $R_L = -5$ Å and $R_R = +5$ Å, respectively. The middle ion is allowed to move on the internuclear axis. Additionally, now two electrons move on the same axis. The resulting Hamiltonian with three degrees of freedom reads (in a.u.):

$$H(x, y, R) = -\frac{1}{2}\frac{\partial^2}{\partial x^2} - \frac{1}{2}\frac{\partial^2}{\partial y^2} - \frac{1}{2M}\frac{\partial^2}{\partial R^2} + V(x, y, R) \tag{6.10}$$

Here, x and y denote the electronic coordinates, R is the position of the nucleus. The mass M of the moving ion was chosen to be that of hydrogen. The potential $V(x, y, R)$ now takes the form:

$$\begin{aligned} V(x, y, R) = {} & \frac{1}{|R_L - R|} + \frac{1}{|R_R - R|} + \frac{erf\left(|x-y|/R_e\right)}{|x-y|} \\ & - \frac{erf\left(|R_L - x|/R_f\right)}{|R_L - x|} - \frac{erf\left(|R_R - x|/R_f\right)}{|R_R - x|} - \frac{erf\left(|R - x|/R_f\right)}{|R - x|} \\ & - \frac{erf\left(|R_L - y|/R_f\right)}{|R_L - y|} - \frac{erf\left(|R_R - y|/R_f\right)}{|R_R - y|} - \frac{erf\left(|R - y|/R_f\right)}{|R - y|} + E_0 \end{aligned} \tag{6.11}$$

The first three terms describe the Coulomb repulsion of the nuclei and the electron-electron repulsion. It should be noted that the third term also was screened by an error function in order to be consistent with the attractive interactions (the two electrons must pass each other which is not possible for a Coulomb repulsion). The other six terms describe the attraction between the electrons and the ions. Again, screened Coulomb interactions are employed. The charges of all ions were chosen to be one. R_f is a fixed cut-off parameter and was chosen as 1.5 Å in all regarded cases. The distance R_e in the third term allows to switch between cases of weak and strong nonadiabatic coupling as in the case of the simpler model (see chapter 3.3). The last term E_0 is chosen such that the global minimum of the potential is shifted to 0 eV.

6.4 Adiabatic potentials and eigenfunctions

In the following we focus on the case of parallel spins ($\alpha\alpha$). We again apply the Born-Oppenheimer approximation (see chapter 3.3) and solve the electronic Schrödinger equation for fixed nuclear coordinate R, which takes now the form (in a.u.):

$$\left\{-\frac{1}{2}\frac{\partial^2}{\partial x^2}-\frac{1}{2}\frac{\partial^2}{\partial y^2}+V(x,y,R)\right\}\varphi_n(x,y,R)=V_n(R)\varphi_n(x,y,R) \tag{6.12}$$

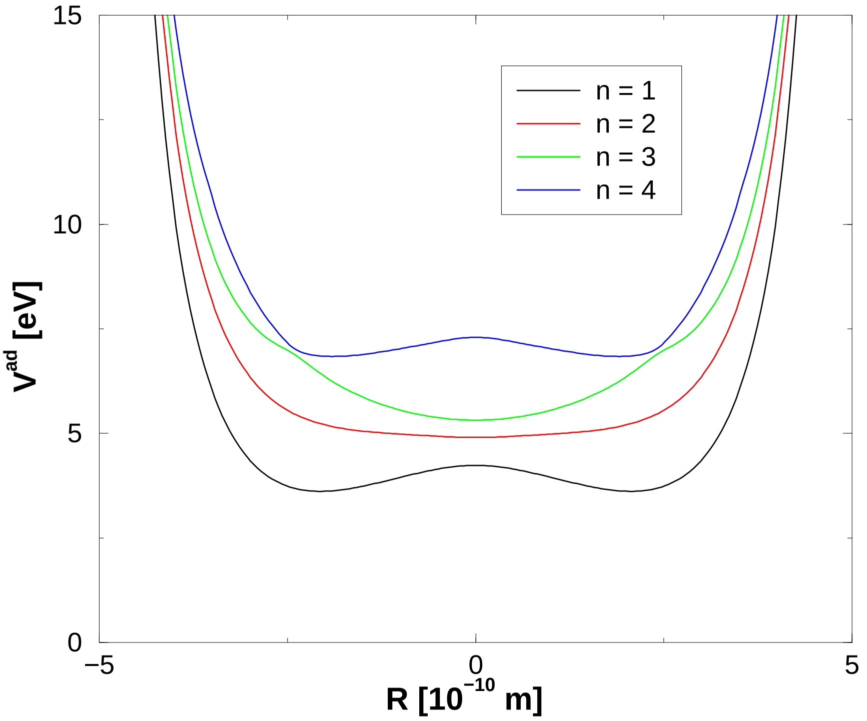

Figure 6.1: Adiabatic potential curves in the spin-parallel case ($\alpha\alpha$) and $R_e = 1.5$ Å for the electronic quantum numbers $n = 1 - 4$.

Figure 6.1 diplays the resulting adiabatic potential curves $V_n(R)$ for parallel electron spins and a parameter of $R_e = 1.5$ Å. The adiabatic ground state potential shows a double minimum structure as in the simpler model system. The higher electronic states ($n = 3, 4$) exhibit avoided crossings at about $R = \pm 2.5$ Å.

The electronic eigenfunctions $\{\varphi_n(x, y, R)\}$ define a complete orthonormal basis set and we may use them to expand the full wave function as:

$$\Psi(x, y, R) = \sum_n \psi_n(R)\varphi_n(x, y, R) \tag{6.13}$$

The expansion coefficients $\psi_n(R)$ depend on the nuclear coordinate and have the meaning of nuclear wave functions. Integration over the modulus squared of the expansion coefficients yields populations in different electronic states (see chapter 3.4.

The electronic functions have to be anti-symmetric with respect to exchange of x and y as the spin function is symmetric in the case of parallel spins. Figure 6.2 displays the electronic ground state wave functions for three different values of R. The symmetrical configurations $R = -3$ Å and $R = +3$ Å (figure 6.2 upper and lower panel) lead to identical probability densities which is due to the symmetry of the potential. The electrons have an equal probability to be located around either of the fixed nuclei at ±5 Å. The wave functions are identical as well, but this is only an artefact of a non-fixed phase factor during the numerical calculation. The symmetric configuration (figure 6.2, middle panel) exhibits a more complex structure: The probability density is concentrated around all three ions, with regions of less density in between.

Figure 6.3 shows the electronic eigenfunctions for the first electronically excited state for a nuclear coordinate of $R = -3, 0$ and $+3$ Å (upper, middle and lower panel). For $R = \pm 3$ Å the electrons have a higher probability to be close to each other and are only located around one fixed ion. For the symmetric configuration the electrons still have a certain probability to be located around all three nuclei, but now an additional node appears perpendicular to the $y = x$ diagonal.

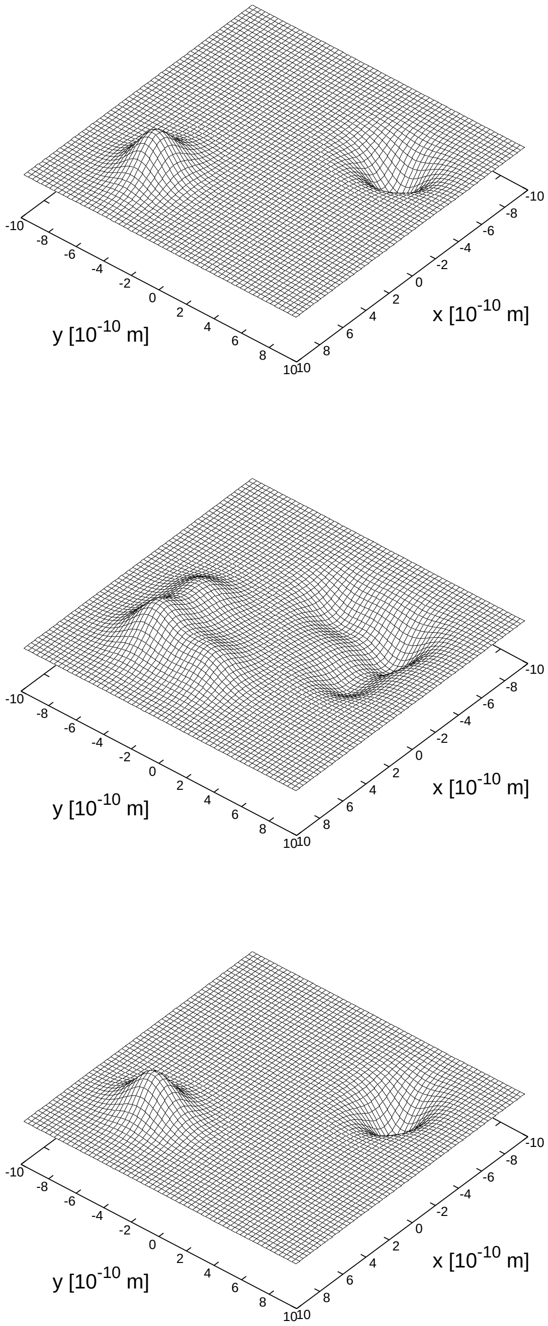

Figure 6.2: Electronic ground state functions in the spin-parallel case for fixed nuclear geometry. Upper panel: $R = -3$ Å, middle panel: $R = 0$ Å, lower panel: $R = +3$ Å. The cut-off parameter R_e was chosen to be 1.5 Å.

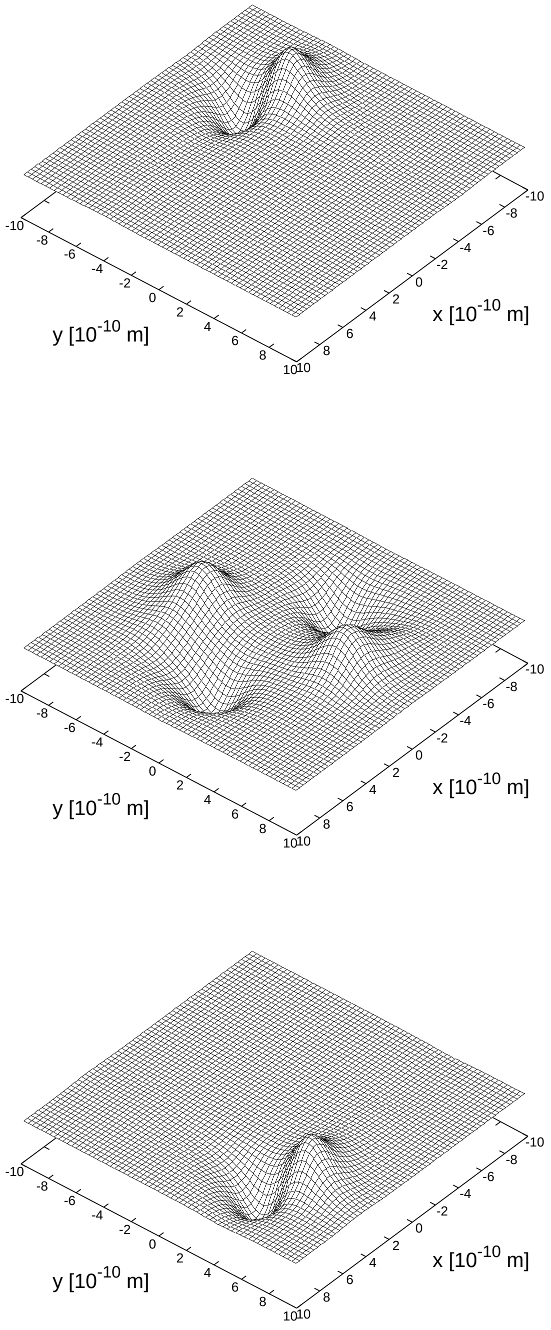

Figure 6.3: First electronic excited state functions in the spin-parallel case for fixed nuclear geometry. Upper panel: $R = -3$ Å, middle panel: $R = 0$ Å, lower panel: $R = +3$ Å. The parameter R_e was chosen to be 1.5 Å.

6.5 Quantum dynamics

In this section we give an example of how the previously defined electron localization function (see section 6.2) can be used to further characterize a time-dependent vibrational motion in an excited electronic state. For that we integrate the time-dependent Schrödinger equation numerically by applying the split-operator algorithm as described in chapter 2.1. The initial wave packet was of the form

$$\Psi(x, y, R, t = 0) = e^{-\beta(R-R_0)^2}\,\varphi_n(x, y, R), \tag{6.14}$$

where $R_0 = -2.7$ Å and $\beta = 0.2646$ Å^{-2}. In the presented example the wave packet was initially located in the first electronically excited state, hence $n = 2$.

In the numerical calculation we used a grid spacing of $\Delta R = 0.047$ Å (256 grid points from -6 to $+6$ Å) for the nucleus. The grids for the electrons had a spacing of $\Delta x = \Delta y = 0.078$ Å (256 grid points from -10 to $+10$ Å). The applied time step in the propagation was $\Delta t = 0.05$ fs.

We again calculate the time-dependent integrated densities which are given by

$$\begin{aligned} \rho(x,t) &= \int |\Psi(x,y,R,t)|^2\, dR\, dy, \\ \rho(R,t) &= \int |\Psi(x,y,R,t)|^2\, dx\, dy. \end{aligned} \tag{6.15}$$

Figure 6.4 displays the calculated nuclear density $\rho(R,t)$ (upper panel) during the vibrational motion. The nuclear wave packet is initially localized in the left half of the potential well and starts moving to the right side where it is repelled by the right fixed ion at about 40 fs. The incoming and the outgoing (reflected) parts of the nuclear wave packet give rise to a pronounced oscillatory structure.

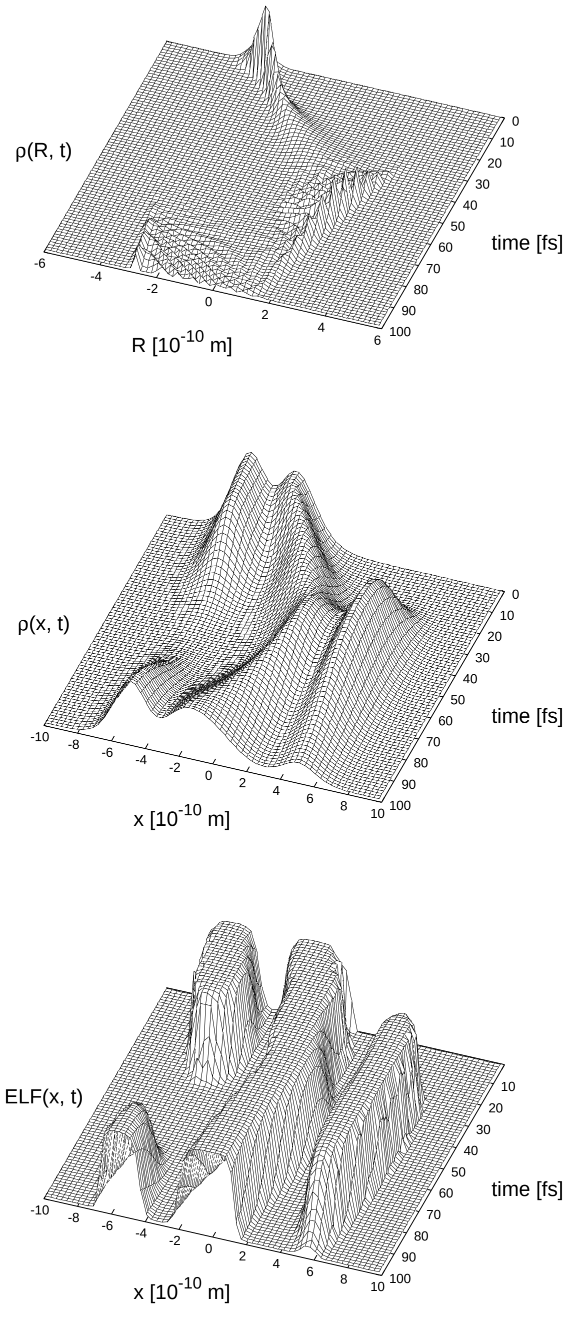

Figure 6.4: Time-dependent densities (upper and middle panel) and ELF (lower panel) for a vibrational motion in the first electronic excited state for the case of parallel spins. R_e was chosen to be 1.5 Å.

After that, the wave packet broadens substantially due to the anharmonicity of the potential. The electron density $\rho(x,t)$ (figure 6.4, middle panel) on the other hand exhibits a very smooth structure during the vibrational motion of the nucleus. At $t=0$ the electron density is accumulated around the left fixed nucleus and the moving ion and reflects the nodal structure of the electronic eigenstate (see figure 6.3). After some time, as the nucleus crosses the origin at $R=0$, the initial density drops to zero and two new maxima occur around the right fixed nucleus and the moving ion. This can be interpreted as a charge transfer from the left fixed ion to the right one due to the motion of the nucleus. However, this situation is not fully reversed at later times because of the broadening of the nuclear probability density, so that the electron density has three maxima at about $t=100$ fs.

From the electron density alone it is not clear how many electrons are involved in the charge transfer from the left to the right fixed ion. In order to shed some light into the process we calculated the *time-dependent electron localization function* $\mathrm{ELF}(x,t)$ [88] which is displayed in figure 6.4 (lower panel). Initially the ELF shows two domains of highly localized electrons: One is located around the left fixed ion at about $x=-5$ Å, the other is near the coordinate origin around $x=0$. The first domain vanishes completely during the vibrational motion of the nucleus (it is restored at later times), while the second one is only slightly modulated. Furthermore, as the mobile ion crosses the origin of the coordinate system, a third domain, located at the right fixed ion ($x=+5$ Å), gets visible which drops to zero again as the vibrational period completes.

The interpretation of the time-dependent ELF is not trivial, but the vanishing of the first domain at $x=-5$ Å and the appearance of a third domain at $x=+5$ Å indicates that one electron must have been removed from the left fixed nucleus and dragged to the right fixed ion as the ELF indicates localization of electron pairs. Now, remembering the fact that the electron density in the left part of the potential drops to zero, one can conclude that both electrons participate in the charge-transfer process. Further studies should be necessary to completely understand the meaning of the time-dependent electron localization function, but, nevertheless, it provides a useful tool to better understand the features of electron and nuclear dynamics in terms of electron localization and correlation.

6.6 Summary

In this chapter we were able to show, how an additional electron can be included into the previously studied simple model system in a straight-forward manner. Complications arise from the fact that one has to explicitly deal with the consequences of the Pauli principle. Also, the concept of “localizing” electrons by calculating the electron density has to be given up. Instead, we re-defined the *electron localization function* for an exact wave function. The ELF has proven to be very useful in chemistry already and should be a valuable tool to investigate time-dependent features of coupled electron and nuclear motion in more detail. The main advantage of our definition of the ELF is the possibility to not only treat the electronic ground state, but also excited states. Furthermore, restrictions imposed by the Born-Oppenheimer approximation can easily be removed. Unfortunately, nowadays computing facilities limit the procedure to systems with only a few degress of freedom. Future work will also have to consider the case of anti-parallel electron spins where a quantity providing the same information as ELF has to be defined. A proposal of how to define such a quantity is presented in the next chapter.

Chapter 7

Outlook: Electron localization in the anti-parallel spin case

In chapter 6.2 we re-defined the electron localization function (ELF) in terms of an exact wave function. This quantity provides useful information about the localization of electrons in the case of parallel electron spins. However, it is not possible to use the ELF in the case of anti-parallel spins in a two-electron system as the conditional probability $P_{\alpha\beta}(x)$ (eqn. (6.3)) vanishes in that case [51].

Returning to the derivation of the ELF for an exact wave function (chapter 6.2), the *conditional probability* to find one electron with spin σ at position x, if we know with certainty that the other electron with spin τ is located at y, is given by

$$P_{\sigma\tau}(x,y) = \frac{D_{\sigma\tau}(x,y)}{\sigma_\tau(y)}. \tag{7.1}$$

In the case of anti-parallel spins $(\alpha\beta)$ $P_{\alpha\beta}(x,y)$ does not vanish if $y \rightarrow x$ and thus the conditional probability is a direct measure for the localization of one electron. Unfortunately, this relation is an indirect one: $P_{\alpha\beta}(x,x)$, in the following denoted as $P_{\alpha\beta}(x)$, is small, if the first electron is strongly localized due to the Coulomb repulsion. In analogy to the definition of the ELF we may define an *anti-parallel spin electron localization function* $\mathrm{ALF}(x)$ which identifies regions in space where electrons of anti-parallel spin are localized:

$$\mathrm{ALF}(x) = \left[1 + (P_{\alpha\beta}(x)/T_{\mathrm{TF}}(x))^2\right]^{-1} \tag{7.2}$$

Here, $T_{\mathrm{TF}}(x)$ is again the Thomas-Fermi kinetic energy density in one dimension for the same spin density $\rho_\alpha(x)$. It takes the form

$$T_{\mathrm{TF}}(x) = \frac{4}{3}\pi^2 \rho_\alpha^3(x), \tag{7.3}$$

where one allows the states to be doubly occupied.

In order to illustrate the "meaning of ALF" let us regard a numerical example: We again employ the extended model Hamiltonian as described in chapter 6.3, but now for the case of anti-parallel spins ($\alpha\beta$). The electronic wave function has to be symmetric with respect to exchange of the electronic coordinates x and y. Choosing $R_e = 2.5$ Å leads to strongly coupled adiabatic states. Figure 7.1 displays the adiabatic potential curves of the lowest four electronic states. Various avoided crossings occur between the ground and the first excited state, but also between the second and third excited state.

It is to be expected that the time-dependent nuclear and electron dynamics exhibit clear signs of nonadiabatic behaviour. We investigate this question by solving the time-dependent Schrödinger equation numerically. The initial wave packet is chosen as

$$\Psi(x, y, R, t = 0) = e^{-\beta(R-R_0)^2}\, \varphi_2(x, y, R), \tag{7.4}$$

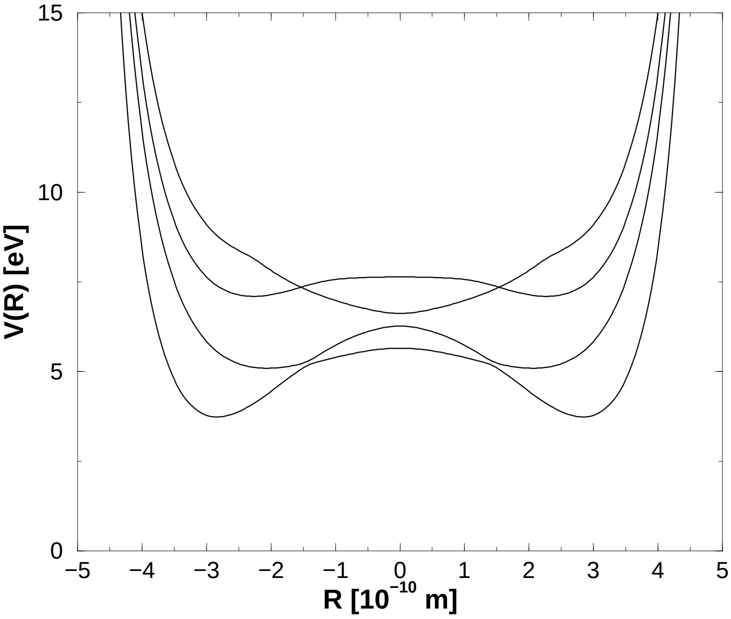

Figure 7.1: Adiabatic potential curves for the spin-parallel case ($\alpha\beta$) and $R_e = 2.5$ Å. The lowest four electronic states are displayed.

where $\varphi_2(x, y, R)$ are the electronic eigenfunctions of the first excited state, $R_0 = -3.5$ Å and $\beta = 0.2646$ Å^{-2}, respectively. The grid was chosen as described in chapter 6.5. The resulting integrated densities $\rho(R, t)$ and $\rho(x, t)$ are plotted in figure 7.2.

The nuclear density $\rho(R, t)$ (figure 7.2, left panel) exhibits the typical picture of a vibrational motion where reflection at an outer turning point results in a large dispersion. This behaviour can be understood, if one takes a look at the populations of the participating electronic states. They are defined as

$$P_n(t) = \int |\langle\varphi_n(x, y, R)|\Psi(x, y, R, t)\rangle_{x,y}|^2 \, dR, \tag{7.5}$$

where $\langle\varphi_n(x, y, R)|\Psi(x, y, R, t)\rangle_{x,y}$ is the component of the full wave function in electronic state n.

The calculated populations for $n = 1, 2$ are displayed in figure 7.3 and we

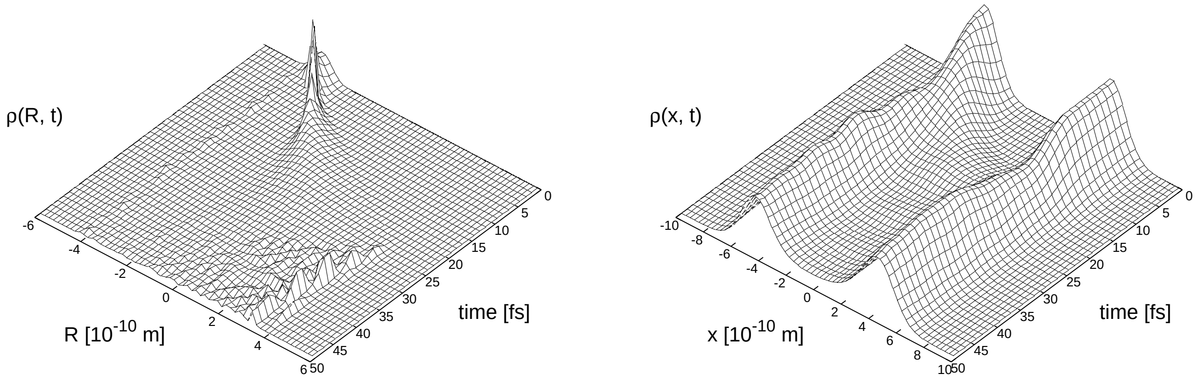

Figure 7.2: Nuclear (left panel) and electron density (right panel) calculated for a vibrational motion starting in the first electronically excited state for anti-parallel ($\alpha\beta$) electron spins. R_e was chosen as 2.5 Å.

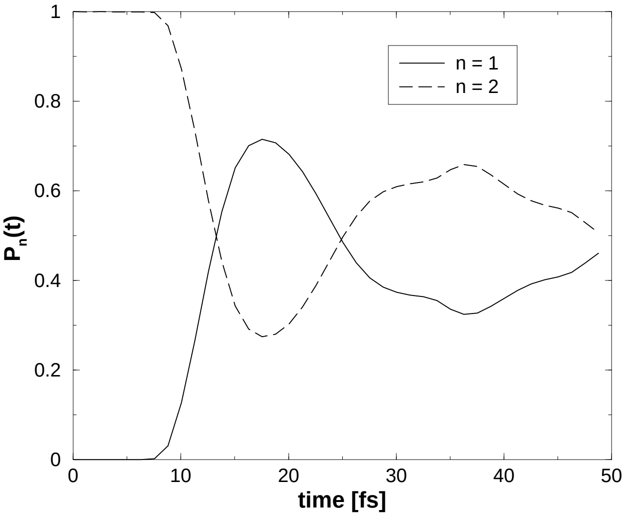

Figure 7.3: Time-dependent populations $P_n(t)$ in the ground ($n = 1$) and first excited ($n = 2$) electronic state.

may now interpret the nuclear motion taking place: Initially the nuclear wave packet is localized in the left well of the first electronically excited state. The initial population in the $n = 2$ state corresponds to the norm of the full wave function. After about 10 fs the wave packet reaches the first coupling region between the ground and first excited state at about $R = -1.5$ Å (see figure 7.1). A substantial amount of population is transferred to the electronic ground state, where the motion proceeds until the moving nucleus reaches the second coupling region around $R = +1.5$ Å at about 25 fs. Now the population gets partially back transferred to the first excited state, where the nuclear wave packet gets repelled by the right fixed ion at about 35 fs which gives rise to a strong oscillatory structure in the nuclear density.

Taking a look at the time-dependent electron density (figure 7.2, right panel), it seems as if hardly anything happens. The initial two maxima of the electron density at $x = \pm 5$ Å are only slightly shifted by the motion of the nucleus. This means, that the electron density exhibits little sign of the nonadiabatically coupled motion that takes place.

In order to gain some insight into the electronic motion which is due to the strong nonadiabatic coupling, we calculate the time-dependent ALF as defined in equation (7.2).

The result is shown in figure 7.4. Initially the $\mathrm{ALF}(x,t)$ resembles the structure of the electron density $\rho(x,t)$ (figure 7.2, right panel). Only some time later the motion of the mobile ion introduces some shaping in the two localization domains. At about 25 fs a considerable amount of population has been transferred to the electronic ground state (figure 7.3) and the right localization domain around $x = +5$ Å has vanished nearly completely. We can understand this result, if we remember that the motion of the nucleus introduces fast changes in the electronic structure and that the nonadiabatic coupling mixes electronic states. By moving the nucleus from near the left fixed ion to the right fixed ion, the

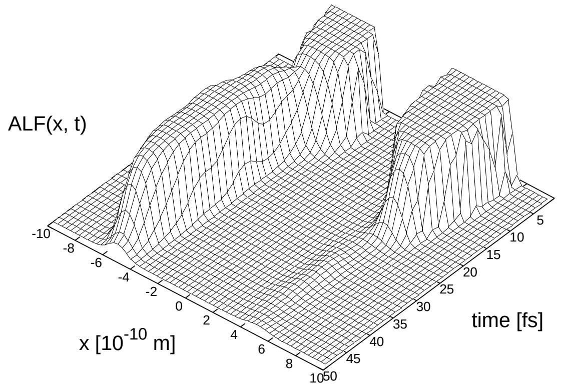

Figure 7.4: Time-dependent ALF in the case of $R_e = 2.5$ Å. Details are given in the text.

initially localized electrons get delocalized in the surroundings of the right fixed nucleus. Simultaneously the localization domain at the left fixed ion gets more compact. Another possible interpretation is in terms of an electronic wave packet generated by the nonadiabatic coupling to the motion of the nucleus which leads to dynamical changes in the localization of the electrons.

Concludingly, we might say, that the concept of electron localization can also be defined in the case of anti-parallel spins through a quantity that is very similar to the ELF. Into this ALF enters the *conditional probability* $P_{\alpha\beta}(x)$ to find an electron at position x, if we know with certainty that there is already another electron with opposite spin, directly. In the regarded example the ALF shows dynamical changes as a function of time due to a nonadiabatically coupled motion of the moving ion and the electrons. On the other hand, the electron density does not reflect these changes and we might conclude that the electron density is not sensitive enough to reveal details of such processes.

As an outlook, motivated by the presented results, the "meaning of ALF" has to be established by applying this new tool to other systems. The careful examination of its static and dynamical features should provide a deeper understanding of how electrons with anti-parallel spin are correlated and how electron localization changes due to nuclear motion or due to an external perturbation. This, of course, also applies to the time-dependent ELF that we introduced in the last chapter.

Summary

Within the framework of the *Graduiertenkolleg 690 "Electron density"* the subject of this work was to investigate the influence of nonadiabatic coupling on the dynamical changes of electronic and nuclear density. Here we enter scientific grounds which have not been cleared before: the properties of electron density have neither been discussed in the non-stationary case, nor for excited electronic states or for a coupled electron and nuclear dynamics. In order to remove these restrictions, it is necessary to describe the quantum mechanical motion of all particles in a system at the same level. This is only possible in very small systems. However, Shin and Metiu [37, 38] developed a model system that contains all necessary physical ingredients to describe a combined electronic and nuclear motion. It consists of only a single nuclear and electronic degree of freedom and the particle interaction is parameterized in such a way as to allow for a flexible switching between an adiabatic (Born-Oppenheimer type) and a strongly coupled dynamics.

We started our investigations by determining the "static" properties of the model system and calculated the electronic eigenfunctions, adiabatic potential curves, kinetic coupling elements and transition dipole moments. The latter are usually hardly accessible as one requires for their calculation the wave functions of electronically excited states; they exhibit singularities in the presence of nonadiabatic coupling. The potentials obtained for different parameterization show two distinct cases: In the first case the ground and first excited state are separated

by a large energetic gap which is the typical Born-Oppenheimer case; the second one exhibits an avoided crossing which results in a breakdown of the adiabatic approximation.

Due to the electronic properties of the system, the quantum dynamics in the two distinct situations is very different, which was illustrated by calculating nuclear and electron densities as a function of time. In the Born-Oppenheimer case, the electron density follows the vibrational motion of the nucleus. This is illustrated by two examples: The first example exhibits a simple vibrational motion taking place in one of the potential minima of the symmetric system. The other example demonstrates an isomerization process between the two stable ground state configurations and the time-dependent electron density reveals a typical charge transfer dynamics between the left and right fixed nucleus.

In the strongly coupled case the wave packet does not exhibit features caused by nonadiabatic coupling. However, a projection of the wave function onto the electronic ground and first excited state yields components of the nuclear wave function. One finds the usual picture obtained from solutions of the nuclear Schrödinger equation involving coupled electronic states. Interestingly, the electron density initially remains stationary in our particular example. Although the motion of the mobile ion extends over a large interval of the nuclear coordinate only small portions of electron density are transferred between the outer ions. Thus, the nuclear motion triggers charge transfer via nonadiabatic coupling.

The Laplacian of the electron density, which is often used in case of static problems, was extended to a time-dependent density and proved to be useful in the characterization of dynamical problems. We discussed the possibility to reverse the Born-Oppenheimer approximation and solve the nuclear Schrödinger equation for fixed electronic coordinates. This led to potential energy surfaces for the motion of the electrons. However, the neglected kinetic coupling elements between electronic and nuclear motion are much larger than those in the Born-

Oppenheimer approximation, leading to an, in principle, unphysical description of the regarded system.

The second part of this work showed that the model system can easily be modified to mimic often found bonding situations in diatomic molecules. The different situations can be characterized in terms of bound and dissociative adiabatic potential curves. We focussed our investigation on the case of an electronic predissociation: the electronic ground state is dissociative in the asymptotic limit of large internuclear distances. At small distances the ground and first excited state exhibit an avoided crossing leading to a "quasi-bound" situation. Such a problem is usally tackled by solving the nuclear Schrödinger equation with coupled potential surfaces in the diabatic description. This is not necessary within our model system and we were able to demonstrate how the character of the electron density changes during the fragmentation process. The nonadiabatic coupling mixed the properties of different electronic states and gave rise to a complicated transient electronic structure of the system.

In the third part we investigated, within our simple model, the influence of external electric fields on the correlated dynamics of electron and nucleus. Employing adiabatic potential curves, the structure of absorption spectra can be understood within the weak-field limit. For the above described Born-Oppenheimer case the adiabatically calculated spectrum was in very good agreement with the exact one. Still, even the existence of a small nonadiabatic coupling produces additional peaks in the spectrum unexplainable within an adiabatic description. In the strongly coupled case the spectrum obtained from an adiabatic approximation was not able to resemble the exact one. A simple *ad-hoc* diabatization yielded much better results.

Regarding the dynamics during a laser excitation process the electronic part of the wave function reached a stationary state on a very short time scale (in the sense that its structure did no longer change). The nuclear wave function stayed essentially frozen during this short time interval and only at longer times settled into a stationary state. In terms of time-dependent electron and nuclear densities this illustrates the famous *Franck-Condon principle*.

During the interaction with strong laser pulses many bound electronic and vibrational states are excited. The electron density reflected the classical-like quiver motion of the electron induced by the fast variations of the electric field. The nucleus did not follow these fast oscillations because of its much larger mass. The interaction produced an electronic and vibrational wave packet which should in principle be visible in any observable depending on the electronic and nuclear coordinates or momenta. This was demonstrated by means of the expectation value of the dipole moment which characterizes the polarization in the system.

The last part of this work then extended the original model system by adding another electron. This yields one nuclear and two electronic degrees of freedom. Within the new model it is necessary to explicitly deal with the consequences of the *Pauli principle*. The configuration space wave function is either symmetric or anti-symmetric with respect to an exchange of the two electrons. This corresponds to anti-parallel or parallel electron spins, respectively. As before, the parameterization of the particle interaction allows to switch between adiabatic and strongly coupled electron-nuclear dynamics.

The advantage of the extended model is that it already contains the physical properties of a many-electron system. Solving the time-dependent Schrödinger equation for a typical vibrational wave packet motion clearly indicated that the electron density is no longer suited to “localize” single electrons. The *electron localization function* (ELF) has proven to be very useful in chemistry for the description of bonding phenomena in molecules, clusters or intermetallic phases. We re-defined the ELF for an exact wave function and investigated for a simple wave packet dynamics in the case of parallel spins, how the ELF can be used to further characterize coupled electron and nuclear motion. The ELF exhibited changes in the localization domains during this process and could in principle be used to monitor the breaking and building of chemical bonds. The advantage of our definition of the ELF is that we are not restricted to the electronic ground state, but can also treat excited states. Furthermore, the restrictions imposed by the Born-Oppenheimer approximation can easily be removed.

Finally, we gave an outlook of how to define electron localization in the case of anti-parallel electron spins. We derived a quantity similar to the ELF denoted *anti-parallel spin electron localization function* (ALF) and demonstrated that the ALF allows to follow time-dependent changes of the electron localization by a numerical example. The time-dependent ALF clearly showed how electrons get delocalized by a coupled electronic and nuclear motion, whereas the time-dependent electron density did not reflect these changes.

In the future it is necessary to extend the concept of time-dependent ELF (and ALF) to more examples in order to gain an understanding of how dynamical changes in the electron and nuclear density influences the localization of the electrons. Nowadays, we are still rather limited in the number of degrees of freedom we can treat exactly as was done within this work. Nevertheless, a full understanding of time-dependent quantum processes can only be achieved by treating all particles quantum mechanically. While computers become constantly faster and acquire larger memory, the investigation of small model systems and molecules can provide usefull information that can be generalized to larger systems. As the ELF is one of the most popular tools used by chemists to visualize chemical bonding, the time-dependent ELF *might* be the tool to describe the changes in electron localization during chemical reactions in the future. With the emerging technologies to produce sub-femtosecond laser pulses which are, in principle, able to time-resolve the motion of electrons the field of electron dynamics has just begun.

Zusammenfassung

Gegenstand dieser Arbeit war es, im Rahmen des *Graduiertenkollegs 690 „Elektronendichte“*, den Einfluss nichtadiabatischer Kopplung auf die dynamischen Änderungen von Elektronen- und Kerndichten zu untersuchen. An dieser Stelle betreten wir wissenschaftliches Neuland: Die Eigenschaften der Elektronendichte wurden bisher weder für den nicht-stationären Fall, noch für angeregte elektronische Zustände oder für eine gekoppelte Elektronen- und Kerndynamik diskutiert. Um diese Einschränkung zu überwinden, ist es notwendig, die quantenmechanische Bewegung aller Teilchen eines Systems auf dem gleichen Niveau zu beschreiben. Dies ist nur für sehr kleine Systeme überhaupt möglich. Shin und Metiu [37,38] entwickelten ein Modellsystem, das alle notwendigen Voraussetzungen erfüllt, um eine gekoppelte Elektronen- und Kernbewegung zu untersuchen. Das Modell enthält jeweils nur einen Freiheitsgrad für Kerne und Elektronen und die Teilchenwechselwirkung ist so parametrisiert, dass ein flexibles Umschalten von einer adiabatischen (Born-Oppenheimer-Fall) zu einer stark gekoppelten Dynamik möglich wird.

Wir begannen unsere Arbeit mit einer Bestimmung der „statischen“ Eigenschaften des Modellsystems; so wurden elektronische Eigenfunktionen, adiabatische Potentialkurven, kinetische Kopplungselemente und Übergangsdipolmomente berechnet. Letztere sind selten verfügbar, da ihre Berechnung die Wellenfunktionen elektrisch angeregter Zustände erfordert und sie im Falle nichtadiabatischer Kopplung Singularitäten aufweisen. Die Potentiale, die man für verschiedene Parametrisierungen erhält, zeigen zwei deutlich unterschiedliche Fälle: Im ersten Fall, einer gültigen Born-Oppenheimer-Näherung, sind der Grund- und erste angeregte Zustand durch einen großen Energieunterschied voneindander getrennt. Der zweite Fall zeigt eine vermiedene Kreuzung, was zu einem Zusammenbruch der adiabatischen Näherung führt.

Aufgrund der elektronischen Eigenschaften des Systems unterscheidet sich die Quantendynamik in den beiden betrachteten Fällen grundlegend. Dies wurde durch die Berechnung zeitabhängiger Kern- und Elektronendichten veranschaulicht. Im Born-Oppenheimer-Fall folgt die Änderung der Elektronendichte der Schwingungsbewegung des Kerns, was durch zwei Beispiele belegt wurde: Das erste Beispiel zeigt eine einfache Schwingungsbewegung, die in einem der Potentialtöpfe des symmetrischen Systems stattfindet. Das andere Beispiel stellt eine Isomerisierung zwischen den zwei stabilen Grundzustandskonfigurationen dar, und die zeitabhängige Elektronendichte lässt die typische Dynamik eines Ladungstransfers zwischen Atomkernen erkennen.

Im Falle starker Kopplung zeigt das Wellenpaket keine Anzeichen einer nichtadiabatischen Kopplung. Die Komponenten der Kernwellenfunktion im Grund- und ersten elektronisch angeregten Zustand lässt sich jedoch durch Projektion auf die zugehörigen Zustände berechnen. Man findet das übliche, aus der Lösung der Schrödingergleichung der Kerne für gekoppelte elektronische Zustände, erhältliche Bild. Interessanterweise bleibt die Elektronendichte in unserem Beispiel anfangs stationär. Obwohl sich die Bewegung des Kernes über ein großes Intervall der Kernkoordinate erstreckt, werden nur kleine Teile der Elektronendichte zwischen den äußeren Kernen übertragen. Das heißt, die Bewegung des Kerns verursacht einen Ladungstransfer aufgrund nichtadiabatischer Kopplung.

Die oft für zeitunabhängige Fragestellungen herangezogene zweite Ableitung der Elektronendichte wurde auf eine zeitabhängige Dichte erweitert und erwies sich ebenfalls zur Untersuchung dynamischer Prozesse als nützlich. Das „Umkehren“ der Born-Oppenheimer-Näherung und Lösen der Schrödingergleichung der Kerne für feste Elektronenkoordinaten ergab Potentialflächen für die Bewegung der Elektronen. Allerdings sind die vernachlässigten Kopplungselemente zwischen Elektronen- und Kernbewegung viel größer als die in der Born-Oppenheimer-Näherung, was letztendlich zu einer nicht-physikalischen Beschreibung des betrachteten Systems führt.

Der zweite Teil der Arbeit zeigte, dass das Modellsystem leicht modifiziert werden kann, um in realen Molekülen vorhandene Bindungsituationen zu simulieren. Die verschiedenen Fälle sind durch gebundene und dissoziative adiabatische Potentialkurven charakterisiert. Speziell untersuchten wir eine elektronische Prädissoziation: Das bedeutet, dass der elektronische Grundzustand im asymptotischen Grenzfall großer Kernabstständee dissoziativ ist. Der Grund- und erste angeregte Zustand besitzen für kleine Kernabstände eine vermiedene Kreuzung, was zu einer Kopplung gebundener Zustände an das Kontinuum führt. Normalerweise löst man in solch einem Falle die Schrödingergleichung der Kerne für gekoppelte Potentialflächen im diabatischen Bild. Innerhalb unseres Modellsystems ist das nicht notwendig und wir konnten zeigen, wie sich die Elektronendichte während des Fragmentierungsprozesses ändert. Die nichtadiabatische Kopplung mischt die Eigenschaften der verschiedenen elektronischen Zustände und führt zu einer komplizierten, transienten elektronischen Struktur.

Im dritten Teil der Arbeit untersuchten wir — wiederum in unserem Modellsystem — den Einfluss externer elektrischer Felder auf die korrelierte Elektronen- und Kerndynamik. Unter Zuhilfenahme adiabatischer Potentiale kann die Struktur von Absorptionsspektren für schwache Felder verstanden werden. Für den oben beschriebenen Fall gültiger Born-Oppenheimer-Näherung, zeigte das adiabatisch berechnete Spektrum sehr gute Übereinstimmung mit dem exakten. Dennoch erzeugt schon eine kleine nichtadiabatische Kopplung zusätzliche Strukturen im Spektrum, die im Rahmen einer adiabatischen Näherung nicht zu erklären sind. Im Falle starker nichtadiabatischer Wechselwirkung konnte ein aus einer adiabatischen Rechnung gewonnenes Spektrum das exakte nicht reproduzieren. Allerdings ist es möglich innerhalb eines einfachen Diabatisierungsschemas bessere Ergebnisse zu erhalten.

Die Berechnung der Dynamik während einer Laseranregung ergab, dass der elektronische Teil der Wellenfunktion schon nach sehr kurzer Zeit einen stationären Zustand erreichte (in dem Sinne, dass sich seine Struktur nicht mehr ändert). Die Kernwellenfunktion blieb in diesem kurzen Zeitraum mehr oder minder eingefroren und erst nach längerer Zeit erreichte auch sie einen stationären Zustand. Im Sinne zeitabhängiger Elektronen- und Kerndichten veranschaulicht dies das *Franck-Condon-Prinzip.*

Während der Wechselwirkung mit starken Laserpulsen werden viele gebundene elektronische und Schwingungszustände angeregt. Die Elektronendichte zeigte die einer klassischen Bewegung sehr ähnliche, Zitterbewegung des Elektrons, die durch die schnellen Änderungen des elektrischen Feldes hervorgerufen wird. Der Kern folgte aufgrund seiner wesentlich höheren Masse diesen schnellen Oszillationen nicht. Die Wechselwirkung generiert ein Schwingungs- und elektronisches Wellenpaket, was sich prinzipiell in jeder Observablen, die von der Kern- oder Elektronenkoordinate oder deren Impulsen abhängt, widerspiegeln sollte. Der Erwartungswert des Dipolmoments, der die Polarisierung im System beschreibt, veranschaulichte dies.

Im letzten Teil dieser Arbeit erweiterten wir das ursprüngliche Modell durch Hinzufügen eines zweiten Elektrons. Man erhält dadurch einen Kern- und zwei elektronische Freiheitsgrade. Innerhalb des neuen Modells ist es allerdings nötig, die Konsequenzen des *Pauli-Prinzips* direkt zu berücksichtigen. Die Wellenfunktion im Ortsraum ist entweder symmetrisch oder anti-symmetrisch bezüglich des Austauschs der beiden Elektronen. Dies entspricht anti-parallelen, bzw. parallelen Spins der Elektronen. Auch hier erlaubt die Parametrisierung zwischen einer adiabatischen und einer stark gekoppelten Elektronen- und Kerndynamik umzuschalten.

Der Vorteil des erweiterten Modells liegt darin, dass es bereits die physikalischen Eigenschaften eines Mehrelektronensystems enthält. Die Lösung der Schrödingergleichung für eine typische Schwingungsbewegung legte nahe, dass die Elektronendichte sich nicht länger eignet, die Lokalisierung der Elektronen zu charakterisieren. In der Chemie hat sich die *Elektronenlokalisierungsfunktion* (ELF) zur Beschreibung der Bindungsituation in Molekülen, Clustern und intermetallischen Phasen als sehr nützlich erwiesen. Durch Neudefinition der ELF für eine exakte Wellenfunktion, konnten wir für eine einfache Wellenpaketdynamik im Falle paralleler Elektronenspins untersuchen, inwieweit sich die ELF eignet, eine gekoppelte Elektronen- und Kernbewegung genauer zu analysieren. Die ELF zeigte die Änderung in den Lokalisierungsdomänen während eines solchen Prozesses und sollte sich prinzipell dazu eignen, den Bruch und die Neubildung chemischer Bindungen zeitaufgelöst zu beobachten. Der Vorteil unserer Definition der ELF ist, dass wir nicht auf den elektronischen Grundzustand beschränkt sind, sondern auch angeregte Zustände betrachten können. Außerdem können die Einschränkungen der Born-Oppenheimer-Näherung leicht überwunden werden.

Schließlich gaben wir einen Ausblick, wie Elektronenlokalisierung im Falle anti-paralleler Spins definiert werden könnte. Die von uns abgeleitete *Elektronenlokalisierungsfunktion für anti-parallelen Spin* (ALF) erlaubt es, die zeitabhängige Änderung der Elektronenlokalisierung zu beobachten, wie wir an einem numerischen Beispiel zeigen konnten. Die zeitabhängige ALF zeigte deutlich, wie Elektronen durch eine gekoppelte Elektronen- und Kernbewegung delokalisiert werden, wohingegen die zeitabhängige Elektronendichte diese Änderungen nicht aufwies.

In der Zukunft wird es notwendig sein, das Konzept der zeitabhängigen ELF (und ALF) auf weiter Beispiele auszudehnen, um ein Verständnis dafür zu gewinnen, wie dynamische Änderungen in der Elektronen- und Kerndichte die Lokalisierung von Elektronen beeinflusst. Wir sind heutzutage in der Anzahl der Freiheitsgrade, die sich — wie in dieser Arbeit geschehen — exakt beschreiben lassen, immer noch sehr eingeschränkt. Trotzdem lässt sich ein volles Verständnis von zeitabhängigen Quantenprozessen nur dann erreichen, wenn alle Teilchen eines Systems quantenmechanisch behandelt werden. In der Zeit, in der Computer schneller und schneller werden und immer mehr Speicher bekommen, kann die Untersuchung kleiner Modellsysteme und Moleküle nützliche Informationen liefern, die sich auf größere Systeme übertragen lassen. Da die ELF eines der beliebtesten Werkzeuge der Chemiker zur Visualisierung der chemischen Bindung ist, *könnte* die zeitabhängige ELF in der Zukunft das Werkzeug sein, mit dessen Hilfe sich Änderungen in der Elektronenlokalisierung während chemischer Reaktionen beschreiben lassen. Mit den gerade aufkommenden Technologien der Erzeugung von sub-Femtosekunden-Laserpulsen, die im Prinzip in der Lage sind, die Bewegung von Elektronen zeitaufzulösen, ist das Forschungsgebiet der Elektronendynamik gerade erst im Entstehen.

Appendix A

Diabatization of two coupled adiabatic potentials

In chapter 5.2 we described shortly how to transform two coupled adiabatic potential curves into a set of two diabatic potentials plus a potential coupling. Here, we describe this procedure in more detail. Starting from the adiabatic curves $V^a(R)$ (figure A.1) in the original model system described in section 3.2, calculated for a cut-off parameter $R_c = 2.5$ Å, we introduce a linear fit to the adiabatic potential curves of the two lowest electronic states at the coupling region at about $R = 0$ Å. This is done by connecting the left branch of the electronic ground state potential with the right branch of the first electronically excited state curve and the other way round.

The two resulting diabatic potential curves $V^d(R)$ are displayed in figure A.2. The unitary transformation from the adiabatic to the diabatic representation is chosen such that the non-adiabatic kinetic coupling elements are minimized. As a result the potential operator matrix is no longer diagonal, but contains off-diagonal coupling elements. The Hamiltonian takes the form

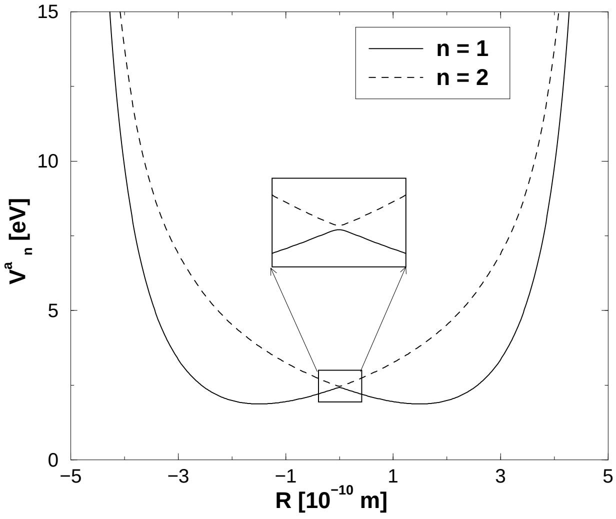

Figure A.1: Adiabatic potential curves for the first two electronic states in the strong-coupling case ($R_c = 2.5$ Å) with zoom into the coupling region around $R = 0$ Å. See chapter 5.2 for details.

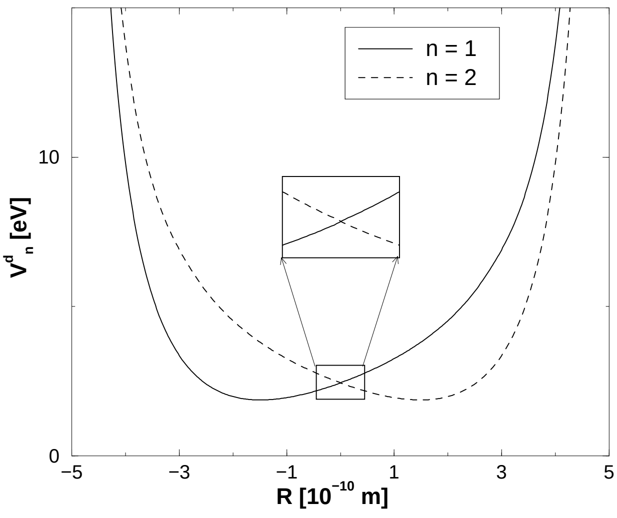

Figure A.2: Diabatic potential curves for the first two electronic states in the strong-coupling case ($R_c = 2.5$ Å) resulting from a linear fit in the coupling region around $R = 0$ Å. See chapter 5.2 for details.

$$\mathbf{H^d} = \begin{pmatrix} V_1^d(R) & V_{12}(R) \\ V_{12}(R) & V_2^d(R) \end{pmatrix} + \begin{pmatrix} T_1(R) & 0 \\ 0 & T_2(R) \end{pmatrix}. \tag{A.1}$$

The potential matrix $\mathbf{V}$ is diagonal in the adiabatic representation. This means that the unknown coupling element $V_{12}(R)$ can be calculated by solving the following system of linear equations

$$\begin{vmatrix} V_1^d(R) - \lambda & V_{12}(R) \\ V_{12}(R) & V_2^d(R) - \lambda \end{vmatrix} = 0, \tag{A.2}$$

where $\lambda = V_n^a(R)$ $(n = 1, 2)$ are the adiabatic potential curves. It follows that $V_{12}(R)$ takes the form:

$$V_{12}(R) = \sqrt{\left(V_2^a(R) - \frac{V_1^d(R) + V_2^d(R)}{2}\right)^2 - \frac{\left(V_1^d(R) - V_2^d(R)\right)^2}{4}} \tag{A.3}$$

Appendix B

Thomas-Fermi kinetic energy density in one dimension

In the definition of the ELF the Thomas-Fermi kinetic energy density of the uniform electron gas serves as a normalization function. In order to derive this quantity for a one-dimensional problem we follow the derivation given in reference [89].

To calculate the kinetic energy density of uniformly distributed electrons in one dimension, space is divided in small intervals of length l. Each interval contains a fixed number of electrons ΔN (which may be different in different intervals), but are restricted to spin σ (either only α or only β). Furthermore, it is assumed that the electrons behave like independent fermions at the temperature $T = 0K$. The intervals are all treated as being independent from each other.

The energy levels of a particle in a one-dimensional box are given by

$$\epsilon(n) = \frac{h^2 n^2}{8ml^2}, \tag{B.1}$$

where $n = 1, 2, 3, ...$ and m is the mass. For large quantum numbers n the number of distinct energy levels with energy smaller than ϵ can be approximated as

$$\Phi(\epsilon) = \frac{n}{2} = \frac{l}{2h}(8m\epsilon)^{\frac{1}{2}}. \tag{B.2}$$

The number of energy levels between ϵ and $\epsilon + \delta\epsilon$ is then

$$g(\epsilon) = \frac{d}{d\epsilon}\Phi(\epsilon) = \frac{l}{4h}(8m)^{\frac{1}{2}}\epsilon^{-\frac{1}{2}}. \tag{B.3}$$

$g(\epsilon)$ is called the *density of states.* To calculate the total energy of an interval with ΔN electrons, one needs the probability for a state with energy ϵ to be occupied. This probability is given by the Fermi-Dirac distribution $f(\epsilon)$, where μ is the chemical potential and $\beta = 1/kT$:

$$f(\epsilon) = \frac{1}{1 + e^{\beta(\epsilon - \mu)}} \tag{B.4}$$

$f(\epsilon)$ reduces to a step function at $T = 0K$:

$$f(\epsilon) = \left\{ \begin{array}{c} 1,\ \epsilon < \epsilon_F \\ 0,\ \epsilon > \epsilon_F \end{array} \right\} \text{as}\, \beta \to \infty \tag{B.5}$$

ϵ_F is the so-called *Fermi energy.* All states with energy smaller ϵ_F are occupied, those with energy greater than ϵ_F are unoccupied. The Fermi energy is the zero-temperature limit of the chemical potential μ.

The total energy of the electrons in an interval is the sum over all contributions from different states:

$$\begin{aligned}\Delta E &= \int \epsilon f(\epsilon) g(\epsilon)\, d\epsilon \\ &= \frac{l}{4h}(8m)^{\frac{1}{2}} \int\limits_0^{\epsilon_F} \epsilon^{\frac{1}{2}}\, d\epsilon \\ &= \frac{l}{4h}(8m)^{\frac{1}{2}}\, \frac{2}{3}\, \epsilon_F^{\frac{3}{2}} = \frac{l}{6h}(8m)^{\frac{1}{2}}\, \epsilon_F^{\frac{3}{2}}\end{aligned} \tag{B.6}$$

Usually a factor of 2 enters here, because each level can be doubly occupied by one electron with spin α and another with spin β. As we restrict the electrons to only have spin α or β, we consequently omitted this factor. The Fermi energy ϵ_F is related to the number of electrons ΔN in an interval by:

$$\begin{aligned}\Delta N &= \int f(\epsilon) g(\epsilon)\, d\epsilon \\ &= \frac{l}{4h}(8m)^{\frac{1}{2}} \int\limits_0^{\epsilon_F} \epsilon^{-\frac{1}{2}}\, d\epsilon \\ &= \frac{l}{2h}(8m)^{\frac{1}{2}}\, \epsilon_F^{\frac{1}{2}}\end{aligned} \tag{B.7}$$

Now taking the expression for ϵ_F from equation (B.7), the Fermi energy can be eliminated from equation (B.6) leading to:

$$\begin{aligned}\Delta E &= \frac{l}{6h}(8m)^{\frac{1}{2}} \left(\frac{2\Delta N h}{l(8m)^{\frac{1}{2}}}\right)^3 \\ &= \frac{lh^2}{6m}\left(\frac{\Delta N}{l}\right)^3\end{aligned} \tag{B.8}$$

Equation (B.8) is a relation between the total kinetic energy and spin density $\rho_\sigma = \Delta N/l$ for each interval of length l. Summing up over all contributions from different intervals, replacing l by a grid spacing Δx and taking the limit $l \to 0$ ($\Delta x \to 0$), we find (in a.u.):

$$
\begin{aligned}
T_\sigma[\rho] &= \lim_{\Delta x \to 0} \sum \frac{2}{3}\pi^2 \rho_\sigma^3(x)\,\Delta x \\
&= \frac{2}{3}\,\pi^2 \int \rho_\sigma^3(x)\,dx \qquad \text{(B.9)}
\end{aligned}
$$

In our treatment the electron density and the two-body density matrix were normalized to **1**, i.e., $\int \rho_\sigma(x)\,dx = 1$. However, integration of the electron density over the complete space must yield the number of particles N_σ with spin σ [89]:

$$\int \rho_\sigma(x)\,dx = N_\sigma \qquad \text{(B.10)}$$

As the TF energy is an integral over the third power of the electron density, we can finally write the normalized TF energy density as

$$T_\sigma^0(x) = \frac{2}{3}\pi^2 N^3 \rho_\sigma^3(x). \qquad \text{(B.11)}$$

For our system consisting of two electrons with the same spin $N = 2$ which yields equation (6.9).

Bibliography

[1] J. Manz, *Molecular Wavepacket Dynamics: Theory for Experiments 1926–1996*, in: V. Sundström (ed.), *Femtochemistry and Femtobiology: Ultrafast Reaction Dynamics at Atomic–Scale Resolution*, Nobel Symposium 101, Imperial College Press, London **1997**.

[2] A. H. Zewail, *Femtochemistry Vol. 1, 2*, World Scientific, Singapur **1994**.

[3] D. Gottlieb, S. S. Orszag, *Numerical analysis of Spectral Methods: Theory and Applications*, SIAM, Philadelphia **1977**.

[4] M. D. Feit, F. A. Fleck, Jr., *Appl. Opt.* **1980**, *19*, 2240.

[5] C. Leforestier, R. H. Bisseling, C. Cerjan, M. D. Feit, R. Friesner, A. Guldberg, A. Hammerich, G. Jolicard, W. Karrlein, H.-D. Meyer, N. Kipkin, O. Roncero, R. Kosloff, *J. Comput. Phys.* **1991**, *94*, 59.

[6] H. Tal-Ezer, R. Kosloff, *J. Chem. Phys.* **1984**, *81*, 3967.

[7] I. B. Bersuker, *Chem. Rev.* **2001**, *101*, 1067.

[8] G. Herzberg, *Spectra of Diatomic Molecules*, van Nostrand Reinhold, New York **1950**.

[9] E. S. Medvedev, V. I. Osherov, *Radiationless Transitions in Polyatomic Molecules*, Springer Series in Chemical Physics 57, Springer-Verlag, Berlin, Heidelberg **1995**.

[10] *Conical Intersections: Electronic Structure, Dynamics and Spectroscopy*, edited by: W. Domcke, D. R. Yakony, H. Köppel, World Scientific, Singapore, **2004**.

[11] W. Domcke, G. Stock, *Adv. Chem. Phys.* **1997**, *100*, 1.

[12] R. H. Bisseling, R. Kosloff, B. Gerber, M. A. Ratner, L. Gibson, C. Cerjan, *J. Chem. Phys.* **1987**, *87*, 2760.

[13] M. H. Beck, A. Jäckle, G. A. Worth, H.-D. Meyer, *Physics Reports* **2000**, *324*, 1.

[14] G. Worth, H.-D. Meyer, L. S. Cederbaum, *J. Chem. Phys.* **1996**, *105*, 4412.

[15] D. K. Remler, P. A. Madden, *Mol Phys.* **1990**, *70*, 921.

[16] M. C. Payne, M. P. Teter, D. C. Allan, T. A. Arias, J. D. Joannopoulos, *Rev. Mod. Phys.* **1992**, *64*, 339.

[17] E. Deumens, A. Diz, R. Longo, Y. Öhm, *Rev. Mod. Phys.* **1994**, *66*, 917.

[18] E. Deumens, Y. Öhrn, *J. Phys. Chem. A* **2001**, *105*, 2660.

[19] K. C. Kulander, K. R. Sandhya Devi, S. E. Koonin, *Phys. Rev. A* **1982**, *25*, 2968.

[20] D. Tiszauer, K. C. Kulander, *Phys. Rev. A* **1984**, *29*, 2909.

[21] D. Tiszauer, K. C. Kulander, *Comput. Phys. Commun.* **1991**, *63*, 351.

[22] K. Runge, D. A. Micha, E. Q. Feng, *Int. J. Quantum Chem.: Quantum Chem. Symp.* **1990**, *24*, 781.

[23] D. A. Micha, K. Runge, *Electronic energy and charge transfer in slow atomic collisions: a time-dependent molecular orbital approach*, in: *Time-Dependent Quantum Molecular Dynamics*, edited by J. Broeckhove and L. Lathouwers, Plenum, New York **1992**.

[24] K. Runge, *A Time-Dependent Many-Electron Apporach to Atomic and Molecular Interactions*, Ph.D. thesis, University of Florida, Gainesville **1993**.

[25] M. J. Field, *J. Chem. Phys.* **1992**, *96*, 4583.

[26] K. V. Mikkelsen, E. Dalgaard, P. Swanstrom, *J. Phys. Chem.* **1989**, *91*, 3081.

[27] S. Chelkowski, T. Zuo, O. Atabek, A. D. Bandrauk, *Phys. Rev. A* **1995**, *52*, 2977.

[28] S. Chelkowski, M. Zamojski, A. D. Bandrauk, *Phys. Rev. A* **2001**, *63*, 023409.

[29] H. Yu, T. Zuo, A. D. Bandrauk, *Phys. Rev. A* **1996**, *54*, 3290.

[30] S. Chelkowski, C. Foisy, A. D. Bandrauk, *Phys. Rev. A* **1996**, *57*, 1176.

[31] I. Kawata, H. Kono, A. D. Bandrauk, *Phys. Rev. A* **2001**, *64*, 043411.

[32] D. G. Lappas, R. van Leeuwen, *J. Phys. B* **1998**, *31*, L249.

[33] M. Lein, E. K. U. Gross, V. Engel, *J. Phys. B* **2000**, *33*, 433.

[34] M. Lein, E. K. U. Gross, V. Engel, *Phys. Rev. Lett.* **2000**, *85*, 4707.

[35] M. Lein, V. Engel, E. K. U. Gross, *Phys. Rev. A* **2001**, *64*, 023406.

[36] M. Lein, T. Kreibich, E. K. U. Gross, V. Engel, *Phys. Rev. A* **2002**, *65*, 033403.

[37] S. Shin, H. Metiu, *J. Chem. Phys.* **1995**, *102*, 9285.

[38] S. Shin, H. Metiu, *J. Phys. Chem.* **1996**, *100*, 7867.

[39] M. Born, K. Huang, *Theory of Crystal Lattices*, Oxford University Press, London **1954**.

[40] F. Jensen, *Introduction to Computational Chemistry*, John Wiley & Sons, New York **1999**.

[41] N. C. Handy, A. M. Lee, *Chem. Phys. Lett.* **1996**, *252*, 425.

[42] I. N. Levine, *Quantum chemistry*, 3rd edition, Allyn and Bacon Inc., Boston **1983**.

[43] W. P. Schleich, *Quantum Optics in Phase Space*, Wiley-VCH, Berlin, New York **2001**.

[44] Christoph Meier, *Theoretische Untersuchungen zur Photoelektronenspektroskopie kleiner Moleküle mit kurzen und intensiven Laserpulsen*, Dissertation, Universität Freiburg i. Br. **1995**.

[45] R. Schinke, *Photodissociation Dynamics*, Cambridge University Press, Cambridge **1993**.

[46] Ch. Meier, V. Engel, *Pump-Probe Ionization Spectroscopy of a Diatomic Molecule: The Sodium Dimer as a Prototype Example*, in: J. Manz, L. Wöste (eds.), *Femtosecond Chemistry*, p. 369 ff., VCH, Weinheim **1995**.

[47] G. Baym, *Lectures on Quantum Mechanics*, Addison-Wesley, New York **1993**.

[48] P. H. Bucksbaum, A. Zavriyev, in: A. D. Bandrauk, S. C. Wallace (eds.), *Coherence Phenomena in Atoms and Molecules in Laser Fields*, Plenum, New York **1992**.

[49] R. Loudon, *The Quantum Theory of Light*, Clarendon, Oxford **1983**.

[50] J. K. Burdett, T. A. McCormick, *J. Phys. Chem. A* **1998**, *102*, 6366.

[51] A. D. Becke, K. E. Edgecombe, *J. Chem. Phys.* **1990**, *92*, 5397.

[52] A. D. Becke, *J. Chem. Phys.* **1988**, *88*, 1053.

[53] A. D. Becke, M. R. Roussel, *Phys. Rev. A* **1989**, *39*, 3761.

[54] A. D. Becke, *Int. J. Quantum Chem.* **1985**, *27*, 585.

[55] R. McWeeny, B. T. Sutcliffe, *Methods of Molecular Quantum Mechanics*, Academic Press, London **1976**.

[56] Y. Tal, R. F. W. Bader, *Int. J. Quantum Chem. Quantum Chem. Symp.* **1978**, *12*, 153.

[57] M. D. Feit, J. A. Fleck, Jr., A. Steiger, *J. Comp. Phys.* **1982**, *47*, 412.

[58] J. A. Fleck, Jr., J. R. Morris, M. D. Feit, *Appl. Phys.* **1976**, *10*, 129.

[59] M. Frigo, S. G. Johnson, *ICASSP conference proceedings* **1998**, *3*, 1381.

[60] A. D. Bandrauk, H. Shen, *Chem. Phys. Lett.* **1991**, *176*, 428.

[61] H. Yoshida, *Phys. Lett. A* **1990**, *150*, 262.

[62] R. Kosloff, H. Tal-Ezer, *Chem. Phys. Lett.* **1986**, *127*, 223.

[63] A. Messiah, *Quantum Mechanics*, Volumes I and II, North-Holland, Amsterdam **1972**.

[64] J. H. Eberly, N. B. Narozhny, J. J. Sanchez-Mondragon, *Phys. Rev. Lett* **1080**, *44*, 1323.

[65] L. Sh. Averbukh, N. F. Perelman, *Phys. Lett. A* **1989**, *139*, 449.

[66] O. Knospe, R. Schmidt, *Phys. Rev. A* **1996**, *54*, 1154.

[67] C. Leichtle, I. Sh. Averbukh, W. P. Schleich, *Phys. Rev. Lett* **1996**, *77*, 3999.

[68] V. A. Ermoshin, M. Erdmann, V. Engel, *Chem. Phys. Lett* **2002**, *356*, 29.

[69] R. F. W. Bader, *Atoms in Molecules*, Clarendon, Oxford, **1994**.

[70] H. Köppel, W. Domcke, L. S. Cederbaum, *Adv. Chem. Phys.* **1984**, *57*, 59.

[71] M. S. Child, *Molecular Collision Theory*, Dover Publications, Mineola, **1996**.

[72] B. H. Bransden, M. R. C. Mcdowell, *Charge Exchange and the Theory of Ion-Atom Collisions*, Clarendon Press, Oxford **2003**.

[73] C. A. Mead, *J. Chem. Phys.* **1979**, *70*, 2276.

[74] V. Engel, H. Metiu, *J. Chem. Phys.* **1989**, *90*, 6117.

[75] M. Grønager, N. Henriksen, *J. Chem. Phys.* **1998**, *109*, 4335.

[76] E. J. Heller, *Acc. Chem. Res.* **1981**, *14*, 368.

[77] V. Sidis, *Adv. Chem. Phys.* **992**, *82*, 73.

[78] T. Pacher, L. S. Cederbaum, H. Köppel, *Adv. Chem. Phys.* **1993**, *84*, 293.

[79] J. Alvarellos, H. Metiu, *J. Chem. Phys.* **1988**, *88*, 4957.

[80] G. Herzberg, *Molecular Spectra and Molecular Structure I, Spectra of Diatomic Molecules*, Van Nostrand, New York **1950**.

[81] R. W. Heather, *Comput. Phys. Commun.* **1991**, *63*, 446.

[82] J. A. Yeazell, in *The Physics and Chemistry of Wave Packets*, edited by J. A. Yeazell and T. Uzer, Chap. 3, Wiley, New York, **2000**.

[83] A. Giusti-Suzor, F. H. Mies, L. F. DiMaruo, E. Charron, B. Yang, *J. Phys. B* **1995**, *28*, 309.

[84] K. Burnett, V. C. Reed, J. Cooper, P. L. Knight, *Phys. Rev. A* **1992**, *45*, 3347.

[85] A. Savin, R. Nesper, S. Wengert, T. F. Fässler, *Angew. Chem.* **1997**, *109*, 1892.

[86] T. Kato, *Commun. Pure Appl. Math.* **1957**, *10*, 151.

[87] R. T. Pack, W. B. Brown, *J. Chem. Phys.* **1966**, *45*, 556.

[88] M. A. L. Marques, E. K. U. Gross, *Annu. Rev. Phys. Chem.* **2004**, *55*, 427.

[89] R. G. Parr, W. Yang, *Density-Functional Theory of Atoms and Molecules*, in: *The International Series of Monographs on Chemistry*, edited by: R. Breslow, J. B. Goodenough, J. Halpern, J. S. Rowlinson, Oxford University Press, New York **1989**.

Dank

Mein Dank gilt auch hier in erster Linie meinem Betreuer Prof. Volker Engel. In den knapp vier Jahren der Diplom- und Doktorarbeit gab es nicht nur viel zu lernen, sondern auch viel zu lachen. Volker war es nie müde, einem Chemiker die Niederungen der Quantenmechanik zu erklären. Dank ihm hatte ich auch die Gelegenheit, meine „verbalen“ Fähigkeiten zu trainieren: Zahlreiche Vorträge auf DPG-Konferenzen und im Rahmen des Graduiertenkollegs ließen nie Langeweile aufkommen. Sein Duett mit Prof. Dietmar Stalke in Klingenberg wird mir wohl besonders in Erinnerung bleiben.

Besonders bin ich natürlich meinen Eltern und Großeltern zum Dank verpflichtet. Meiner Mutter, die mich in all den Jahren finanziell und menschlich unterstützt hat, meinem Vater, der die Fertigstellung dieser Arbeit nicht mehr erleben durfte, und meinen Großeltern, die immer den Kopf über den Enkel schüttelten...

Patrick Musch danke ich für das Korrekturlesen und für die endlosen Diskussionen über Computer, Filme, Studenten und natürlich Programmieren. Für ihre Geduld und ihr Verständnis danke ich Simone Falk und ihrer Familie.

Nicht vergessen seien auch die Mitglieder der anderen Arbeitsgruppen auf unserem Stockwerk: Horia-Sorin Andrei, Stefan Dümmler, Wolfgang Roth, Thomas Schüssler, Nicola Solca, Matthias Zierhut und deren Chefs Otto Dopfer und Prof. Ingo Fischer. Dank auch an die wichtigste Frau auf dem Flur, unsere immer hilfsbereite Sekretärin Elvira König.

Am Schluss bleibt jetzt noch, den aktiven und ehemaligen Mitgliedern der Arbeitsgruppe zu danken: Manfred Lein, der mich im F-Praktikum betreut hat, brachte mir die grundlegenden Dinge über Fortran und UNIX bei. Steffi Gräfe danke ich für das Korrekturlesen, die vielen fachlichen und weniger fachlichen Gespräche und die Verpflegung. Philipp Marquetand hat durch seine Arbeit entscheidend zu dieser Dissertation beigetragen. Auf seinen Schultern lastet jetzt die Verantwortung für den CIP-Pool. Silvia Baumann wagte sich kurz an die Prädissoziation. Und dann waren da noch die „Jungs“: Jochen Beck und Theo Lohmüller, deren gute Laune immer ansteckend war.

Lebenslauf

Persönliche Daten:

Name:	Marco Werner Erdmann
Geburtsdatum:	26.5.1975
Geburtsort:	Würzburg
Staatsangehörigkeit:	deutsch

Schulbildung:

1981–1985	Besuch der Grundschule an der Verbandschule Margetshöchheim
1985–1994	Friedrich-Koenig-Gymnasium, Würzburg, mathematisch-naturwissenschaftlicher Zweig
1994	Abiturprüfung

Grundwehrdienst:

Okt. 1994-Sept.1995	Fernmelderegiment 220, Donauwörth

Studium und berufliche Tätigkeiten:

seit 1995	Studium der Chemie an der Universität Würzburg
Okt. 2000	Diplomprüfung in Chemie
Nov. 2000 – Juni 2001	Diplomarbeit im Arbeitskreis von Prof. V. Engel, Institut für Physikalische Chemie
Juni 2001	Abschluss als Diplom-Chemiker Univ.
Aug. 2001 – Juni 2004	Promotion im Arbeitskreis von Prof. V. Engel.